University of South Carolina
Scholar Commons

Theses and Dissertations

1-1-2013

Design and Synthesis of Polymer-Based Advanced Nanomaterials Using Raft Polymerization and Click Reaction

Junting Li
University of South Carolina

Follow this and additional works at: https://scholarcommons.sc.edu/etd

 Part of the Chemistry Commons

Recommended Citation

Li, J.(2013). *Design and Synthesis of Polymer-Based Advanced Nanomaterials Using Raft Polymerization and Click Reaction.* (Doctoral dissertation). Retrieved from https://scholarcommons.sc.edu/etd/2393

This Open Access Dissertation is brought to you by Scholar Commons. It has been accepted for inclusion in Theses and Dissertations by an authorized administrator of Scholar Commons. For more information, please contact digres@mailbox.sc.edu.

DESIGN AND SYNTHESIS OF POLYMER-BASED ADVANCED NANOMATERIALS USING RAFT POLYMERIZATION AND CLICK REACTION

by

Junting Li

Bachelor of Science
East China University of Science and Technology, 2006

Master of Science
East China University of Science and Technology, 2008

Submitted in Partial Fulfillment of the Requirements

For the Degree of Doctor of Philosophy in

Chemistry and Biochemistry

College of Arts and Sciences

University of South Carolina

2013

Accepted by:

Brian C. Benicewicz, Major Professor

Chuanbing Tang, Committee Member

Thomas Vogt, Committee Member

Harry Ploehn, Committee Member

Lacy Ford, Vice Provost and Dean of Graduate Studies

© Copyright by Junting Li, 2013
All Rights Reserved.

ACKNOWLEDGEMENTS

First, I would like to thank my advisor Prof. Brian Benicewicz for giving me the opportunities to achieve this intriguing and innovative research. His support and encouragement for me had never changed even after many times of failures in my experiments, and his insight and profound expertise served as the best guidance throughout my Ph.D. studies. I also want to thank all my committee members: Prof. Chuanbing Tang, Prof. Tomas Vogt and Prof. Harry Ploehn for their useful suggestions regarding my proposal and my Ph.D. research.

I would like to acknowledge my collaborators – Prof. Linda Shadler and Dr. Jianing Gao at Rensselaer Polytechnic Institute, Prof. Sanat Kumar and Dr. Yuping Xie at Columbia University for their valuable contributions and advices to this work. The experience working with these knowledgeable and helpful people in the interdisciplinary projects let me have a higher version of the material science and learn more extensive beyond chemistry.

Many thanks are due to the members of Benicewicz group past and present for their constant assistance and suggestions. In particular, I want to thank Dr. Yu Li and Dr. Cash Brandon for being the best mentors I could have had.

Last but not least, I want to express my greatest gratitude to my parents and my fiancée – Di Song. This achievement could not have been possible without their love, encouragement, and support.

ABSTRACT

This research focuses on exploring new synthetic approaches to prepare polymer-based advanced nanomaterials using highly efficient chemical tools, such as reversible addition-fragmentation chain transfer (RAFT) polymerization and click reactions.

In the first project, novel synthetic routes to produce fullerene-based polymers were designed. First, mono-alkynyl functionalized fullerene was prepared starting with pristine fullerene (C_{60}). Methyl methacrylate and 6-azido hexyl methacrylate were then randomly copolymerized via RAFT polymerization with well-controlled molecular weights and copolymer compositions. Finally, the two moieties were covalently assembled into a series of well-defined side-chain fullerene polymers (SFP's) via the copper-catalyzed click reaction. The TGA and UV-vis analyses demonstrated consistent and high conversions for most of the samples. Furthermore, the SEM images of these polymers showed the formation of various supramolecular nanoparticle assemblies and crystalline-like clusters depending on the fullerene contents and polymer chain lengths. Additionally, "tadpole-like" fullerene polymers (TFP) were generated from bi-alkynyl functionalized fullerene, followed by a click reaction to anchor azido-capped polymers as "tails". The resultant polymers behaved as surfactants to significantly improve the solubility of graphene. The UV-vis and FT-IR spectra indicated the strong π-π stacking interactions between the TFP's and graphene. TEM images also displayed different dispersions of the complexes of TFP's and graphene in various solvents.

Another aspect of this Ph.D. research was the fabrication of Janus nanoparticles (NP's). A critical challenge in NP functionalization has been the preparation of polymer-grafted asymmetric (Janus) NP's (dia. <100 nm). After multiple trials using different protection-deprotection methods and face-blocking moieties, such as wax beads and planar silica wafers, we designed a robust and cyclic method to synthesize such NP's involving a reversible click reaction and a "grafting to" strategy. A novel mechanochemical approach was introduced into the particle interactions to selectively achieve the protection-deprotection of NP's, which was combined with polymer modification of the unprotected surfaces of the NP's via a "grafting to" approach. The azide-functionalized larger particles could be recycled as face-blocking moieties. Using this pathway, we prepared 15 nm silica NP's that were partially functionalized with poly(methyl methacrylate). Additionally, the unique self-assembly behaviors of the resultant Janus NP's and their interactions with isotropic NP's were investigated in different solvents and concentrations by TEM and AFM analyses.

The dispersion of NP's in polymer matrices is a critical factor in determining the properties of the resulting nanocomposites. In the last part, we studied on NP's modification via surface-initiated RAFT polymerization using various functional monomers, and the dispersion of the NP's in different polymer matrices. Kinetic studies were investigated for each polymerization to demonstrate the controlled nature of the polymerization on the surface of the NP's. In addition to the homopolymers, multi-layers of block copolymer brushes were grafted on silica NP's by sequential RAFT polymerizations. Moreover, "pseudo" gradient copolymer brushes were also prepared by inserting a third random copolymer block into the middle of the two homopolymer

blocks, which was established as an easy and straightforward method to synthesize gradient brushes on NP's.

TABLE OF CONTENTS

LIST OF TABLES

LIST OF FIGURES

LIST OF SCHEMES

CHAPTER 1

INTRODUCTION

1.1 Reversible Addition-fragmentation Chain Transfer Polymerization

Reversible addition-fragmentation chain transfer (RAFT) polymerization has become one of the three best-developed living radical polymerization processes (or formally named as reversible deactivation radical polymerization) [1] over the past three decades, together with nitroxide mediated polymerization (NMP) and atom transfer radical polymerization (ATRP). These polymerization processes enable researchers to simultaneously control the molecular weight and molecular weight distribution, and provide "living" characteristics to the polymer chains. In particularly, RAFT polymerization has been widely applied to prepare many types of polymer-based advanced architectures due to the relatively mild reaction conditions and the tolerance to a variety of functional groups.[2-4]

The RAFT process is similar to conventional free radical polymerization with the addition of thiocarbonylthio compounds (Z-(C=S)-SR) as the chain transfer agents (CTA's), which are crucial to control the polymerization through a two-step addition-fragmentation mechanism. The whole mechanism of RAFT polymerization is shown in Scheme 1.1.[5] The living characteristics rely on the dynamic equilibrium between the active propagating radicals ($P_n\cdot$ and $P_m\cdot$) and the dormant polymeric thiocarbonylthio species. The equilibrium must be faster than the propagation, ensuring that all the

polymer chains grow with the same possibility. Additionally, the reinitiation and propagation should also be fast enough to suppress the termination. To optimize the control in RAFT polymerization, choosing appropriate CTA's for different monomers is very necessary.

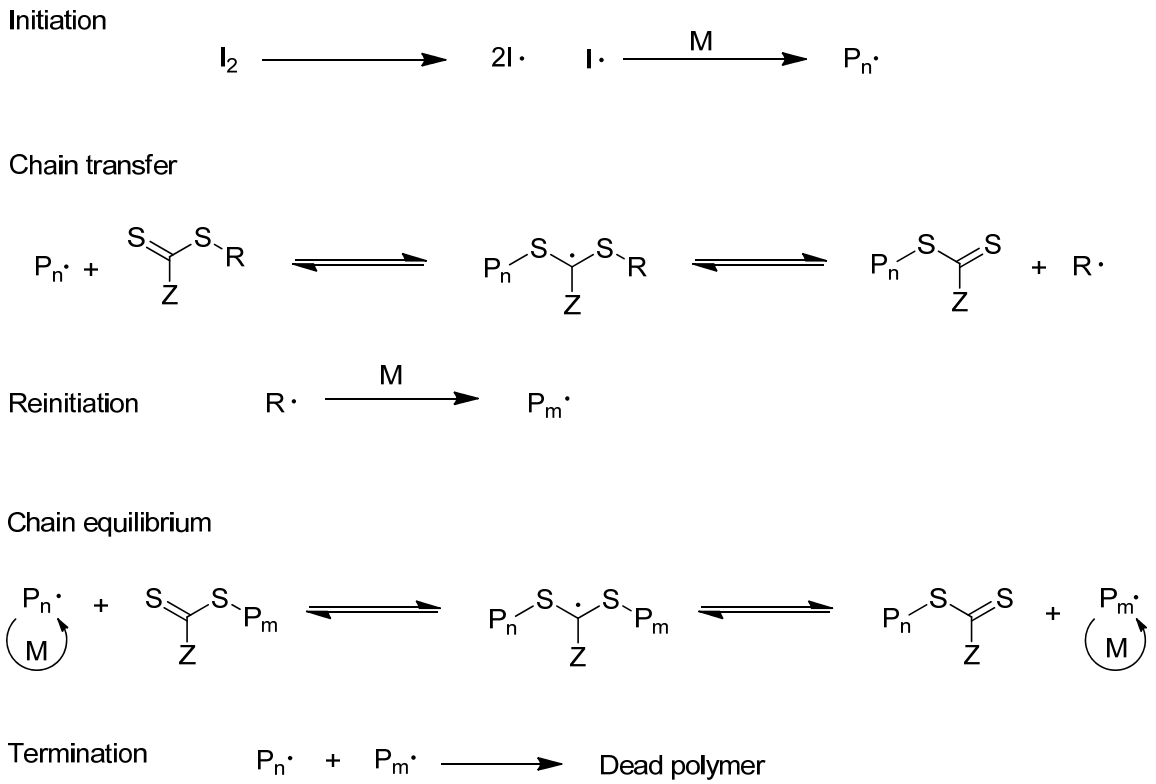

Scheme 1.1 General mechanism of RAFT polymerization.

After more than ten years of development of RAFT polymerization, the correlation between CTA structures and polymerization control has been fully studied.[6] We have known that both the 'Z' and 'R' groups of the CTA play critical roles in determining the outcome of the polymerization. The 'Z' group determines the reaction rates of the dynamic equilibrium, and generally, the rate constant of the equilibrium must be greater than the rate of propagation. With different 'Z' groups, the compounds used as CTA's include dithioesters (Z = alkyl or aryl), trithiocarbonates (Z = SR'), xanthates (Z = OR')

and dithiocarbamates (Z = NR'R"). Generally, dithioesters and trithiocarbonates are more active than xanthates and dithiocarbamates, since the lone pair on nitrogen or oxygen adjacent to the thiocarbonyl of the latter two kinds of CTA's can reduce the transfer coefficients in terms of their zwitterionic canonical forms. General guidelines for selection of 'Z' groups are summarized in Figure 1.1.

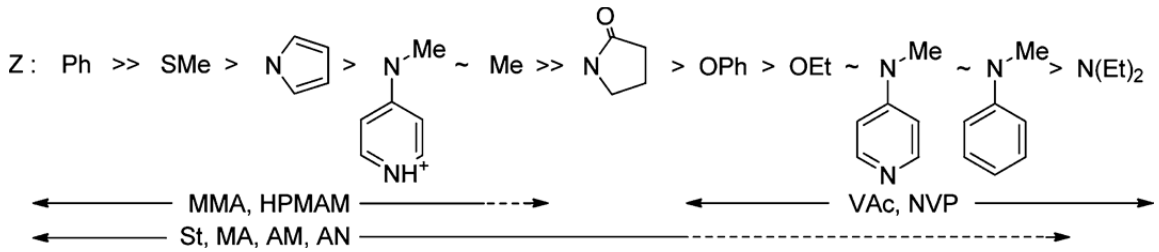

Figure 1.1 Guidelines for selection of the 'Z' group of RAFT agents (ZC(=S)SR) for various monomers.[6]

On the other hand, the 'R' group of the CTA must be a good leaving group, and the expelled radical (R·) should also be able to reinitiate polymerization efficiently. Otherwise, retardation and termination will occur. General guidelines for selection of 'R' groups are summarized in Figure 1.2.

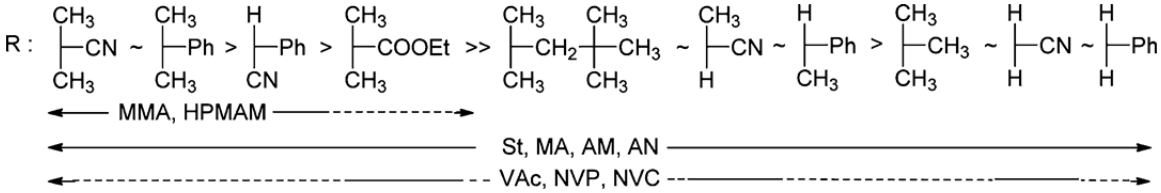

Figure 1.2 Guidelines for selection of the 'R' group of RAFT agents (ZC(=S)SR) for various monomers.[6]

1.2 Reversible Copper-mediated Click Reaction in Polymer Chemistry

In 2001, K. Barry Sharpless proposed the concept of "click chemistry". Actually, click chemistry is not a scientific definition, but rather a synthetic philosophy inspired by the simple but efficient organic reactions that takes place in nature. In Sharpless' opinion, all reactions having the characteristics below are "click reactions".[7]

- The reaction must be modular, wide in scope, stereospecific (but not necessarily enantioselective), and give very high yields.
- Only inoffensive byproducts are generated that can be removed by non-chromatographic methods, such as crystallization or distillation.
- The required process characteristics include simple reaction conditions (ideally, the process should be insensitive to oxygen and water), readily available starting materials and reagents, the use of a solvent that is benign (such as water) or easily removed or solventless, and simple product isolation.

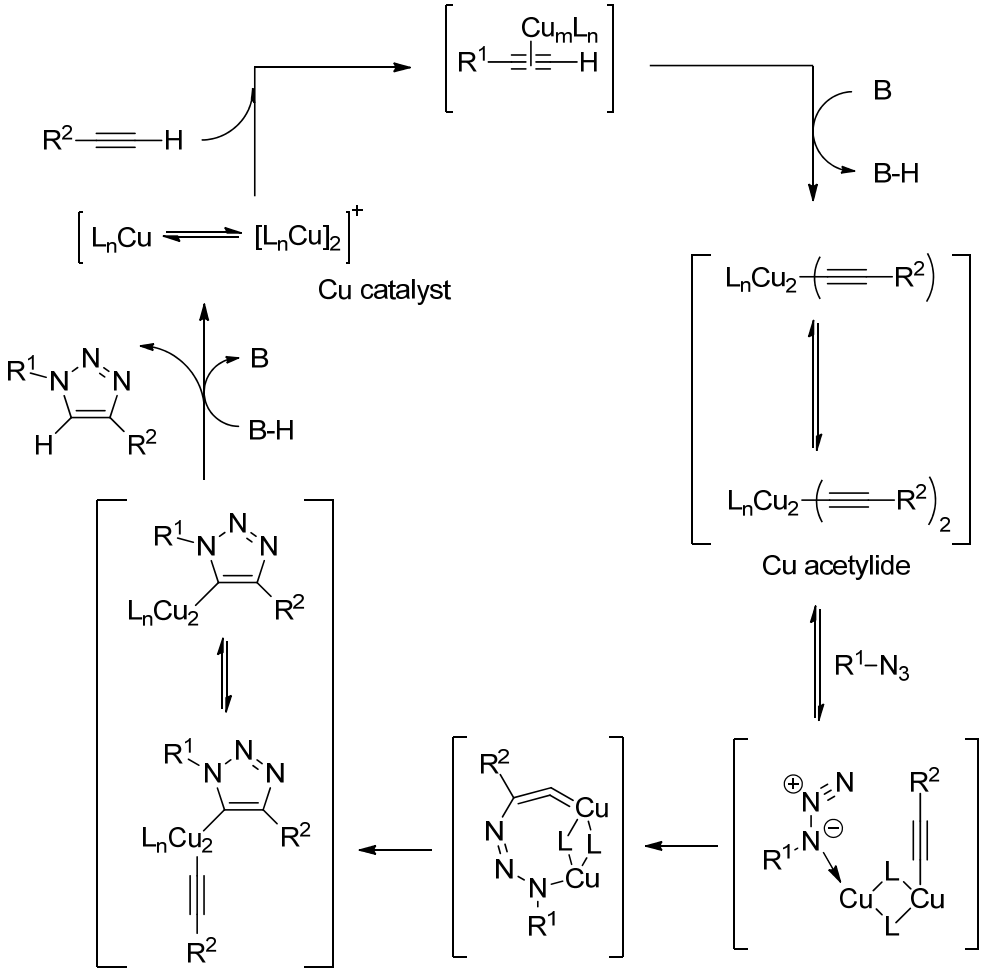

Scheme 1.2 Proposed mechanism of Cu(I)-mediated azide-alkyne cycloaddition.[8]

The copper-catalyzed dipole cycloaddition of azides and alkynes, named the Huisgen cycloaddition, is one of the most powerful reactions in this family. In the absence of a proper catalyst, this cycloaddition is usually quite slow, because the ending alkynes are not good 1,3-dipole accepters. However, when copper (I) is introduced, which can bind to the alkynes (Scheme 1.2), the reaction rates increase dramatically with high regioselectivity and yields.

The copper-mediated click reaction shows many advantages, such as:

- introduction of azides is easily accomplished via reduction of primary amine or substitution of halide;
- azides are very stable against dimerization, hydrolysis and other organic synthesis conditions;
- the reaction can be performed in various solvents including aqueous solution.

While there have been many types of click reactions developed to date, such as the thiol-ene reaction,[9, 10] thiol-yne reaction,[11] and Diels-Alder reaction,[12] the copper-mediated click reaction is still the most popular click reaction for many applications, especially in the area of polymer synthesis.[13]

The copper-mediated click reaction is commonly used to either build up linear polymers through step polymerization with azido/alkynyl functionalized monomers,[14] or to form dendrimers, brush polymers and block copolymers when combined with other polymerization tequiques,[15-18] such as living radical polymerization, ring opening polymerization (ROP), and ring-opening metathesis polymerization (ROMP). For example, the strategy developed by Li and Benicewicz was used to synthesize a variety of side-chain functionalized polymers by postfunctionalization through the click reaction,

following the RAFT polymerization of azide-containing monomers at a relatively low temperature (40 °C) to prevent the degradation of the azides.[15] Figure 1.3 shows all the possible polymer architectures which can be generated via combination of ATRP and the click reaction. In addition, the click reaction also provides an effective linkage to achieve the "grafting to" strategy for surface modification,[19, 20] which will be discussed later.

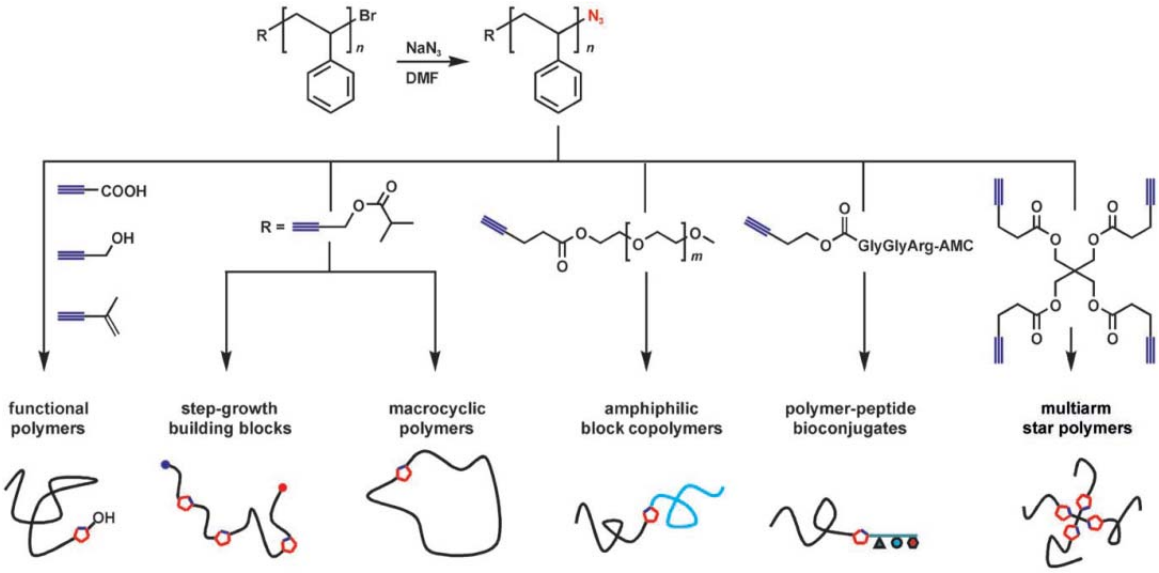

Figure 1.3 Functional group interconversion for ATRP products.[20]

Moreover, the importance of the copper-catalyzed click reaction for polymer chemistry is not only because it is an efficient method for forming covalent linkages, but also because it can be used in an opposite way – cleavage of polymer chains. The 1,2,3-triazole ring formed in the click reaction is extremely robust, and for a long time it was widely believed that the cycloreversion was not as efficient. Recently, Bielawski and coworkers found that this linkage can be mechanically broken to recover the original azides and alkynes by means of an ultrasound technique, if the triazole ring is in the middle of a long polymer chain (Figure 1.4).[21, 22] This mechanically-driven reaction undergoes a totally different mechanism from its reverse reaction, where the mechanical

forces are presumed to promote the reaction through ground-state destabilization of the reactants (as a result of changes in molecular geometry) or the stabilization of reactive intermediates at or near the transition state of the reaction coordinate. Unquestionably, this discovery will widely broaden the application of this classic reaction in the future as it provides a simple and powerful synthetic pathway to reversible covalent connections.

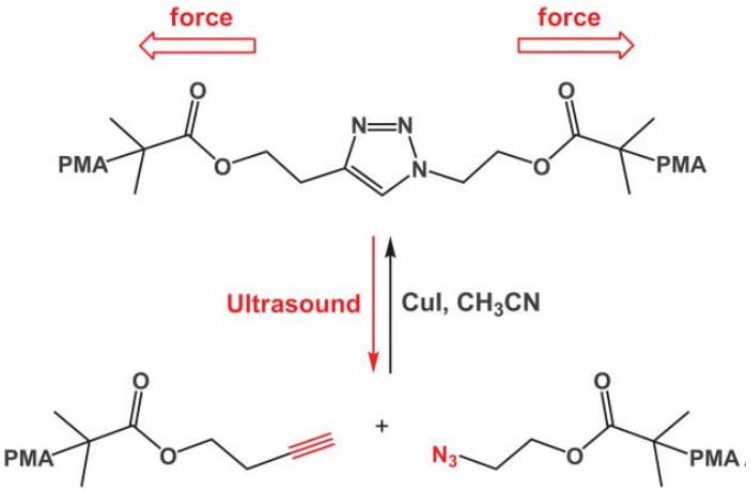

Figure 1.4 Reversible formation and cleavage of 1,2,3-triazole ring embedded within a poly(methyl acrylate) chain.[21]

1.3 Synthesis of Fullerene Polymers

In 1985, Kroto and coworkers first reported the existence of buckminsterfullerene (C_{60}).[23] Five years later, the preparation of fullerene was scaled up to multigram quantities by evaporating graphite electrodes.[24] Since then, fullerene has attracted much attention due to its unique and interesting properties, such as superconductivity, ferromagnetism, anti-HIV bioactivity, and optical nonlinearity. Especially in the application of polymer-based solar cells, fullerene has become the ubiquitous electron acceptor because of the high electron affinity and ability to transport charge effectively.[25] However, its applications are seriously limited because pristine fullerene has very poor compatibility with most other materials.

Covalent combination of fullerene with polymers is an effective strategy to overcome this disadvantage and create novel fullerene-based architectures. After two decades of development, a variety of fullerene-polymer structures have been synthesized through different chemical routes. Generally, fullerene-based polymers can be classified into the following types according to the different positions of fullerene moieties in the polymer structures: main-chain fullerene polymers, side-chain fullerene polymers, fullerene-capped polymers, star-shaped fullerene polymers and fullerene dendrimers.[26, 27]

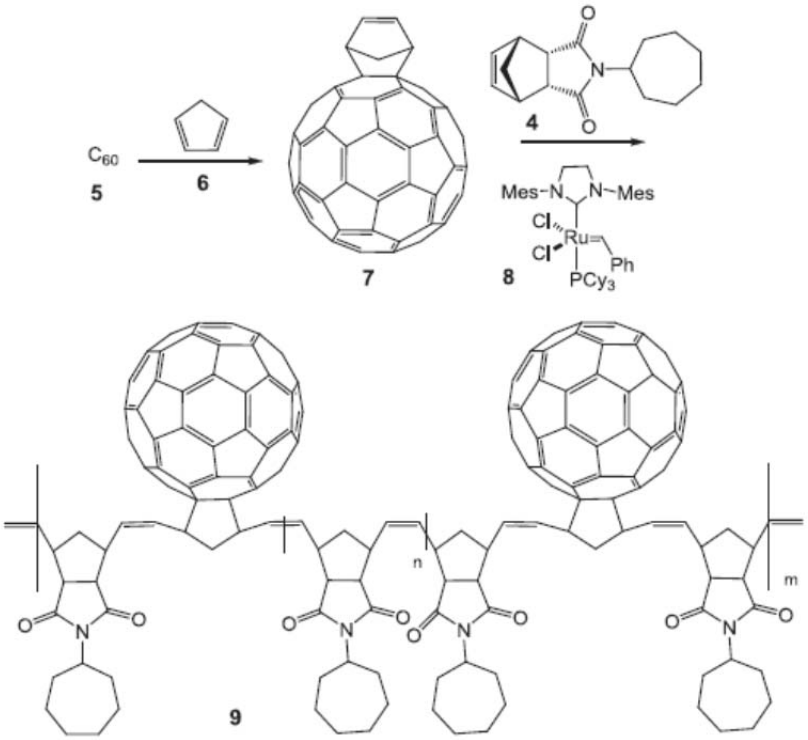

Scheme 1.3 Synthesis of C_{60}-cyclopentadiene cycloadduct – N-(cycloheptyl)-endo-norbornene-5,6-dicarboximide polymers by ROMP.[28]

Memo and coworkers synthesized a main-chain fullerene polymer using ROMP.[28] They first functionalized pristine fullerene with cyclopentadiene first via a Diels-Alder reaction. Then the C_{60}-cyclopentadiene cycloadduct was copolymerized with N-

(cycloheptyl)-endo-norbornene-5,6-dicarboximide using a Grubbs second-generation ruthenium catalyst (Scheme 1.3).

For the synthesis of a side-chain fullerene polymer, Hadziioannou *et al.* produced styrene-based copolymers by nitroxide-mediated radical polymerization and then introduced C_{60} to the side chains through either atom-transfer radical addition (ATRA)[29] or cycloaddition to C_{60} [30].

Yagci and coworkers reported the fabrication of fullerene-capped polystyrene by converting the RAFT chain end of polystyrene to a thiol group, which could subsequently react with C_{60} through a thiol-ene click reaction.[31] This method could be performed using mild conditions and short reaction times.

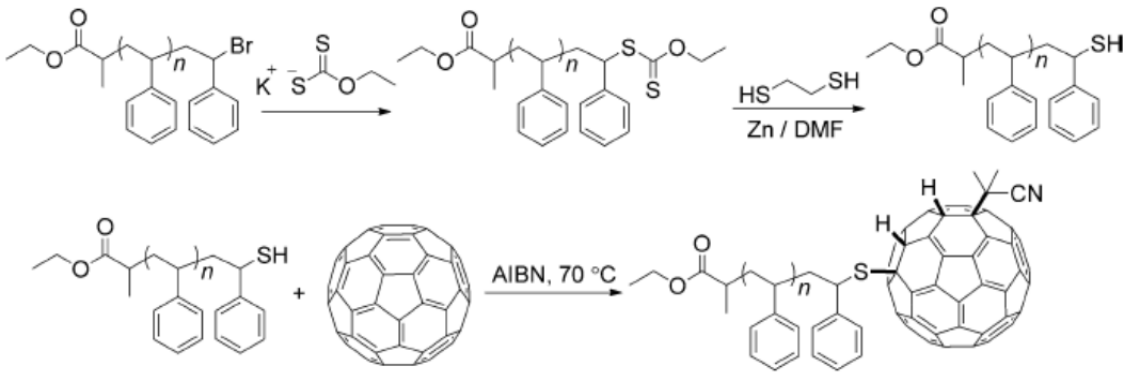

Scheme 1.4 Synthesis of C_{60} end-capped polystyrene using thiol-ene chemistry.[31]

Natori and coworkers grafted poly(1,3-cyclohexadienyl)lithium on fullerene to form a star-shaped fullerene polymer.[32] They found that the reaction efficiency was strongly dependent on the nucleophilicity of the polymer carbanions and the molecular weight. Due to the steric hindrance of the attached arm and the negative charge generated on the C_{60} core, up to four arms could be grafted on each fullerene molecule.

There are two architectures of fullerene dendrimers with the fullerene moiety located either on the braches or in the core. An example of the former type is the fullerene-rich

dendron synthesized by Yang and coworkers, which could be further polymerized as a macromonomer through ROMP (Scheme 1.5).[33] In contrast, Martin *et al.* made amphiphilic dendrofullerenes with fullerene in the core and carboxylic acids on the branches, which displayed very interesting self-assemblies forming micelles, nanorods, or hollow vesicles depending on the concentration.[34]

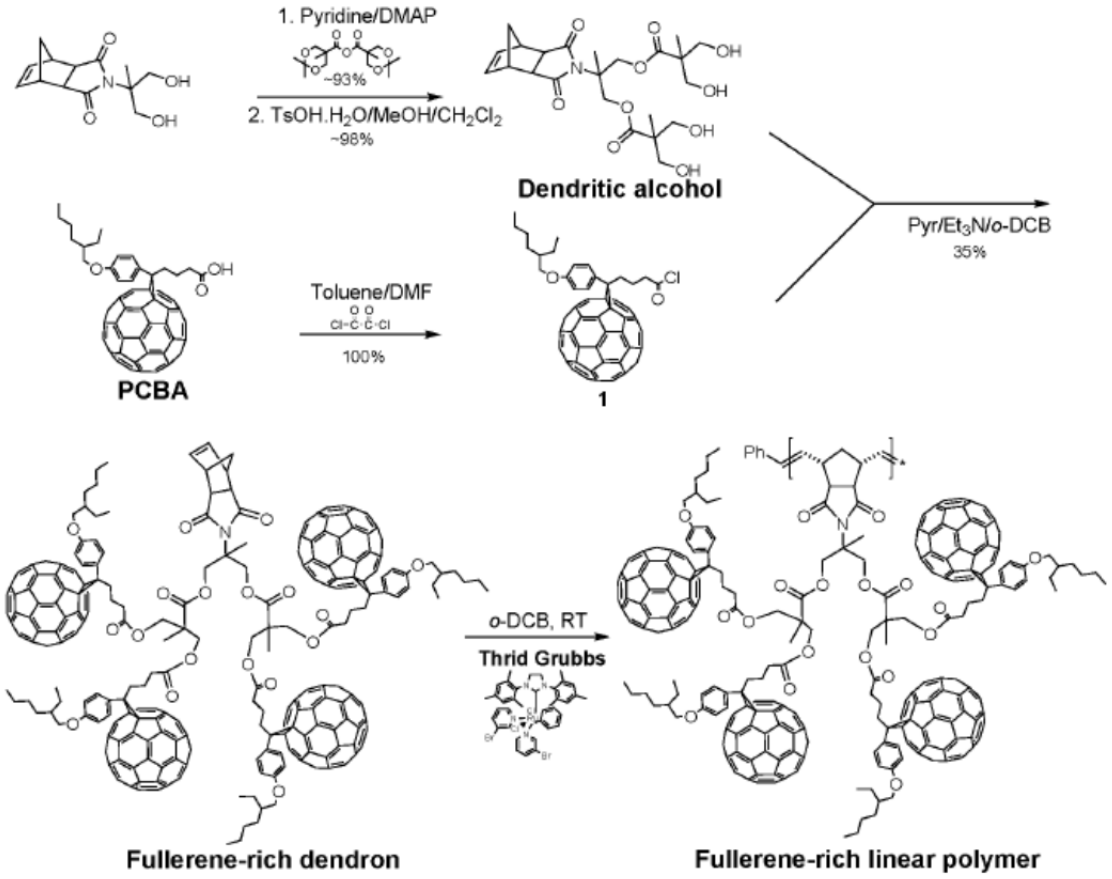

Scheme 1.5 Synthetic route to fullerene-rich dendron and its linear polymer.[33]

For the solar cell applications, there is a class of fullerene polymers named double-cable polymers, which consists of π-conjugated backbones (donor cable) bearing covalently connected fullerenes (acceptor cable).[35, 36] This design is used to overcome the poor compatibility between the conjugated polymer and the fullerene components, which could decrease the effective donor-acceptor interaction as well as the charge transport of

the photogenerated electrons and holes. Another approach to solve this problem is to generate block copolymers bearing both conjugated blocks and fullerene blocks,[37, 38] since the micro-phase separation of amphiphilic block copolymers has been well studied.

1.4 Surface Modification of Nanoparticles with Polymers

Nanoparticles are of great scientific and practical interest as they are effectively a bridge between bulk materials and molecular structures, and display many intriguing size-dependent properties. Covalently grafting polymer brushes on their surface has extensively broadened the applications of nanoparticles in recent years, as the modification can greatly improve their compatibility with organic/polymer matrices, and optimize the surface chemistry for optical, mechanical and biomedical applications.[39-43]

Overall, there are two principal synthetic strategies for grafting polymers on nanoparticles: the "grafting to" and "grafting from" strategies (Figure 1.5). As the term implies, in the "grafting to" approach polymers are produced first, and then attached to the surface of nanoparticles with proper end functional groups.[44-48] Since polymer synthesis and grafting are performed in separate steps, this approach is universal and many types of polymerization methods can be applied regardless of the surface chemistry of nanoparticles. However, it is not possible to attain high graft densities using "grafting to" strategies because it is difficult for the end-functionalized polymer chains to diffuse near the nanoparticle surface after some grafting sites have been occupied by the earlier-grafted polymers due to steric hindrance, especially when the molecular weight of the polymer is high. Moreover, the existence of many free polymers after the grafting can create difficulties in purification. In contrast, chain initiators are anchored on the nanoparticle surface in the "grafting from" strategies, which can usually have a relatively high graft density ascribed to their smaller size. Then, monomers are added to the

initiators during the polymerization, and polymers grow from the surface.[49-52] The success of this strategy only requires the diffusion of small monomeric species to the surface of the nanoparticles. While very few polymerization methods can tolerate the extremely high local concentration of chain initiators on the nanoparticle surface and still maintain good control, so far living radical polymerization is the most popular method for grafting polymer "from" the surface of nanoparticles.

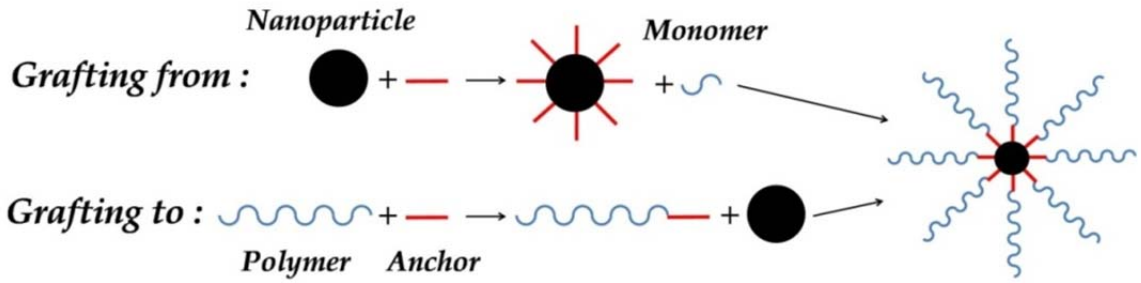

Figure 1.5 The "grafting to" and "grafting from" strategies for grafting polymers on nanoparticles.

Nanoparticle modification via RAFT polymerization has been investigated for more than ten years due to its versatility and simplicity,[53] which is usually achieved by anchoring either the "Z" group or the "R" group of CTA on the nanoparticle surface. Following the "Z" approach, polymer brushes act as the leaving groups ($P_n\cdot$) and are not always attached on the surface of the nanoparticles. Thus, the propagation actually occurs in the solution, so it is more like a "graft to" strategy.[54, 55] However, to undergo a well-controlled RAFT polymerization, the propagating polymer radicals have to be close to the surface to maintain the chain-transfer reaction with the CTA's. Because of the steric hindrance of the neighboring grafted polymer chains, the polymerization control of the "Z" approach is relatively poor. The propagating polymer radicals may drift away from the nanoparticle surface during the polymerization, leading to decreased graft density and free polymers in the solution.

On the other hand, the "R" approach can overcome these disadvantages and has attracted more attention from the scientific community. Since the "R" groups are anchored on the surface, the whole nanoparticle acts as part of the leaving groups. Thus, the propagating polymer radicals are always on the surface during the polymerization. In previous work from our group, Li and Benicewicz have designed a mature pathway to anchor a CTA – 4-cyanopentanoic acid dithiobenzoate (CPDB) on silica nanoparticles (SiO_2) with precisely tunable graft density (Scheme 1.6), and conducted well-controlled RAFT polymerization of different monomers on the nanoparticles.[56] In addition to dithioester-type CTA's, trithiocarbonates have also been anchored on nanoparticles, which are claimed to be more robust and universal.[57]

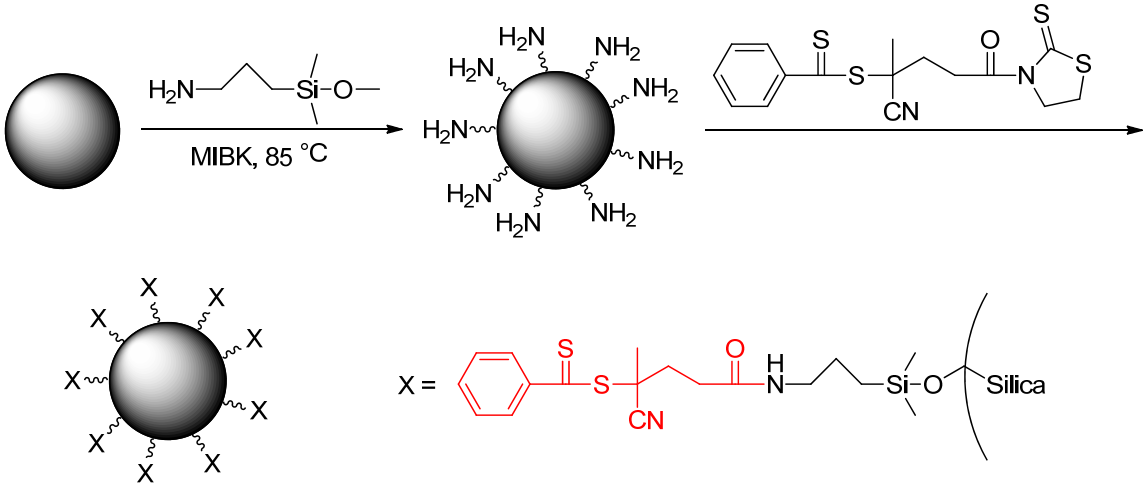

Scheme 1.6 Synthesis of CPDB functionalized silica nanoparticles.

Although the previous discussion has focused on uniformly-functionalized homopolymer-grafted nanoparticles, more complicated architectures composed of polymer brushes and nanoparticles can be conducted with appropriate graft strategies. In terms of polymer composition, random copolymers, block copolymers, and even gradient copolymers can be grafted on nanoparticles. Also, the nanoparticles can be functionalized

with more than one kind of species, such as binary brush grafted nanoparticles.[58, 59] There have also been attempts to prepare nanoparticles that are asymmetrically functionalized with different polymers to form Janus nanoparticles. These advanced structures will open up many new possibilities for the application of nanoparticles as smart or multi-functioned materials.

1.5 Synthesis of Janus particles

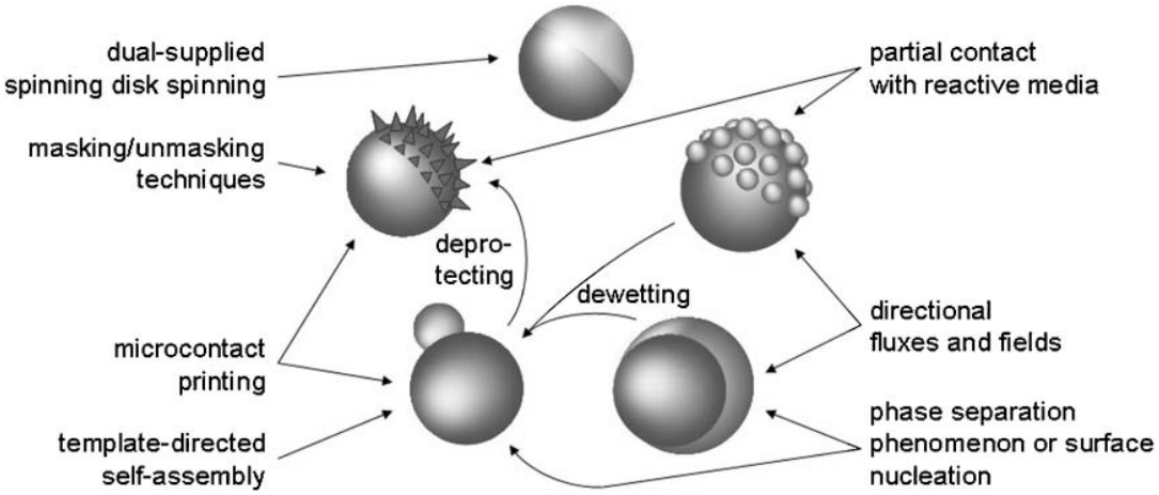

Figure 1.6 Schematic representation of the synthetic routes yielding Janus particles.[64]

The introduction of anisotropy into micro or nano sized particles is an intriguing and challenging research area in current materials science, since it has been theoretically predicted that anisotropic particles could be very useful for controlling molecular recognition and self-assembling processes.[60-62] Janus particles, were first proposed by P-G. de Gennes,[63] and are a type of particle that contains different chemistries on the two hemispheres of the particle. In 2005, Perro *et al*. reviewed the research on Janus particle synthesis after fifteen years of development and summarized the most typical synthetic routes for preparing Janus particles (Figure 1.6).[64] At that time, most of the reported

Janus particles were fairly large with diameters ranging from hundreds of nanometers to dozens of micrometers.

More recently, research efforts have focuses on even smaller particles with more precise control over the geometry of the Janus particles. For instance, Wang and coworkers stabilized negatively charged gold nanoparticles (Au NPs) in organic solvents assisted by amphiphilic poly(ethylene glycol)-octa-functionalized polyhedral oligomeric silsesquioxane, and then mixed it with an aqueous solution containing positively charged silica nanoparticles (SiO_2 NPs), inducing the interface conjugation of negative Au NPs and positive SiO_2 NPs through electrostatic interactions and leading to the formation of patchy Janus nanoparticles.[65] Paunov and Cayre used a gel trapping technique to form monolayers of polystyrene microparticles on an oil-water interface, and then lifted off the particles by casting with PDMS elastomer to generate Janus particles.[66] Similarly, Tang and coworkers prepared monolayers of microparticles on glass slides and coated the exposed surface of the particles with gold. After release from the glass slides by sonication, the two hemispheres of the Janus particles were functionalized by two kinds of proteins using different chemistry for potential biomedical applications.[67]

The emulsion approach developed by Granick *et al* is one of the most successful synthetic routes for Janus particles so far, and gram-sized quantities could be achieved using this approach.[68] At the liquid-liquid interface of emulsified molten wax and water, untreated silica particles adsorb and are frozen in place when the wax solidifies. The exposed surfaces of the immobilized particles are modified chemically. After the wax is dissolved, the inner surfaces can be modified with a different chemistry (Scheme 1.7). By adding surfactants to the interface or changing pH and salt concentration, the contact

angle of silica particles on the interface can be varied. Consequently, the ratio of the two hemispheres of the Janus particles can be adjusted.[69] Moreover, they also developed a two-step μ-contact printing method to form a more complicated structure – trivalent patchy particles.[70]

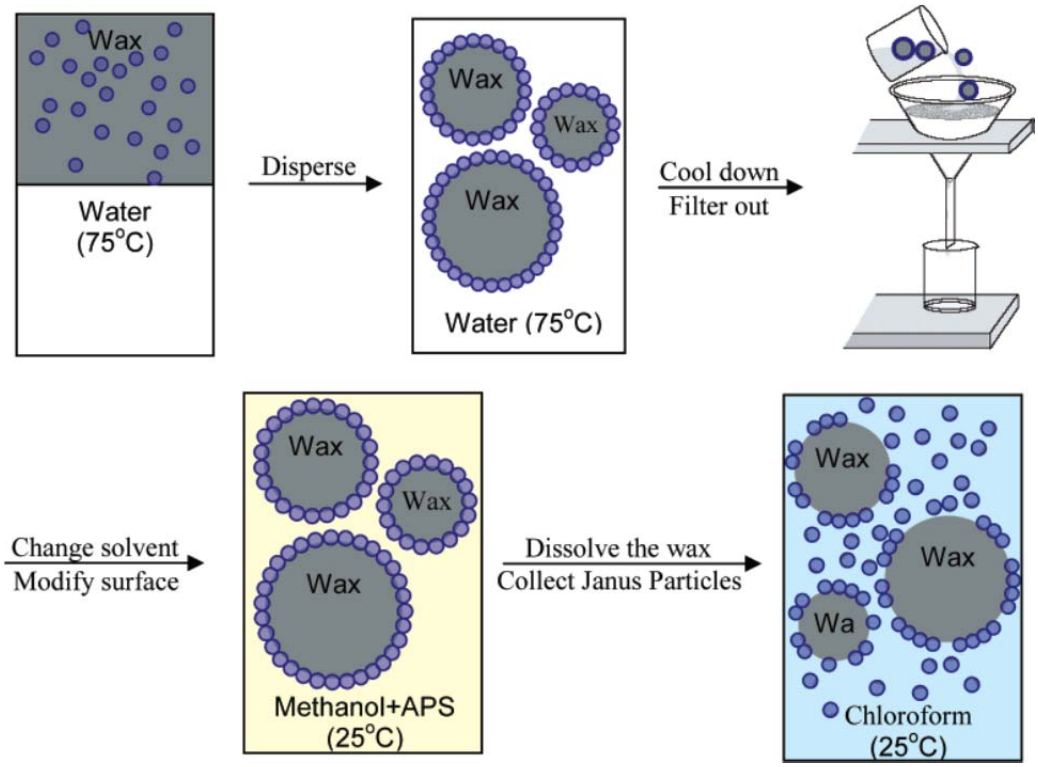

Scheme 1.7 Janus nanoparticle synthesis using an emulsion process.[68]

1.6 Motivation and outline

The development of modern synthetic techniques in organic and polymer chemistry has introduced many novel and efficient reactions into the toolbox for polymer synthesis and nanoparticle modification.[15,71] In this research, we used these modern synthetic tools to overcome two major challenges in polymer functionalized nanomaterials and advance our understanding of their self-assembly behaviors.

In the first part of this work, carbon-nased materials ,such as fullerene, graphene, etc, are generally not miscible with most other materials as discussed above. By

functionalizing them with polymers, an improved compatibility in organic solvents and polymer matrices is expected. As described in Chapter 2 of this dissertation, both side-chain fullerene polymers and "tadpole-like" fullerene polymers were designed through a combination of RAFT polymerization and click reaction. Due to the high efficiency of the two techniques, the molecular weight, fullerene loading and polymer architecture of the side-chain fullerene polymers were controlled precisely and simultaneously, which represnts a significant progress in comparison to the previously reported synthetic approaches. Additionally, the ability of the "tadpole-like" fullerene polymers to function as surfactants was studied to stabilize graphene in different solvents through strong π-π stacking interactions.

Another aspect of this research was focused on the surface modification of silica nanoparticles with polymers in unique ways. In Chapter 3, a novel, mechanochemically-driven and cyclic synthetic route is designed for the fabrication of polymer-grafted Janus nanoparticles, using the recently-reported reversible click reaction, Previous to this research there were no effective synthetic methods reported in this field to prepare polymer-grafted Janus nanoparticles with diameters less than 100 nm. Additionally, growing polymer brushes is an effective strategy to adjust the dispersion of the nanoparticles in polymeric nanocomposites. Therefore, the final chapter focuses on exploring the polymerizations of different functional monomers on silica nanoparticles via surface-initiated RAFT polymerization, and studying the dispersions of the resultant polymer-grafted nanoparticles in the corresponding matrices. In addition to homopolymers, sequential RAFT polymerizations on silica nanoparticles were also

investigated to form multi layers of polymer brushes, capable of creating pseudo-gradient brush structures in a robust and straightforward manner.

1.7 References

1. Jenkins, A. D.; Jones, R. G.; Moad, G. *Pure Appl. Chem.* **2010,** *82*, 483-491.

2. Hrsic, E.; Zografou, I.; Schulte, B.; Pich, A.; Keul, H.; Moller, M. *Polymer* **2013,** *54*, 495-504.

3. Quek, J. Y.; Roth, P. J.; Evans, R. A.; Davis, T. P.; Lowe, A. B. *J. Polym. Sci. Pol. Chem.* **2013,** *51*, 394-404.

4. Xu, J. X.; Xiao, X.; Zhang, Y. Y.; Zhang, W. Q.; Sun, P. C. *J. Polym. Sci. Pol. Chem.* **2013,** *51*, 1147-1161.

5. Moad, G.; Chiefari, J.; Chong, Y. K.; Krstina, J.; Mayadunne, R. T. A.; Postma, A.; Rizzardo, E.; Thang, S. H. *Polym. Int.* **2000,** *49*, 993-1001.

6. Keddie, D. J.; Moad, G.; Rizzardo, E.; Thang, S. H. *Macromolecules* **2012,** *45*, 5321-5342.

7. Kolb, H. C.; Finn, M. G.; Sharpless, K. B. *Angew. Chem. Int. Edit.* **2001,** *40*, 2004-2021.

8. Bock, V. D.; Hiemstra, H.; van Maarseveen, J. H. *Eur. J. Org. Chem.* **2005**, 51-68.

9. Lowe, A. B. *Polym. Chem.* **2010,** *1*, 17-36.

10. Kotsuchibashi, Y.; Ebara, M.; Aoyagi, T.; Narain, R. *Polym. Chem.* **2012,** *3*, 2545-2550.

11. Fairbanks, B. D.; Sims, E. A.; Anseth, K. S.; Bowman, C. N. *Macromolecules* **2010,** *43*, 4113-4119.

12. Blackman, M. L.; Royzen, M.; Fox, J. M. *J. Am. Chem. Soc.* **2008,** *130*, 13518-13519.

13. Lutz, J.-F. *Angew. Chem. Int. Edit.* **2007,** *46*, 1018-1025.

14. Chernykh, A.; Agag, T.; Ishida, H. *Polymer* **2009,** *50*, 382-390.

15. Li, Y.; Yang, J.; Benicewicz, B. C. *J. Polym. Sci. Pol. Chem.* **2007,** *45*, 4300-4308.

16. Opsteen, J. A.; van Hest, J. C. M. *Chem. Commun.* **2005**, 57-59.

17. Wu, P.; Feldman, A. K.; Nugent, A. K.; Hawker, C. J.; Scheel, A.; Voit, B.; Pyun, J.; Frechet, J. M. J.; Sharpless, K. B.; Fokin, V. V. *Angew. Chem. Int. Edit.* **2004,** *43*, 3928-3932.

18. Chen, J. C.; Xiang, J. M.; Cai, Z. W.; Yong, H.; Wang, H. D.; Zhang, L. H.; Luo, W. Q.; Min, H. *J. Macromol. Sci. Part A-Pure Appl. Chem.* **2010,** *47*, 655-662.

19. An, Z.; Tang, W.; Wu, M.; Jiao, Z.; Stucky, G. D. *Chem. Commun.* **2008**, 6501-6503.

20. Liu, J.; Nie, Z.; Gao, Y.; Adronov, A.; Li, H. *J. Polym. Sci. Pol. Chem.* **2008,** *46*, 7187-7199.

21. Brantley, J. N.; Wiggins, K. M.; Bielawski, C. W. *Science* **2011,** *333*, 1606-1609.

22. Leibfarth, F. A.; Hawker, C. J. *Science* **2011,** *333*, 1582-1583.

23. Kroto, H. W.; Heath, J. R.; O'Brien, S. C.; Curl, R. F.; Smalley, R. E. *Nature* **1985,** *318*, 162-163.

24. Kratschmer, W.; Lamb, L. D.; Fostiropoulos, K.; Huffman, D. R. *Nature* **1990,** *347*, 354-358.

25. Thompson, B. C.; Frechet, J. M. J. *Angew. Chem. Int. Edit.* **2008,** *47*, 58-77.

26. Giacalone, F.; Martin, N. *Chem. Rev.* **2006,** *106*, 5136-5190.

27. Wang, C. C.; Guo, Z. X.; Fu, S. K.; Wu, W.; Zhu, D. B. *Prog. Polym. Sci.* **2004,** *29*, 1079-1141.

28. Mamo, M. A.; Freitas, F. S.; Forbes, R. P.; Black, R. S.; Nogueira, A. F.; van Otterlo, W. A. L.; Coville, N. J. *Fuller. Nanotub. Carbon Nanostruct.* **2013,** *21*, 198-212.

29. de Boer, B.; Stalmach, U.; van Hutten, P. F.; Melzer, C.; Krasnikov, V. V.; Hadziioannou, G. *Polymer* **2001,** *42*, 9097-9109.

30. Barrau, S.; Heiser, T.; Richard, F.; Brochon, C.; Ngov, C.; van de Wetering, K.; Hadziioannou, G.; Anokhin, D. V.; Ivanov, D. A. *Macromolecules* **2008,** *41*, 2701-2710.

31. Iskin, B.; Yilmaz, G.; Yagci, Y. *Chem.-Eur. J.* **2012,** *18*, 10254-10257.

32. Natori, I.; Natori, S. *J. Polym. Sci. Pol. Chem.* **2008,** *46*, 3282-3293.

33. Kim, J.; Yun, M. H.; Lee, J.; Kim, J. Y.; Wudl, F.; Yang, C. *Chem. Commun.* **2011,** *47*, 3078-3080.

34. Munoz, A.; Illescas, B. M.; Sanchez-Navarro, M.; Rojo, J.; Martin, N. *J. Am. Chem. Soc.* **2011,** *133*, 16758-16761.

35. Lanzi, M.; Paganin, L.; Errani, F. *Polymer* **2012,** *53*, 2134-2145.

36. Miyanishi, S.; Zhang, Y.; Hashimoto, K.; Tajima, K. *Macromolecules* **2012,** *45*, 6424-6437.

37. Heuken, M.; Komber, H.; Erdmann, T.; Senkoyskyy, V.; Kiriy, A.; Voit, B. *Macromolecules* **2012,** *45*, 4101-4114.

38. Bicciocchi, E.; Chen, M.; Rizzardo, E.; Ghiggino, K. P. *Polym.Chem.* **2013,** *4*, 53-56.

39. Lin, I. C.; Liang, M. T.; Liu, T. Y.; Jia, Z. F.; Monteiro, M. J.; Toth, I. *Bioorg. Med. Chem.* **2012,** *20*, 6862-6869.

40. Park, J. T.; Roh, D. K.; Patel, R.; Kim, E.; Ryu, D. Y.; Kim, J. H. *J. Mater. Chem.* **2010,** *20*, 8521-8530.

41. Shi, H. Y.; Yuan, L.; Wu, Y. F.; Liu, S. Q. *Biosens. Bioelectron.* **2011,** *26*, 3788-3793.

42. Tao, P.; Li, Y.; Rungta, A.; Viswanath, A.; Gao, J. N.; Benicewicz, B. C.; Siegel, R. W.; Schadler, L. S. *J. Mater. Chem.* **2011,** *21*, 18623-18629.

43. Yang, J.; Deng, L. H.; Han, C. R.; Duan, J. F.; Ma, M. G.; Zhang, X. M.; Xu, F.; Sun, R. C. *Soft Matter* **2013,** *9*, 1220-1230.

44. Lowe, A. B.; Sumerlin, B. S.; Donovan, M. S.; McCormick, C. L. *J. Am. Chem. Soc.* **2002,** *124*, 11562-11563.

45. Lupitskyy, R.; Motornov, M.; Minko, S. *Langmuir* **2008,** *24*, 8976-8980.

46. Feng, L. B.; He, L.; Ma, Y. X.; Wang, W. *Mater. Chem. Phys.* **2009,** *116*, 158-163.

47. Thong-On, B.; Rutnakornpituk, B.; Wichai, U.; Rutnakornpituk, M. *J. Nanopart. Res.* **2012,** *14*.

48. Wang, Y. Z.; Fan, D. Q.; He, J. P.; Yang, Y. L. *Colloid Polym. Sci.* **2011,** *289*, 1885-1894.

49. Bartholome, C.; Beyou, E.; Bourgeat-Lami, E.; Chaumont, P.; Zydowicz, N. *Macromolecules* **2003,** *36*, 7946-7952.

50. Li, C. Z.; Benicewicz, B. C. *Macromolecules* **2005,** *38*, 5929-5936.

51. Pyun, J.; Jia, S. J.; Kowalewski, T.; Patterson, G. D.; Matyjaszewski, K. *Macromolecules* **2003,** *36*, 5094-5104.

52. Rutot-Houze, D.; Fris, W.; Degee, P.; Dubois, P. *J. Macromol. Sci. Pure* **2004,** *A41*, 697-711.

53. Raula, J.; Shan, J.; Nuopponen, M.; Niskanen, A.; Jiang, H.; Kauppinen, E. I.; Tenhu, H. *Langmuir* **2003,** *19*, 3499-3504.

54. Stenzel, M. H.; Zhang, L.; Huck, W. T. S. *Macromol. Rapid Commun.* **2006,** *27*, 1121-1126.

55. Zhao, Y.; Perrier, S. *Macromolecules* **2006,** *39*, 8603-8608.

56. Li, C.; Han, J.; Ryu, C. Y.; Benicewicz, B. C. *Macromolecules* **2006,** *39*, 3175-3183.

57. Ohno, K.; Ma, Y.; Huang, Y.; Mori, C.; Yahata, Y.; Tsujii, Y.; Maschmeyer, T.; Moraes, J.; Perrier, S. *Macromolecules* **2011,** *44*, 8944-8953.

58. Rungta, A.; Natarajan, B.; Neely, T.; Dukes, D.; Schadler, L. S.; Benicewicz, B. C. *Macromolecules* **2012,** *45*, 9303-9311.

59. Zhao, B.; He, T. *Macromolecules* **2003,** *36*, 8599-8602.

60. Vaia, R. A.; Wagner, H. D. *Mater. Today* **2004,** *7*, 32-37.

61. Zhang, Z. L.; Glotzer, S. C. *Nano Letters* **2004,** *4*, 1407-1413.

62. Vanakaras, A. G. *Langmuir* **2006,** *22*, 88-93.

63. Degennes, P. G. *Angew. Chem. Int. Edit.* **1992,** *31*, 842-845.

64. Perro, A.; Reculusa, S.; Ravaine, S.; Bourgeat-Lami, E. B.; Duguet, E. *J. Mater. Chem.* **2005,** *15*, 3745-3760.

65. Wang, F.; Phonthammachai, N.; Mya, K. Y.; Tjiu, W. W.; He, C. *Chem. Commun.* **2011,** *47*, 767-769.

66. Paunov, V. N.; Cayre, O. J. *Adv. Mater.* **2004,** *16*, 788-791.

67. Tang, J. L.; Schoenwald, K.; Potter, D.; White, D.; Sulchek, T. *Langmuir* **2012,** *28*, 10033-10039.

68. Hong, L.; Jiang, S.; Granick, S. *Langmuir* **2006,** *22*, 9495-9499.

69. Jiang, S.; Granick, S. *Langmuir* **2008,** *24*, 2438-2445.

70. Jiang, S.; Granick, S. *Langmuir* **2009,** *25*, 8915-8918.

71. Li, Y.; Benicewicz, B. C. *Macromolecules* **2008,** *41*, 7986-7992.

CHAPTER 2

SYNTHESIS OF FULLERENE POLYMER VIA COMBINATION OF RAFT POLYMERIZATION AND CLICK REACTION

2.1 Introduction

As discussed in Chapter 1, the covalent incorporation of fullerene into polymer architectures can significantly improve the compatibility of fullerene and expand it applications. According to the different positions of C_{60} moieties in the polymer structures, fullerene-based polymers can be categorized into the following types: main-chain fullerene polymers, side-chain fullerene polymers (SFP's), fullerene-capped polymers, star-shaped fullerene polymers and dendrimers.[1,2] Synthesis of polymers with C_{60} units in the main chain involves fullerene-based monomers having two reacting sites, which are relatively difficult to produce and purify, and a slight amount of multi-functionalized fullerene impurities can result in severe cross-linking during the polymerization.[3] Fullerene star-shaped polymers have also been prepared.[4] These polymers usually exhibit excellent solubility and compatibility due to the high content of polymer portion, but cannot have high C_{60} loadings because fullerene moieties only exist in the cores of the "stars". C_{60}-containing dendrimers are another type of interesting architecture, but typically prepared as low molecular weight materials.[5-7]

In contrast, SFP's can have relatively well-defined strucutres, high C_{60} loadings and molecular weights simultaneously, although their syntheses can be quite challenging. Wudl et al. first tried to prepare SFP's by step polymerization using C_{60}-containing

monomers.[8] Because of the steric hindrance of the C_{60} moieties, the degree of polymerization was very low. Alternatively, anchoring C_{60} moieties on preformed polymers ("grafting to" strategy) can avoid the steric hindrance during polymerization, but an efficient reaction is needed to achieve a controlled attachment. In a recent publication from the same group, a "rod-coil" diblock copolymer containing poly(3-hexylthiophene) (P3HT) and fullerene was synthesized through a combination of RAFT polymerization strategy and a subsequent polymer-analogous cycloaddition.[9] A similar block copolymer was reported by Jo *et al.*, but the "coil" block was formed by ATRP and the attachment was achieved via a carboxylic acid-alcohol coupling reaction.[10] Hadziioannou *et al.* copolymerized 4-chloromethylstyrene and styrene by NMP and then attached C_{60} through via an atom-transfer radical addition (ATRA) or a cycloaddition to C_{60}.[11,12] Through a direct fullerenation, Celli *et al.* prepared polysulfone with fullerene randomly connected to the side chains.[13] Yang *et al.* postfunctionalized the side chain of a P3HT derivative with C_{60} by adding sarcosine to create a phenyl linking bridge.[14] Also, Rusen *et al.* made C_{60}-grafted polyethylene at 100 °C based on the reaction of C_{60} with amino groups which were introduced earlier along the polymer main chains.[15] However, in most of these cases the architectures and C_{60} loadings were not well controlled, because it was difficult to prevent multiple reactions on the same C_{60} molecule when pristine fullerene was involved in the attachment process. Generally, the methods of attachment were not effective enough to make polymers possessing carefully adjustable fullerene contents.

Herein, we describe our work on the fabrication of SFP's by combining RAFT polymerization and the copper-mediated click reaction. Since both of these techniques

feature good control, mild reaction conditions and functional group tolerance, the combination is expected to be a convenient approach to prepare well-defined linear SFP's. Methacrylate-based monomers were chosen to prepare the backbones because of its relatively good compatibility with fullerene,[10,16,17] and also its mechanical properties, optical transparency and stability to photo ageing.[18] Moreover, the synthesis of a soluble and mono-functionalized fullerene derivative for the post-functionalization is depicted which prevented cross-linking of the polymer chains.

Additionally, the assembly behaviors of the prepared polymers were investigated in solution by gel permeation chromatography (GPC) and dynamic light scattering (DLS), and on solid substrates using scanning electron microscopy (SEM). The SFP's displayed a variety of self-aggregation behaviors. The SEM images of the SFP's on silica wafers showed the formation of various nanoparticle assemblies and crystalline-like clusters depending on fullerene contents and chain lengths of the SFP samples. The study of the self-assembly of fullerene derivatives into supramolecular architectures is always a significant challenge.[19-21] Although many such investigations were performed on fullerene dendrimers [7,22] and fullerene-capped polymers [23-25], to the best of our knowledge, detailed morphology studies on SFP's had not been reported by the time when we started this research.

On the other hand, graphene has become one of the most popular carbon materials in recent years because its unique two dimensional hexagonal carbon network leads to extraordinary mechanical properties, high thermal conductivity, and interesting optical properties.[26] However, single graphene sheets have strong tendency to agglomerate ascribed to the attractive interactions between each other. Therefore, graphene oxide has

been widely used instead, which has better solubility, but the defects in the aromatic structure may impair the outstanding properties in contrast with graphene. Liu and coworkers utilized pyrene-terminal polymers to functionalize graphene through π-π stacking interactions and produced thermosensitive graphene nanocomposites.[27] This kind of non-covalent attachment between pyrene and graphene resulted in a greatly enhanced solubility of graphene without damaging its aromatic structure.

In this context, we designed a fullerene-capped polymer with two polymeric tails and named it as "tadpole-like" fullerene polymer (TFP). The tail parts were synthesized by RAFT polymerization involving azido-capped CTA's, and then anchored on the fullerene "head" though a copper-mediated click reaction. The amphiphilic TFP bearing two solvophilic tails and a "graphene-philic" head were further studied as surfactant to improve the solubility of graphene in diverse solvents. Using this method, polymer tails are supposed to stabilize the graphene sheets in a variety of solvents or matrices depending on the nature of polymer. Meanwhile, the combination of fullerene and graphene is expected to create a new class of photovoltaic active materials with a strong electron-accepting capability of fullerene and good charge transport properties associated with graphene.[28,29] UV-vis and FT-IR spectroscopies were applied to demonstrate the π-π stacking interactions between the TFP and graphene.

2.2 Experimental Section

2.2.1 Materials

Fullerene (C_{60}) was purchased from SES Research and used as received. Tetrahydrofuran (THF) (99.9%, Acros) was dried over CaH_2 overnight and distilled before use. 4-Cyanopentanoic acid dithiobenzoate (CPDB) was purchased from Strem Chemical Inc. and used as received. Methyl methacrylate (99%, Acros) was passed

through a basic alumina column to remove inhibitors before use. 2,2'-Azobis(4-methoxy-2,4-dimethyl valeronitrile) (V-70) was purchased from Wako Chemicals and used as received. Graphene was purchased from Angstron Materials and used as received. Unless otherwise specified, all chemicals were purchased from Fisher Scientific and used as received.

2.2.2 Instrumentation

Nuclear magnetic resonance (NMR) spectra were recorded on Varian Mercury 300 and 400 spectrometers using $CDCl_3$ as the solvent. Matrix-assisted laser desorption-ionization time-of-flight mass spectrometry (MALDI-TOF-MS) was performed with a Bruker Ultraflex MALDI tandem time-of-flight mass spectrometer. Fourier transform infrared spectroscopy (FT-IR) spectra were recorded using a PerkinElmer Spectrum 100 FT-IR Spectrometer. Molecular weights and polydispersity indices (PDI = M_w/M_n) were determined using a Waters gelpermeation chromatograph equipped with a 515 HPLC pump, a 2410 refractive index detector, and three Styragel columns (HR1, HR3, HR4 in the effective molecular weight range of 100-5000, 500-30 000, and 5000-500 000, respectively) with THF as the eluent at 30 °C and a flow rate of 1.0 mL/min. The GPC system was calibrated with poly(methyl methacrylate) from Polymer Laboratories. The thermal stability of the polymers was determined by thermogravimetric analysis (TGA) performed on vacuum-dried polymer samples from 30 °C to 600 °C using a TA Instruments Q5000 with a nitrogen flow rate of 20 mL/min and heating rate of 10 °C/min. UV-vis absorption spectra were taken on a Perkin-Elmer Lamda 4C UV/vis spectrophotometer. The glass transition temperatures (T_g) of the polymer samples were measured by differential scanning calorimetry (DSC) using a TA Instruments Q2000 with a nitrogen flow rate of 50 mL/min. The analysis was done by heating samples from 30 ºC

to 150 °C at a heating rate of 10 ºC/min, which were then cooled from 150 °C to 30 ºC at a heating rate of 20 ºC/min, followed by a second-round heating step at a heating rate of 20 ºC/min. The DSC curves were obtained from the second heat cycle. The DLS experiment was carried out using a Zetasizer Nano S instrument. The laser wavelength was 633 nm and the detector position was at 173°. SEM images were captured using a Zeiss Ultraplus Thermal Field Emission Scanning Electron Microscope, and the samples were prepared on silicon wafers by spin-coating.

2.2.3 Synthesis of 3,5-bis(octyloxy)phenyl methanol (2) and 3-(3,5-bis (octyloxy)benzyl oxy)-3-oxopropanoic acid (3)

The syntheses of **compounds 2** and **3** were carried out according to the methods in the literature.[30]

2.2.4 Synthesis of 3,5-bis(octyloxy)benzyl propy-2-nyl malonate (4)

Compound 3 (6.31 g, 14 mmol), propargyl alcohol (788 mg, 14 mmol) and 4-(dimethylamino) pyridine (DMAP) (512 mg, 4.7 mmol) were dissolved in methylene chloride (100 mL). Dicyclohexylcarbodiimide (DCC) (2.89 g, 14 mmol) in 30 mL of methylene chloride was added dropwise into the solution with stirring at 0 °C. The mixture was allowed to slowly warm to room temperature and, after stirring overnight, filtered and evaporated. Silica gel column chromatography (3:2 mixture of hexane and methylene chloride) yielded **compound 4** as a colorless oil (5.41 g, 79%). ^{1}H NMR (300 MHz, $CDCl_3$): δ = 0.88 (t, J = 6.6 Hz, 6H, C**H**$_3$), 1.37 (m, 20H, $CH_3(C\mathbf{H}_2)_5CH_2CH_2O$), 1.74 (m, 4H, $CH_3(CH_2)_5C\mathbf{H}_2CH_2O$), 2.49 (t, J = 2.3 Hz, 1H, C≡C**H**), 3.48 (s, 2H, OCC**H**$_2$CO), 3.92 (t, J = 6.5 Hz, 4H, $CH_3(CH_2)_6C\mathbf{H}_2O$), 4.73 (d, J = 1.2 Hz, 2H, C**H**$_2$C≡CH), 5.09 (s, 2H, PhC**H**$_2$O), 6.40 (d, J = 2.4 Hz, 1H, Ar), 6.46 (d, J = 2.1 Hz, 2H, Ar). ^{13}C NMR (400 MHz, $CDCl_3$): δ = 14.06, 22.65, 26.04, 29.22, 29.24, 29.34, 31.81,

41.04, 52.75, 67.20, 67.93, 75.42, 75.50, 101.09, 106.31, 137.19, 160.41, 165.53, 165.75. FT-IR: 1741 cm^{-1} (C=O) and 3291 cm^{-1} (C≡CH). HRMS (EI): calcd. for $C_{29}H_{44}O_6$ $[M]^+$ 488.3124; found 488.3138.

2.2.5 Synthesis of mono-alkynyl functionalized fullerene (1)

1,8-Diazabicyclo[5.4.0]undec-7-ene (DBU) (0.310 mL, 2.08 mmol) was added at room temperature to a solution of **compound 4** (447 mg, 0.915 mmol), C_{60} (600 mg, 0.832 mmol), and iodine (264 mg, 1.04 mmol) in toluene (600 mL), and the mixture was stirred for 7 hours. The mixture was filtered through a short plug of silica gel and washed by methylene chloride (100 mL). Silica gel column chromatography (1:1 mixture of hexane and toluene) yielded **compound 1** as dark red glassy solids (547 mg, 54%). ^{1}H NMR (300 MHz, $CDCl_3$): δ = 0.89 (m, 6H, C**H**$_3$), 1.36 (m, 20H, $CH_3(CH_2)_5CH_2CH_2O$), 1.75 (m, 4H, $CH_3(CH_2)_5CH_2CH_2O$), 2.60 (t, J = 2.6 Hz, 1H, C≡C**H**), 3.91 (t, J = 6.5 Hz, 4H, $CH_3(CH_2)_6CH_2O$), 5.04 (d, J = 2.1 Hz, 2H, C**H**$_2$C≡CH), 5.45 (s, 2H, PhC**H**$_2$O), 6.42 (d, J = 2.7 Hz, 1H, Ar), 6.61 (d, J = 2.1 Hz, 2H, Ar). ^{13}C NMR (400 MHz, $CDCl_3$): δ = 14.12, 22.68, 26.12, 29.27, 29.39, 31.83, 51.26, 54.41, 68.16, 69.16, 71.18, 101.70, 107.25, 136.42, 138.93, 139.38, 140.89, 140.95, 141.84, 141.86, 142.19, 142.20, 142.96, 142.99, 143.01, 143.05, 143.84, 143.87, 144.53, 144.67, 144.71, 144.90, 144.91, 145.02, 145.15, 145.17, 145.24, 145.29, 160.49, 162.86, 163.13. FT-IR: 1749 cm^{-1} (C=O) and 3302 cm^{-1} (C≡CH). MALDI-TOF-MS: calcd. for $C_{89}H_{42}O_6$ $[M + Na]^+$ 1229.28; found 1229.3.

2.2.6 Synthesis of bi-alkynyl functionalized fullerene (5)

The synthesis of **compound 5** was carried out according to the methods reported in the previous literature.[31]

2.2.7 Synthesis of 6-azidohexyl 4-cyano-4-(phenylcarbonothioylthio)pentanoate (azido-functionalized CPDB).

1-Azido-6-hydroxyhexane was synthesized according to the methods published previously.[32] CPDB (878 mg, 3.15 mmol), 1-azido-6-hydroxyhexane (500 mg, 3.49 mmol), and dicyclohexylcarbodiimide (DCC) (720 mg, 3.49 mmol) were dissolved in 30 mL of dichloromethane. (Dimethylamino)pyridine (DMAP) (128 mg, 1.05 mmol) in 5 mL of dichloromethane was added slowly to the solution, which was stirred at room temperature overnight. The solution was filtered to remove the salt. After removal of solvent and silica gel column chromatography (10:1 mixture of hexane and ethyl acetate), azido-functionalized CPDB, was obtained as a dark red oil (798 mg, 63% yield). ^{1}H NMR (300 MHz, $CDCl_3$): δ = 1.35-1.39 (m, 4H, $N_3CH_2(CH_2)_2$), 1.54-1.66 (m, 4H, $N_3(CH_2)_3(CH_2)_2$), 1.91 (s, 3H, CH_3), 2.36-2.69 (m, 4H, $C(CH_2)_2(C{=}O)O$), 3.24 (t, J = 6.8 Hz, 2H, CH_2N_3), 4.09 (t, J = 6.6 Hz, 2H, $CH_2OC{=}O$), 7.37 (t, J = 7.8 Hz, 2H, Ar), 7.54 (t, J = 7.4 Hz, 1H, Ar), 7.88 (dd, $J_{1,2} = J_{3,4}$ = 1.2 Hz, $J_{1,3} = J_{2,4}$ = 8.4 Hz, 2H, Ar). ^{13}C NMR (400 MHz, $CDCl_3$): δ = 24.09, 25.48, 26.32, 28.39, 28.70, 29.79, 33.40, 45.75, 51.28, 64.94, 118.49, 126.66, 128.57, 133.06, 144.48, 171.54, 222.33. FT-IR: 1181 cm^{-1} (PhC=S), 1732 cm^{-1} (C=O), 2094 cm^{-1} (N_3). HRMS (EI): calcd. for $C_{19}H_{24}N_4O_2S_2$ $[M]^+$ 404.1341; found 404.1347.

2.2.8 Synthesis of 6-azidohexyl methacrylate (AHMA)

The synthesis of AHMA was carried out according to the methods published previously.[32]

Caution: special care should be taken to minimize the possible hazards in the preparation and handling of the azide compounds.

2.2.9 Typical RAFT polymerization of AHMA and MMA

Typically, a solution of AHMA (0.22 g), methyl methacrylate (MMA) (1.0 g), 4-cyanopentanoic acid dithiobenzoate (CPDB) (10.5 mg, 37 μmol/g), V-70 (1.05 mg, 3.4 μmol/g), and THF (1.2 mL) were prepared in a dried Schlenk tube. The mixture was degassed by three freeze-pump-thaw cycles, backfilled with nitrogen, and then placed in an oil bath at 40 °C for various intervals. The polymerization solution was quenched in ice water and poured into an aluminum boat. The solvent and monomer were removed by evaporation in a fume hood overnight and then one day under vacuum. Monomer conversion was determined by gravimetric analysis, molecular weight characteristics were analyzed by GPC, and proportion of each residue analyzed via ^{1}H NMR. The feed ratios varied according to the requirements for different random copolymers.

2.2.10 Typical Click reaction between poly(MMA-*r*-AHMA) and alkynyl functionalized fullerene (1)

A sample of poly(MMA-*r*-AHMA) with a known proportion of each residue was reacted with **compound 1** for example: Poly(MMA-*r*-AHMA) (M_n = 15,718, PDI = 1.15, [AHMA]:[MMA] = 1:11) (200 mg, 1 equiv. of N_3), **compound 1** (202 mg, 1.1 equiv. of alkyne), and N,N,N',N',N''-pentamethyldiethylene triamine (PMDETA) (16 μL, 0.5 equiv.) were dissolved in toluene (50 mL). The solution was degassed by bubbling nitrogen for 30 min and then CuBr (11 mg, 0.5 equiv.) was added. The mixture was stirred under nitrogen protection at room temperature for one day. The mixture was then diluted with methylene chloride and passed through neutral alumina to remove the copper catalyst and unreacted fullerene **compound 1**. After concentration by rotary evaporation, the product was precipitated in hexane, filtered, and dried under vacuum. The feed ratios can be different when polymers with different components involved.

2.2.11 Synthesis of azido-capped poly(methyl methacrylate) (N_3-PMMA).

A solution of MMA (1.0 g, 10 mmol), azido-functionalized CPDB (13.4 mg, 33 μmol), V-70 (3.3 μmol), and THF (1.0 mL) was prepared in a dried Schlenk tube. The mixture was degassed by three freeze-pump-thaw cycles, back filled with nitrogen, and then placed in an oil bath at 40 °C for 15 hours. The polymerization solution was quenched in ice water and the resultant azido-capped polymer was precipitated in hexane. Molecular weight characteristics were analyzed by GPC.

2.2.12 Typical Click reaction for synthesis of fullerene-capped poly(methyl methacrylate) (TFP)

A solution of **compound 5** (7.74 mg, 8 mmol), N_3-PMMA (M_n = 9.9k, PDI = 1.14, 160 mg, 16 mmol) and PMDETA (1.7 μL, 8 mmol) in toluene was degassed by nitrogen flashing for 30 min, and then CuBr (1.2 mg, mmol) was added. The mixture was stirred under nitrogen protection at room temperature for one day. The mixture was then diluted with methylene chloride and passed through neutral alumina to remove the copper catalyst. After concentration by rotary evaporation, the product was precipitated in hexane, filtered, and dried under vacuum. Molecular weight characteristics were analyzed by GPC. The amounts of N_3-PMMA varied depending on diverse molecular weights.

2.3 Results and Discussion

2.3.1 Modification of pristine fullerene

A highly soluble fullerene derivative **compound 1** with a "clickable" functional group was designed to create an exclusive reactive site on C_{60} for the side chain functionalization of prepolymers. The synthesis is depicted in Scheme 2.1. **Compound 3** was produced by following Felder's procedure with 3,5-dihydroxybenzyl alcohol and 1-bromooctane as the starting materials.[30] Then the coupling reaction between the carboxylic acid and propargyl alcohol in the presence of DCC and DMAP generated

compound 4, which was attached onto a C_{60} molecule via a facile Bingel cyclopropanation.[33]

Otherwise, **compound 5** was also afforded through Bingel reaction between pristine fullerene and di(pent-4-ynyl) malonate. At first, it was attempted to anchor **compound 5** on the side chains of polymers, but then the fullerene polymers were obtained with severe cross-linkings shown in the GPC analysis. In spite of this, the bi-functionalized fullerene derivative could benefit the other application for geraphene modification by forming TFP, which will be discussed later.

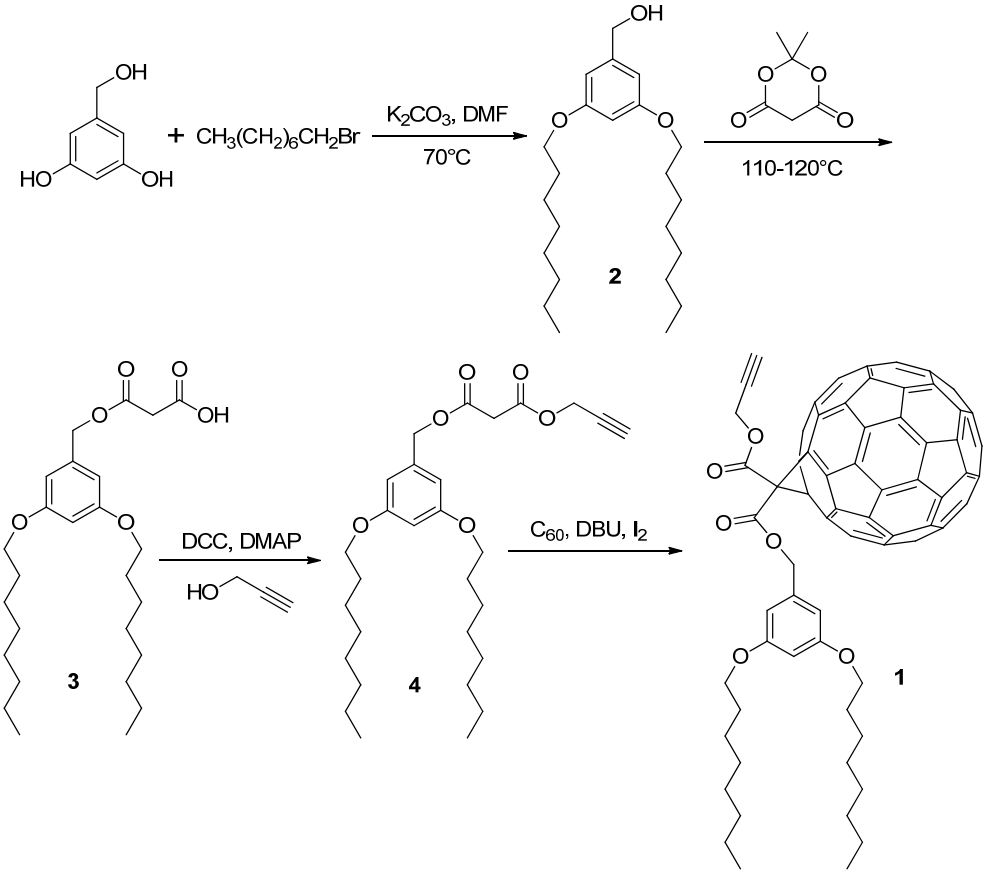

Scheme 2.1 Synthetic route for the mono-alkynyl functionalized fullerene (**compound 1**).

In the final step of Scheme 2.1, an excess amount of **compound 4** (1.1 equiv.) was applied to afford **compound 1** as the major product, which was purified through a silica

gel column and identified by NMR analyses. Since multi-functionalized fullerene can lead to reticulate structures as mentioned earlier, byproducts carrying more than one alkynyl group were highly undesirable. To ensure that the product did not contain this type of impurity, MALDI-TOF-MS was performed for further characterization (Figure 2.1). Two expected charged peaks were displayed at m/z = 1206.3 and 1229.3 (calculated m/z = 1206.29 and 1229.28), corresponding to the molecular ion peak of **compound 1** and $[M+Na]^+$, respectively. If a difunctionalized fullerene was present, peaks at approximately m/z = 1692.6 and 1715.6 would be expected. Therefore, the absence of these peaks demonstrated that only mono-alkynyl functionalized fullerene was obtained.

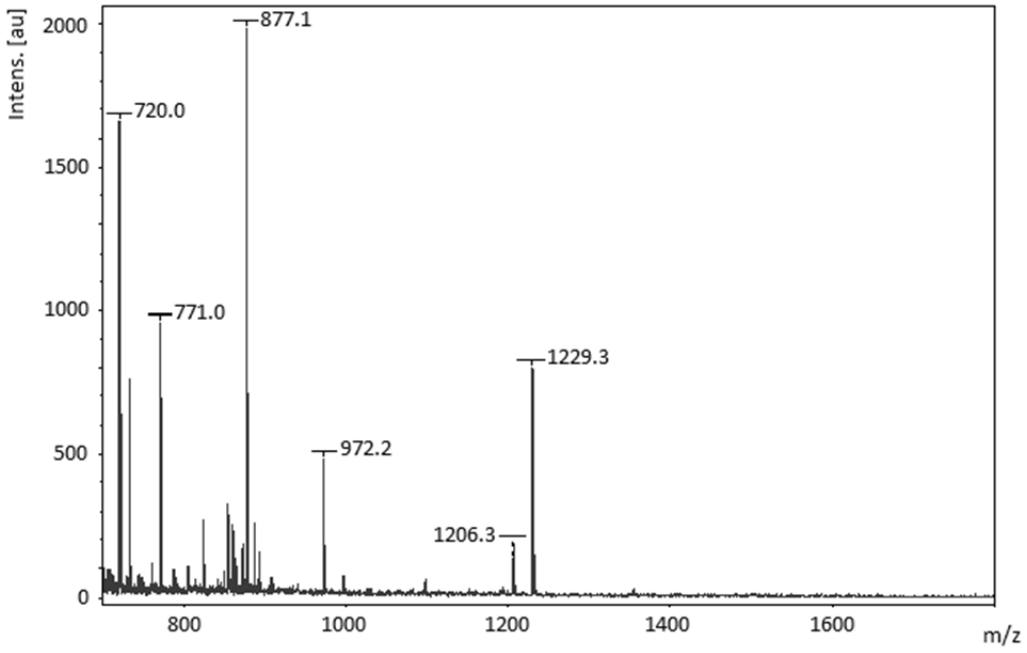

Figure 2.1 MALDI-TOF-MS spectrum of **compound 1**.

In addition, most reactions involving fullerene require a large amount of solvent and produce relatively low yields because of its poor solubility (around 2.8 mg/mL in toluene maximum).[34] In our current design, the fullerene modification not only grafted a mono-alkynyl group on the C_{60} molecules for the further click reaction, but also introduced two

long alkyl chains which significantly improved the solubility in organic solvents, such as toluene, methylene chloride and THF. Both solutions of **compound 1** and **compound 5** in toluene (25 mg/mL) were kept in a refrigerator for one year without precipitation.

2.3.2 RAFT Polymerization involving azido monomer

Azido-containing monomers can be polymerized by living radical polymerization with controlled molecular weight and narrow polydispersity. A relatively low temperature (40 °C) was applied to minimize possible side reactions between the azide and C=C bond of the monomer (AHMA).[32] The six-carbon side chains of the resultant polymer provide relatively long and flexible tethers for the fullerene moieties to ameliorate the rigidity imposed by the backbone.[12] In addition to homopolymer, random copolymers poly(AHMA-*r*-MMA) were prepared by adding MMA in the polymerization to vary the fullerene content along the SFP chains. Thus, both fullerene content and chain length could be adjusted independently to study the effects of these variables on the polymer properties.

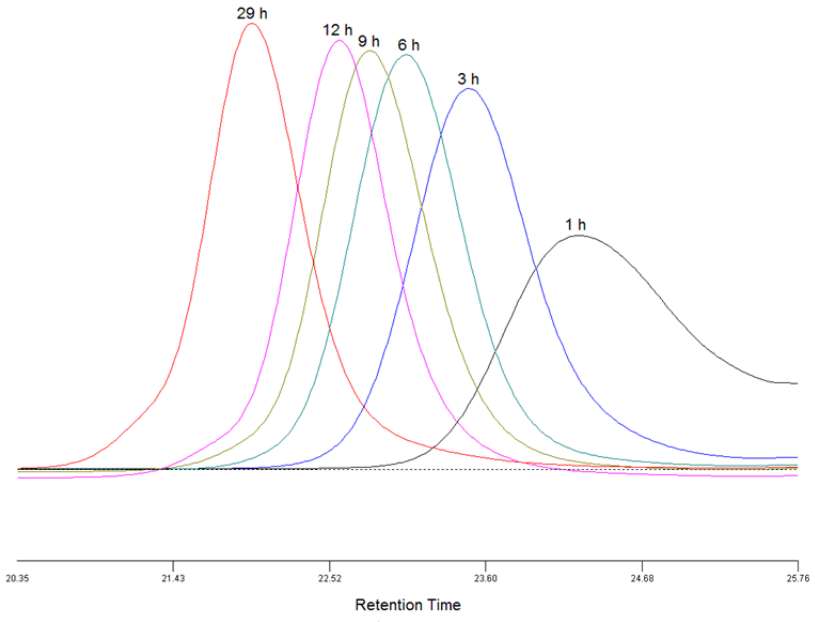

Figure 2.2 GPC traces of prepolymers for kinetics studies.

To demonstrate the controllability of the RAFT copolymerization of AHMA and MMA, a kinetics study (Figure 2.2) was performed with a fixed feed ratio of AHMA to MMA (1:20). Figure 2.3a shows a pseudo-first-order kinetics plot indicating a constant free radical concentration in the polymerization process. The number average molecular weights (M_n) increased linearly with monomer conversion and were in agreement with predictions (Figure 2.3b). Moreover, the PDIs were kept below 1.2 with conversions up to 82%. Generally, the RAFT copolymerization of AHMA and MMA were well-controlled, and the kinetics were similar to the polymerization of other azido-functionalized methacrylate monomers which we previously studied.[35]

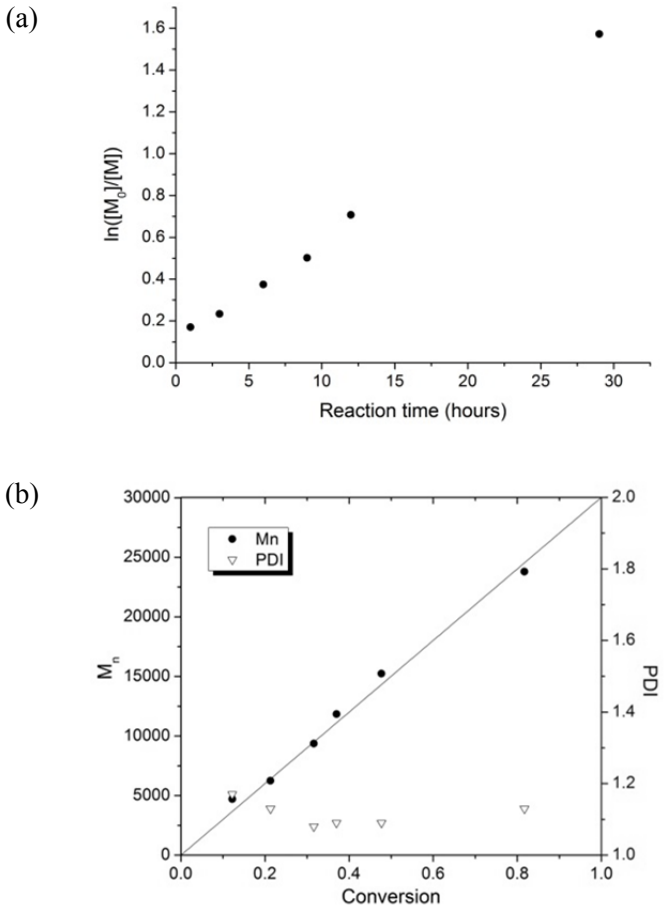

Figure 2.3 (a) Kinetics plot and (b) dependence of the molecular weight and polydispersity on the conversion for the RAFT polymerization of AHMA and MMA

(1:20) ([monomer]: [CPDB]: [V-70] = 300:1:0.1, 40 °C). The solid line represents the theoretical number molecular weights.

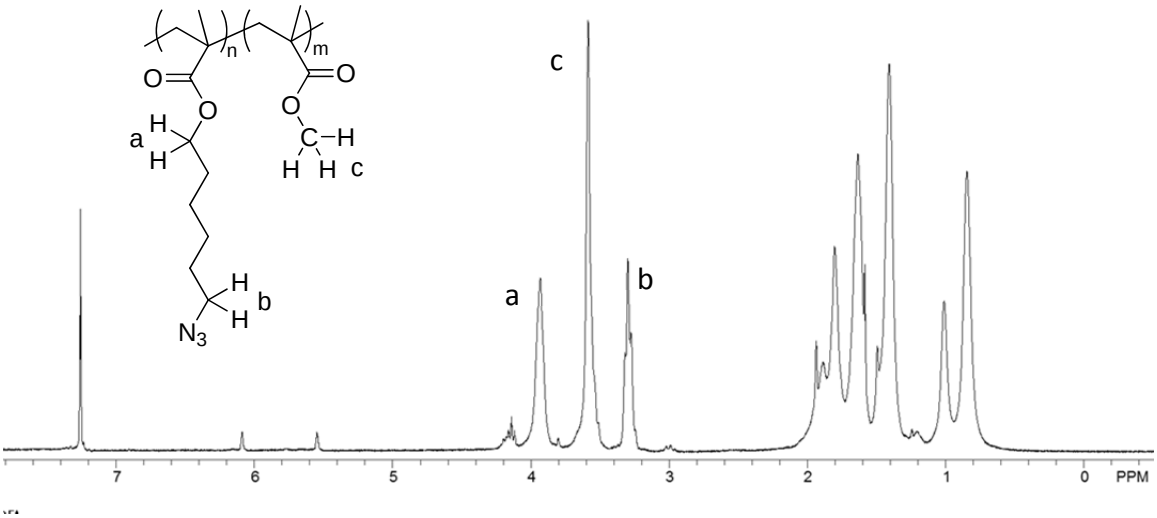

Figure 2.4 ^{1}H NMR spectrum of **prepolymer 2**.

The fullerene loading of the SFP's was adjusted by simply altering the feed ratios of AHMA to MMA in the syntheses of the prepolymers. Consequently, a series of prepolymers with variable molecular weights and compositions were synthesized for the susequent click reactions. Table 2.1 shows that the compositions of the prepolymers were consistent with the feed ratios of the corresponding polymerizations, indicating that AHMA and MMA have similar relative reactivity ratios in this composition range and can be randomly copolymerized. The compositions of the prepolymers were determined by integrated areas of the corresponding peak of each repeat unit in the ^{1}H NMR spectra. Using **prepolymer 2** as an example (Figure 2.4): the methylene protons (next to the oxygen) of AHMA residue at 3.93 ppm and the methyl protons of MMA residue at 3.59 ppm were chosen to calculate the ratio, which can be expressed as: $r = \frac{I_{3.93}/2}{I_{3.59}/3}$.

Table 2.1 RAFT polymerization of AHMA and MMA in THF [a]

Prepolymer	M_n / g mol^{-1}	M_w/M_n	Feed ratio ([AHMA]:[MMA])	Composition [b]
1	15,200	1.23	1:0	1:0
2	32,000	1.23	1:1	1:1
3	18,700	1.21	1:5	1:5
4	15,700	1.15	1:10	1:11
5	11,200	1.08	1:20	1:18
6	33,000	1.12	1:20	1:22
7	53,100	1.13	1:20	1:18
8	20,900	1.13	1:40	1:41

a. In all the polymerizations, [monomer]: [RAFT]: [V-70] = 300:1:0.1, [monomer] = 50 vol%, and all the polymerizations were conducted at 40 °C; b. This represents the experimentally measured average ratio of AHMA to MMA moieties in each polymer chain, determined by ^{1}H NMR.

2.3.3 Click reaction for the SFP synthesis

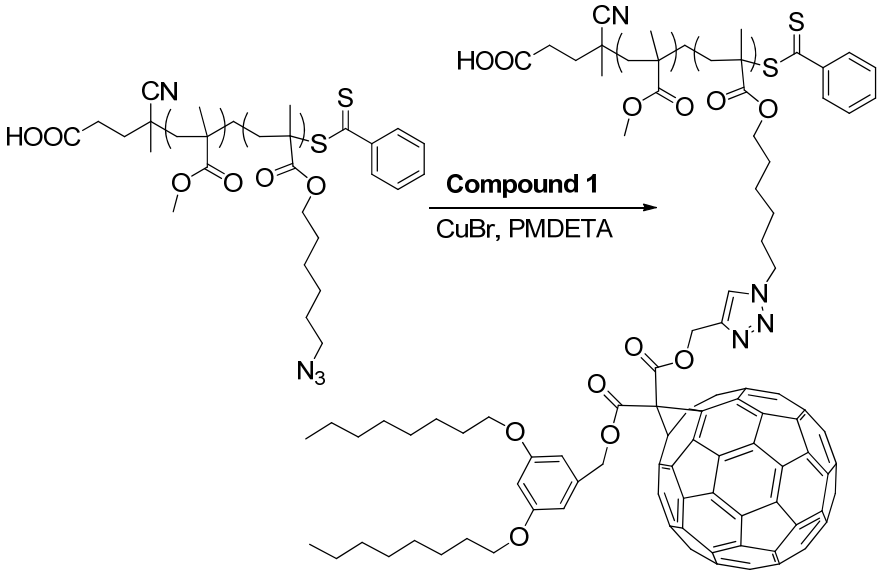

Scheme 2.2 Click reaction for side chain functionalization of prepolymers.

The copper-mediated click reactions between the prepolymers and **compound 1** were performed at room temperature with equivalent amounts of azide and alkyne (Scheme 2.2). FT-IR was applied to monitor the reactions, as a strong and specific absorption at approximately 2100 cm^{-1} ascribed to the azido group disappeared completely after the 1,3-cycloaddition (Figure 2.5), indicating a high conversion of the

click reaction. Also, ^{1}H NMR spectra provided a further confirmation for the reaction involving PAHMA (**prepolymer 1**). Since the azide was converted to triazole, the methylene protons next to the original azido group shifted downfield from 3.30 ppm to 4.37 ppm, and the typical proton on the triazole ring was detected at approximately 7.8 ppm (Figure 2.6). A noteworthy issue is that the ^{1}H NMR signals were too weak to provide quantitative integrations after the click reaction, presumably because of the shielding effect of the fullerene moieties and the limited solubility of the polymers.

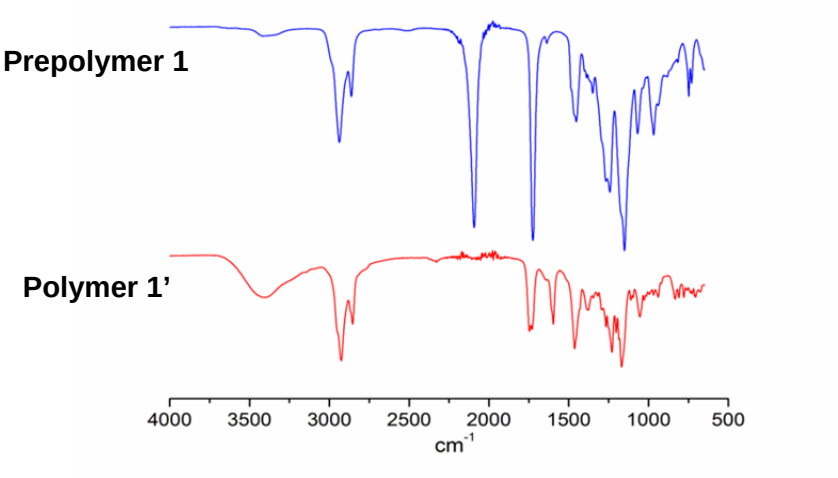

Figure 2.5 IR spectra of **prepolymer 1** and the resultant **polymer 1'**.

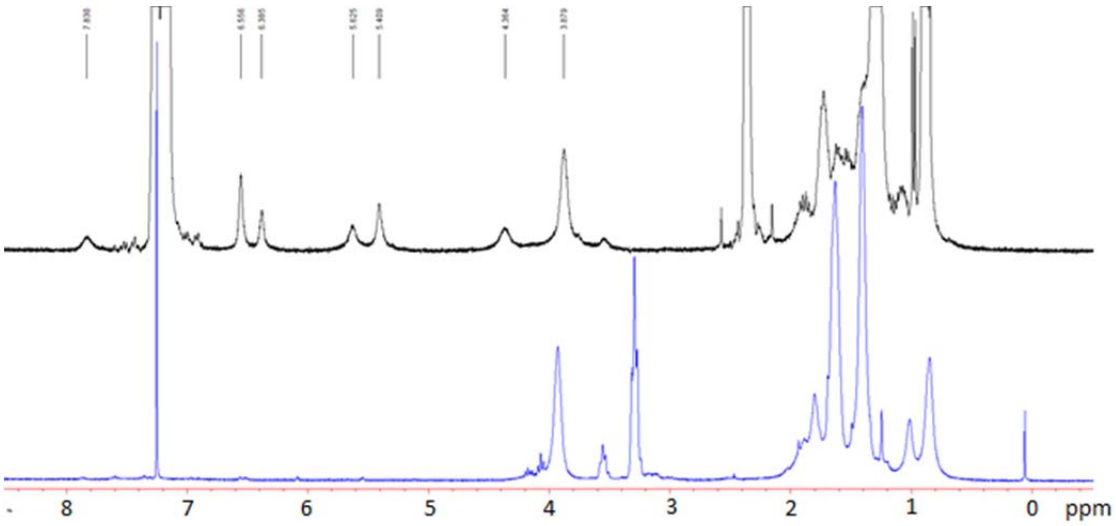

Figure 2.6 The comparison of ^{1}H NMR spectra between **prepolymer 1** (lower) and **polymer 1'** after the click reaction (upper).

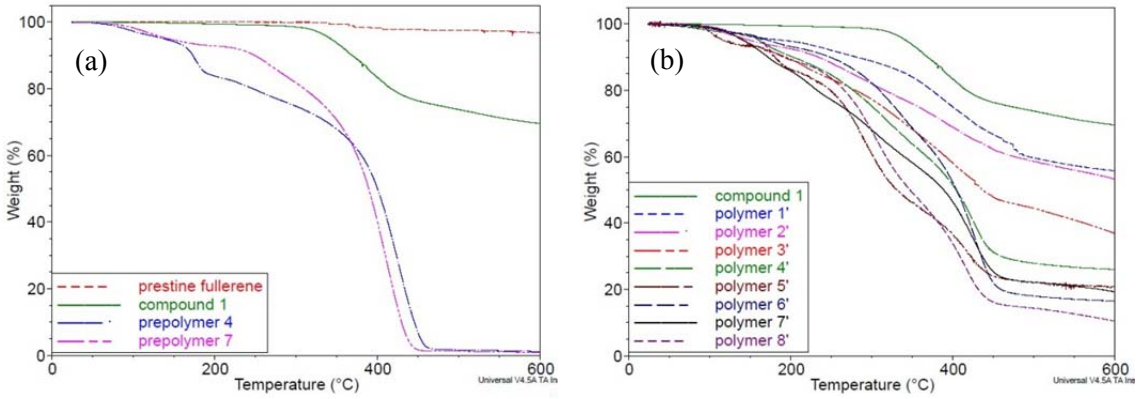

Figure 2.7 (a) TGA scans of pristine C_{60}, **compound 1**, **prepolymer 4** and **7** from 30 °C to 600 °C in nitrogen; (b) TGA scans of **compound 1** and side-chain fullerene polymers with different loadings from 30 °C to 600 °C in nitrogen.

2.3.4 Calculation of fullerene loadings of SFP samples by TGA and UV-vis spectrometry

TGA scans in nitrogen of pristine fullerene, **compound 1**, the prepolymers and the SFP's with diverse fullerene loadings were studied. Pristine fullerene exhibits outstanding thermal stability – 96.7 wt% residue remained when heated to 600 °C (Figure 2.7a). In comparison, **compound 1** had 69.6 wt% char yield at this temperature, which was higher than the theoretical estimation if assuming that the "non-fullerene" moiety had been completely decomposed and removed. Hence, in practice the excess char yield can be ascribed to the residue of the "non-fullerene" moiety of **compound 1**.

TGA in nitrogen showed that the prepolymers were almost completely decomposed after 450 °C. Similar inflection points in the range from 435 °C to 485 °C were also observed on the TGA curves of the SFP samples (Figure 2.7b). The weight changes became smoother and almost parallel with each other after this range, suggesting that they (including **compound 1**) decomposed at similar rates. Thus, it is reasonable to propose that the inflection points indicated the disappearance of the polymer backbones of the SFP's, and the remains after these temperatures corresponded to the residues of

compound 1. On the basis of this hypothesis, fullerene loadings of the SFP's and conversions of the click reactions were calculated using the TGA curve of **compound 1** as reference.[16a]

The weight losses of the SFP's between 150 °C and 550 °C were analyzed for the calculation, because the influence of solvents could be excluded by starting at 150 °C, and 550 °C was right in the "parallel" interval. For instance, **polymer 1'** had 59.5 wt% char yield at 550 °C comparing with that at 150 °C, and **compound 1** had 71.5 wt%. Therefore, the content of **compound 1** moiety in **polymer 1'** was calculated as 59.5 wt% / 71.5 wt% = 83.2 wt%. Because the theoretical content with 100% conversion of the click reaction is 85.1 wt%, the actual conversion could be obtained as 81.0 wt% / 85.1 wt% = 97.8%. Following this method, Table 2.2 summarizes the conversions of all the SFP samples and the average numbers of C_{60} per polymer chain.

Table 2.2 Click conversion efficiency and fullerene loadings calculated by TGA and UV-vis analyses.

Sample*	theoretical loading	# of C_{60} per chain (theoretical)	actual loading (TGA / UV-vis)	Conversion (TGA / UV-vis)	# of C_{60} per chain (TGA / UV-vis)
polymer 1'	85.1%	71	83.2% / 62.5%	97.8% / 73.4%	69 / 52
polymer 2'	79.5%	103	82.2% / 60.0%	103.4% / 75.5%	107 / 78
polymer 3'	62.9%	26	62.7% / 55.6%	99.7% / 88.4%	26 / 23
polymer 4'	47.9%	12	38.7% / 38.2%	80.8% / 79.7%	10 / 10
polymer 5'	37.5%	6	31.9% / 32.3%	85.1% / 86.1%	5 / 5
polymer 6'	33.4%	14	25.3% / 23.7%	75.7% / 71.0%	11 / 10
polymer 7'	37.5%	26	31.3% / 18.7%	83.5% / 49.9%	22 / 13
polymer 8'	21.9%	5	18.3% / 16.7%	83.6% / 76.3%	4 / 4

* The sample IDs of the SFP's were correlated with corresponding prepolymers.

Alternately, UV-vis spectrometry provided a more convenient method to determine the fullerene contents because of its fast measurement and non-destructive nature. Additionally, **compound 1** has only one substituent, which leads to a unique molar

extinction coefficient, so the measurement should be more accurate than that involving fullerene structures with multiple substituents and/or multiple substitution patterns.[15a,36]

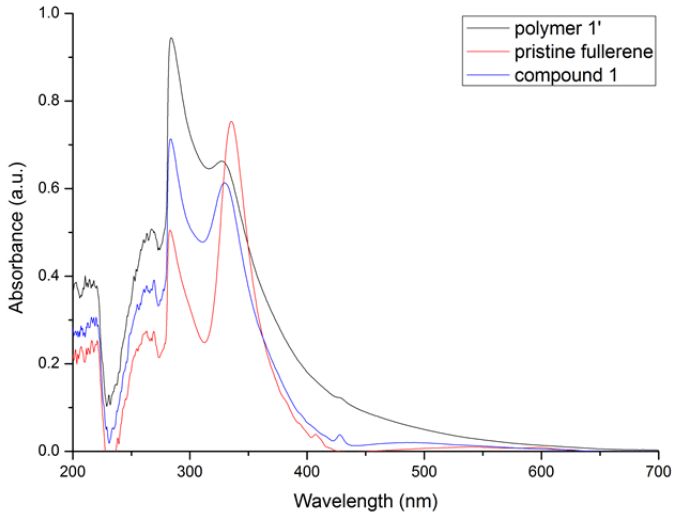

Figure 2.8 UV-vis spectra of pristine fullerene (0.0151 mg/mL), **compound 1** (0.0181 mg/mL) and **polymer 1'** (0.0376 mg/mL) in toluene.

Figure 2.8 shows the UV-vis spectra of pristine fullerene, **compound 1** and **polymer 1'** in toluene. Strong absorption at approximately 284 nm was observed in all the three samples. However, another peak at 330 nm of **compound 1** was blueshifted and weaker in contrast to the absorption at 335 nm of the pristine fullerene, which is probably due to the interaction between the C_{60} moiety and the adjacent aromatic ring in **compound 1**. The UV-vis spectra of **compound 1** and **polymer 1'** are very similar, indicating the similar chemical environment of the fullerene moieties. Therefore, the concentrations of the **compound 1** moiety of the SFP samples in toluene were determined using **compound 1** as an external standard. Subsequently, the contents of **compound 1** moiety in the SFP chains could be calculated with the known concentrations of the SFP samples. A standard dependence of absorbance at 284 nm on the concentration of **compound 1** in

toluene was displayed in Figure 2.9. Fullerene loadings and the conversions of the click reactions estimated by UV-vis spectrometry are also summarized in Table 2.2.

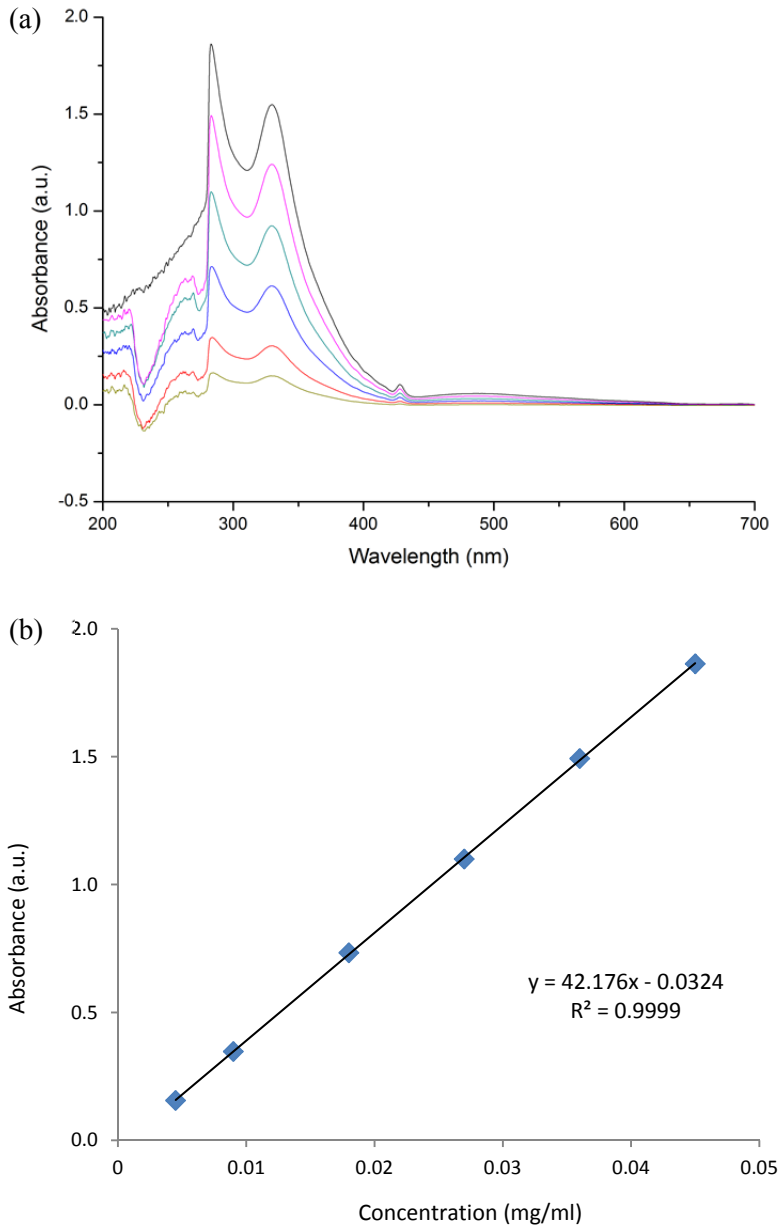

Figure 2.9 (a) UV-vis spectra of **compound 1** with various concentrations in toluene (from 0.0045 mg/ml to 0.045 mg/ml); (b) standard dependence of UV-vis absorption on concentration of **compound 1** at 284 nm in toluene.

The results from TGA and UV-vis were consistent for **polymers 3' – 6'** and **polymer 8'**. However, TGA indicated higher fullerene loadings and conversions with

high azide content prepolymers (**polymer 1'** and **2'**) or when the molecular weight was high (**polymer 7'**). A reasonable explanation is that steric hindrance of the attached fullerene moieties and entanglement of the polymer chains reduced the efficiency of the click reactions resulting in unreacted azido groups in the resultant SFP's, which became severe with an increase of the statistical incorporation of AHMA repeat units and/or the polymer chain length. During the TGA tests at high temperatures, reactions between these azido groups and the fullerene moieties generated cross-linked structures,[12b] which could retard the degradation and result in higher test values.

Except for **polymer 7'**, the SFP's were prepared at high conversions (70% - 90%) as determined from UV-vis. As mentioned above, both steric hindrance and chain entanglement could reduce the efficiency of the fullerene attachment. The relatively low conversion of **polymer 7'** can be rationalized since the effect of chain entanglement is expected to be greater.

In addition, DSC studies (Figure 2.10) showed that the addition of fullerene moieties to the prepolymers increased the T_g of the SFP's except at the lowest loading levels (**polymer 7'** and **8'**). At the highest fullerene loadings (**polymer 1'-3'**), T_g's were not detected up to 150 ˚C. Apparently, the fullerene-fullerene attractions can limit the mobility of the polymer chains and therefore, raise the T_g's. However, for the low-loading samples, this factor may be counteracted by the side chain effect, since the side-chain fullerene moieties also generate free volume and improve the mobility of the polymer chains.

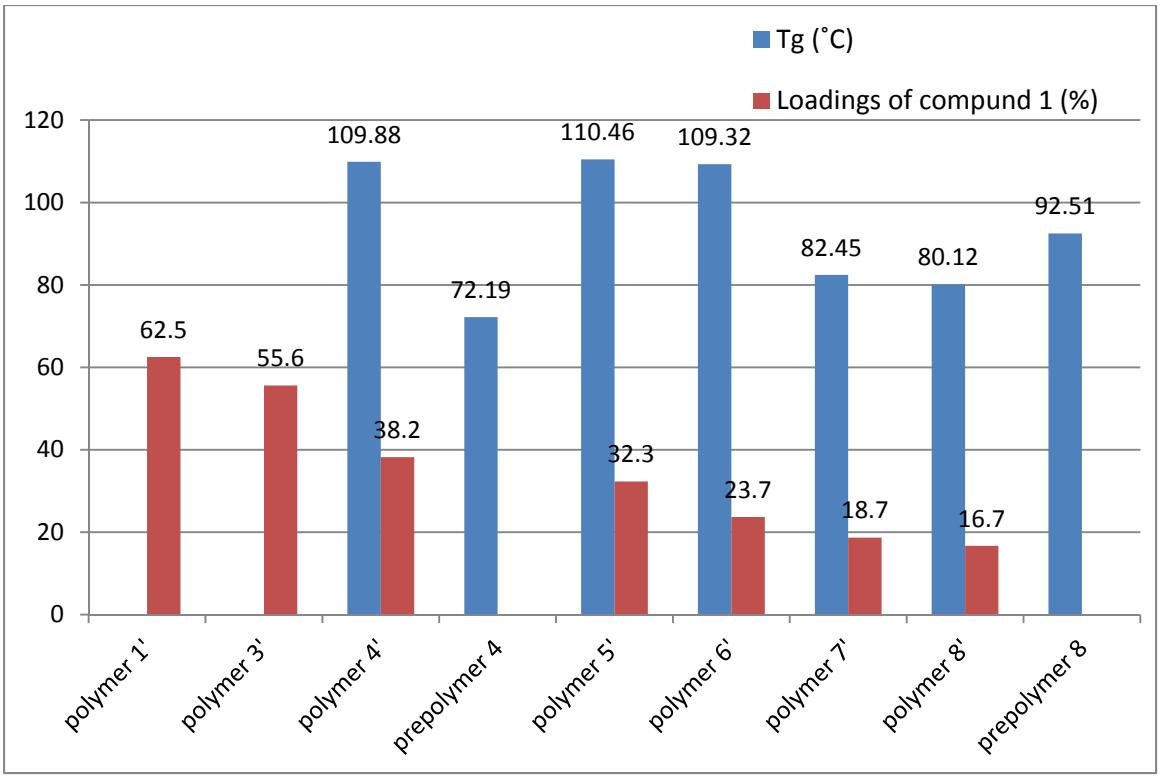

Figure 2.10 Chart of T_g and **compound 1** loadings in different polymer samples.

2.3.5 Morphology studies of the SFP's

C_{60} moieties have very strong π-π stacking interactions with each other (~4.2 kcal/mol in direct contact),[37] which are similar in strength to hydrogen bonding. Thus, most fullerene derivatives are described as solvophobic and often form various aggregates in solution. Accordingly, it was also expected that our SFP's would not exist in solution as individual chains but assemble into nano-complexes, with the solvent-compatible polymer backbones at the exterior surface to reduce direct fullerene-solvent interactions.

GPC analysis was initially used to study this self-aggregation behavior.[16b,38] A mono-modal peak at 22 min, ascribed to individual polymer chains, was detected in the GPC traces of **polymers 3', 4'** and **8'** (Figure 2.11), demonstrating that cross-linking did not occur in the fullerene grafting process. The PDI's of the peaks remained narrow. The

chromatogram of **polymer 8'** exhibits the individual-chain peak exclusively, suggesting little tendency of self-aggregation in solution, which is reasonable considering its low fullerene content. In contrast, in the GPC traces of **polymer 1'**, **3'**and **4',** another group of wide peaks were displayed at very early retention times, which provided strong evidence for the formation of aggregates, although the GPC does not allow measuring molecular weights accurately at this interval. With an increase in the fullerene content, the signals of aggregations became stronger and the peaks of individual chains became weaker. Finally, only aggregation signal was observed for **polymer 1'** while the individual-chain peak disappeared.

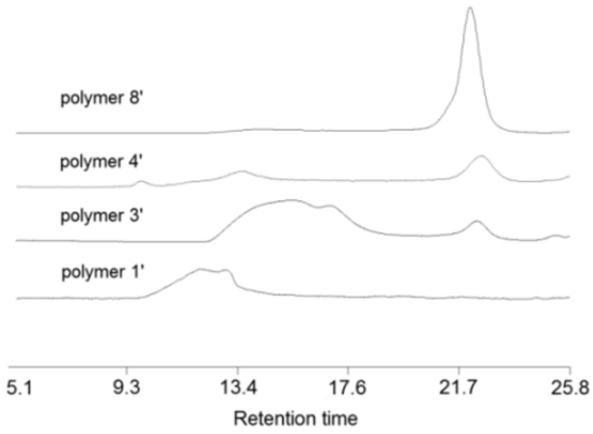

Figure 2.11 GPC traces of side-chain fullerene polymer **1', 3', 4'** and **8'** recorded by refractive index detector.

Moreover, the prepolymers of **polymer 1'** and **4'** had similar molecular weights, but the DLS analyses of the two corresponding fullerene-attached samples showed different size distributions (Figure 2.12). **Polymer 1'** displayed a bimodal size distribution with a Z-average size of 220 nm, and both peaks were larger than the diameter of the individual chains, which further verified the aggregation behavior of the SFP's in solution.

However, the DLS for **polymer 4'** showed a major peak with a Z-average size of 16 nm, which corresponded to the size of the individual chains.

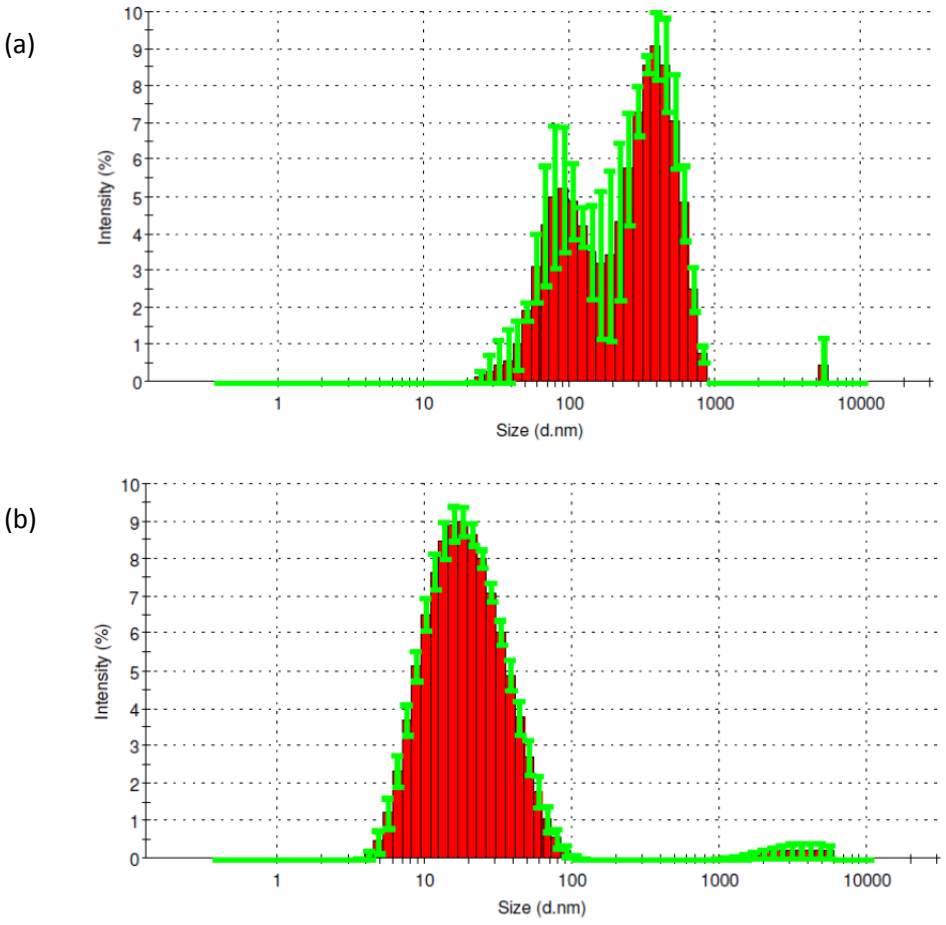

Figure 2.12 Statistical size distributions of (a) **polymer 1'** and (b) **polymer 4'** in toluene tested by DLS. Curves represent the average of three separate measurements.

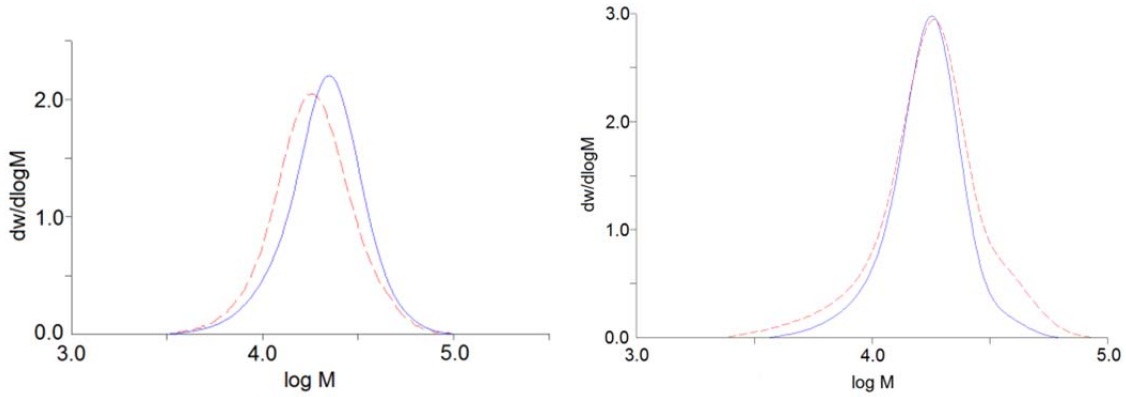

prepolymer 3 and **polymer 3'**

prepolymer 4 and **polymer 4'**

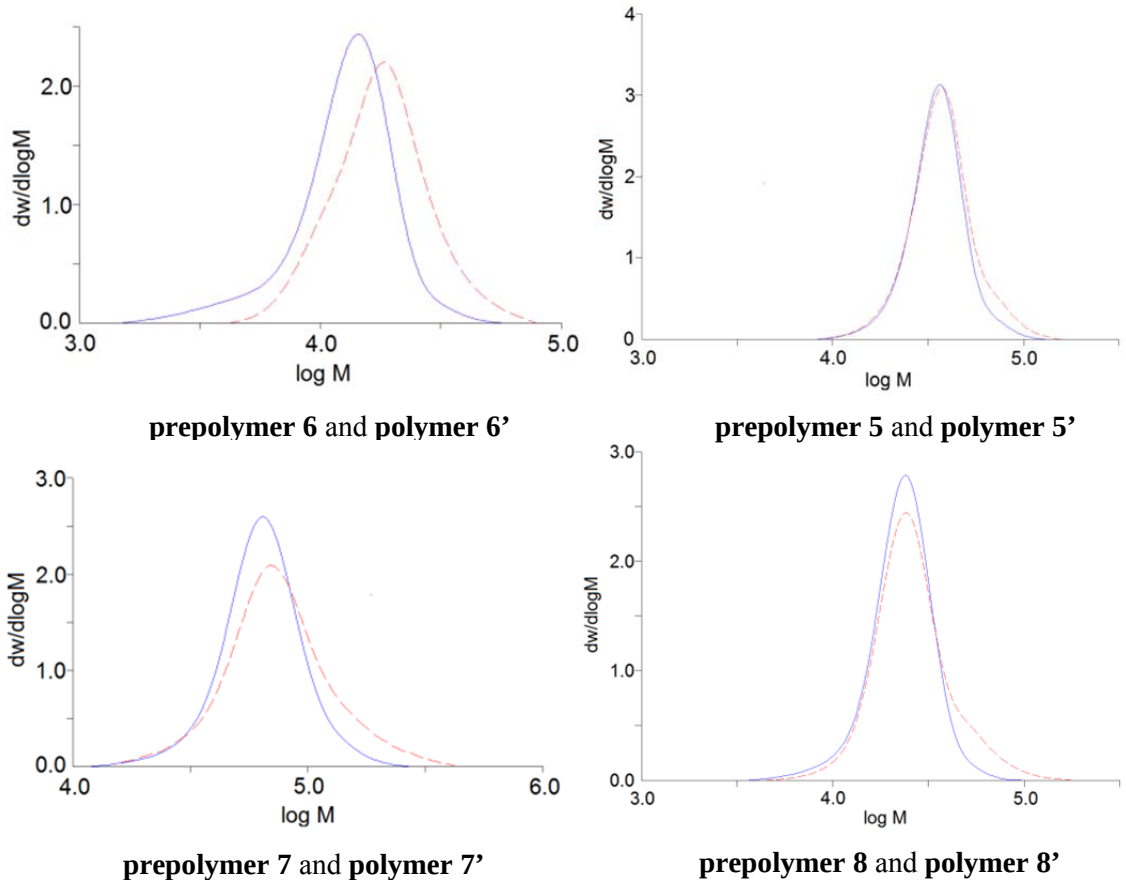

Figure 2.13 Molecular weight distributions of the SFP samples (red dash lines) and their prepolymers (blue solid lines). (*w* stands for mass of polymer with certain molecular weight; and *M* stands for number average molecular weight of polymer.)

In addition, the GPC data were also compared between the SFP samples and their prepolymers (Figure 2.13). Surprisingly, it appears that the molecular weights of the SFP's did not increase after the fullerene grafting. The average molecular weight of **polymer 3'** was even lower than that of its precursor. It is worth noting that the GPC traces recorded by the RI detector indicate the hydrodynamic volume of the polymer chains, and may not reflect the actual changes in molecular weights of the SFP's. On the basis of the backbone modification, the SFP's can be considered as comb- or brush-polymers, and it has been reported that the GPC-measured values underestimated the true molecular weights of such branched polymers by up to a factor of ten.[39] More

importantly, the GPC with RI detector responds to size difference of polymers, and it was possible that the coils of the SFP's were much denser ascribed to the intra-fullerene attractions.

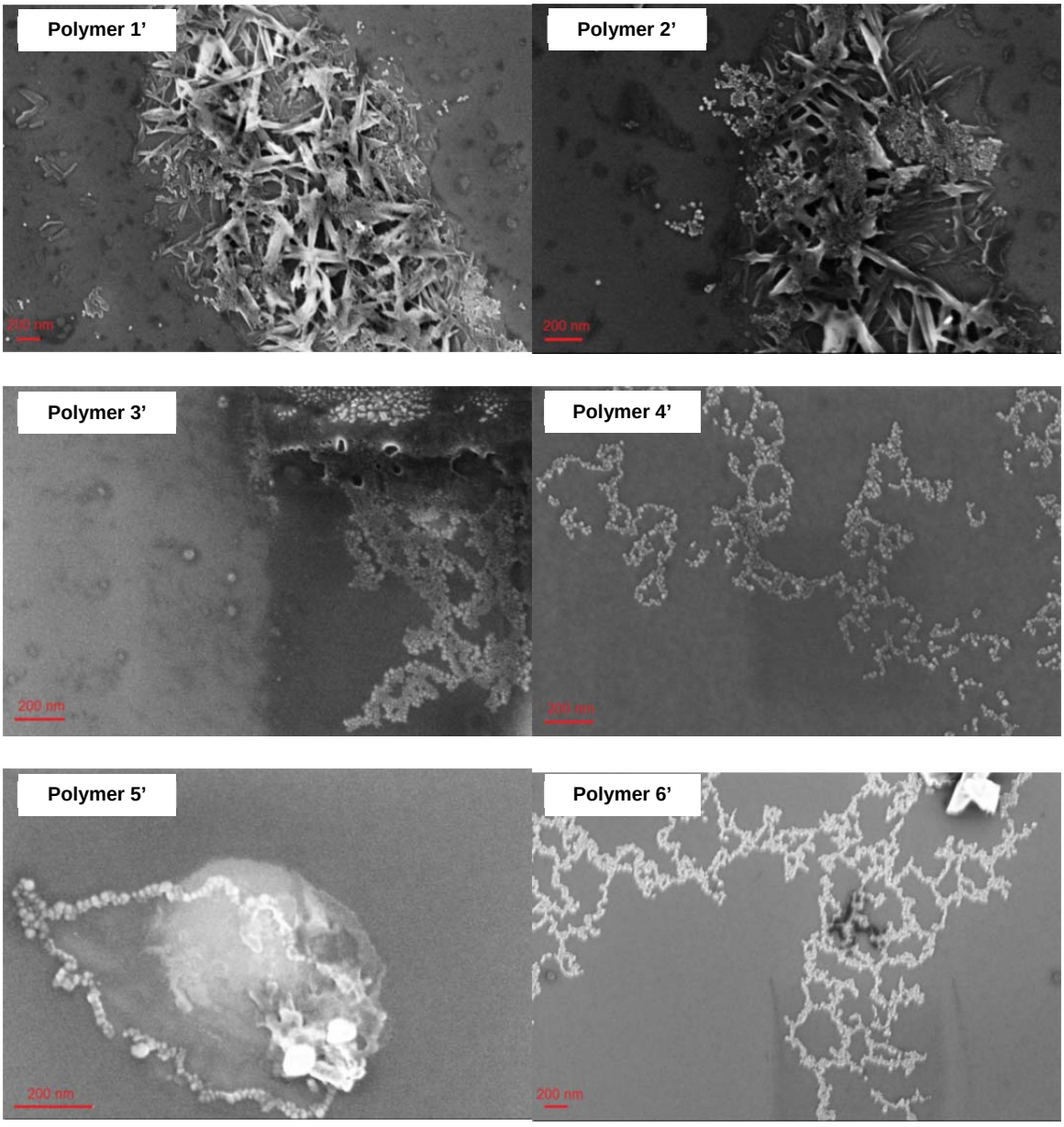

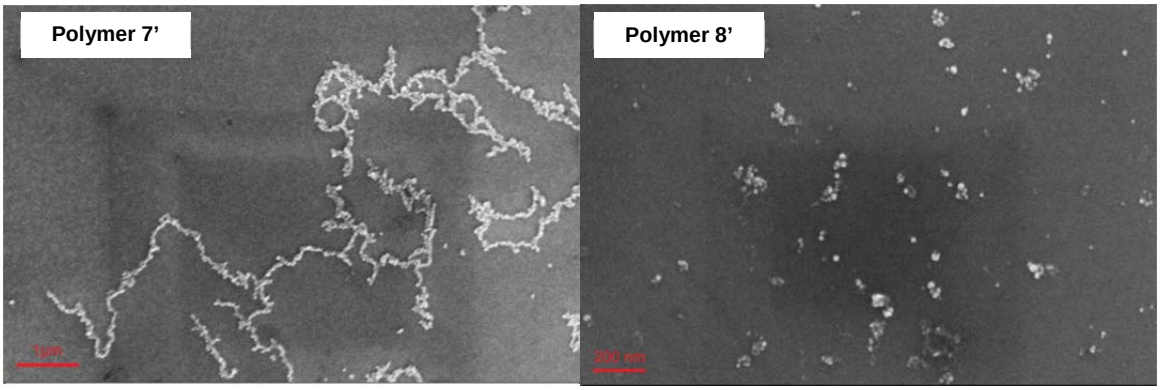

Figure 2.14 SEM images of **polymer 1' – 8'**.

The morphology of the SFP's on silicon wafer was analyzed by SEM (Figure 2.14). All the samples were dissolved in toluene with identical concentrations (1.0 mg/mL) except polymer **1'** and **2'** (0.2 mg/mL) due to their poorer solubility. It was observed that all the SFP's in the SEM images aggregated into nanoparticles as the elementary units for further supramolecular assemblies. The sizes of the nanoparticles in all the batches were generally uniform from 10 nm to 30 nm in diameter, indicating that they were independent of the polymer chain length or the fullerene content of the polymers, and apparently only dependent on the nature of the fullerene moiety itself.

Further assembly into sheets of nanoparticles was detected for **polymers 1' – 3'** while the nanoparticles of **polymers 4' – 7'** tended to form string-like assemblies. The nanoparticles of **polymer 8'** appeared as individual particles or clusters of several nanoparticles rather than micron-size complexes. These complex architectures were likely formed by non-covalent attractions of the fullerene moieties, since both individual nanoparticles and the complex assemblies were observed in many sample preparations thus implying that reversible interactions are the probable driving force for the assembly.

A hypothesis was proposed to explain the relationship between the observed morphology and the variable fullerene loadings of the SFP's. With increasing fullerene

content, there was an increase in the amount of C_{60} exposed on the surface of the resultant nanoparticles, which could act as active sites for the fullerene-fullerene attraction between different nanoparticles. Hence, they were more likely to build up more complex structures, e.g., nanoparticle strings or sheets on the wafer. In contrast lower fullerene loadings resulted in fewer or no active sites on the nanoparticle surfaces since most of the fullerene moieties were encapsulated inside of the nanoparticles and covered by the polymer backbones, and individual nanoparticles or small nanoparticle clusters were preferred.

Although nanoparticle strings were formed in **polymers 4' – 7'**, they were not identical in appearance. **Polymers 4'** and **6'** formed very similar branched nanoparticle networks in a range of a few microns, which may correlate to their similar number of C_{60}'s (10) per chain. In comparison, nanoparticles of **polymer 7'** formed less-branched strings possibly resulting from the lower fullerene content. **Polymer 5'** had only 5 C_{60}'s per chain and formed "necklace-like" nanoparticle structures that were less than one micron in size. This is probably due to both its shorter chain length and fewer number of C_{60} per chain.

Polymers 1' and **2'** not only showed nanoparticle assemblies, but also assembled into ordered or crystalline-like clusters. These polymers are likely to have extended chain conformations due to the highly crowded pendant fullerene moieties which may further facilitate associations that underlie the formation of ordered regions.

In summary, a general assembling tendency of well-defined SFP's to assemble was observed, and the nanoparticles formed by the SFP's on silica wafers were relatively small compared with other nanoparticles assembled by fullerene derivatives that have

been previously reported.[20a,40,41] Interestingly, the size of the nanoparticles was not determined by the fullerene loading or chain length of the SFP's. Due to the interplay of several important molecular variables, a rich variety of nanostructures and morphologies were formed.

2.3.6 Synthesis of TFP

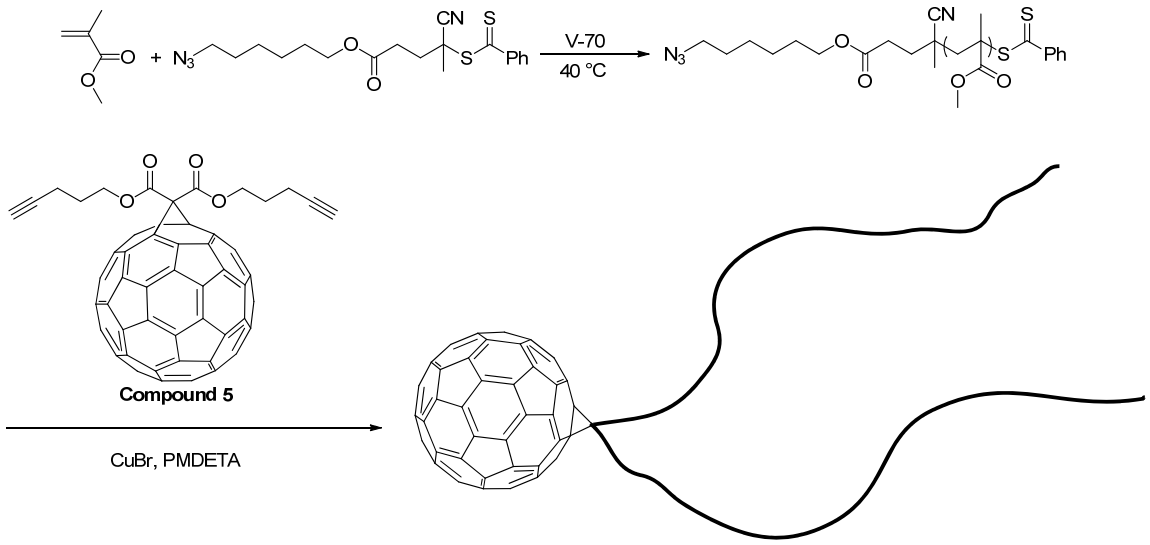

Scheme 2.3 Synthesis of "tadpole-like" fullerene polymer.

The TFP samples were prepared using a copper(I) bromide catalyzed click reaction between **compound 5** and N_3-PMMA, which was previously prepared by RAFT polymerization of MMA with an azide containing CTA (Scheme 2.3). Due to the low content of azide in the polymer chains, the completion of the click reaction could not be verified by FT-IR spectroscopy. However, if the reaction reached a 100% conversion, GPC traces of the TFP should show double the molecular weights of the original polymers, as **compound 5** would behave as a linker to connect two blocks of polymers together. Figure 2.14 shows the GPC analysis of several groups of polymers with increasing molecular weights, comparing the peak shifts before and after the click reactions. The results indicated that the click reaction could reach high conversions with

two tails anchored on the same molecule of **compound 5** only if the molecular weight of N_3-PMMA was less than 20k. Apparently, when the molecular weight of the N_3-PMMA polymer chains increased, it became more difficult for the second N_3-PMMA chain to approach the fullerene surface because of the steric hindrance of the earlier-attached chain. A similar phenomenon is observed in the "grafting to" strategy used for nanoparticle functionalization that limits high graft densities, as discussed in Chapter 1. Nevertheless, a fullerene with only one attached polymer chain can still behave as an amphiphilic macromolecular surfactant. Thus, the architecture of TFP did not need to be precisely controlled to expect amphiphilic properties.

(a)

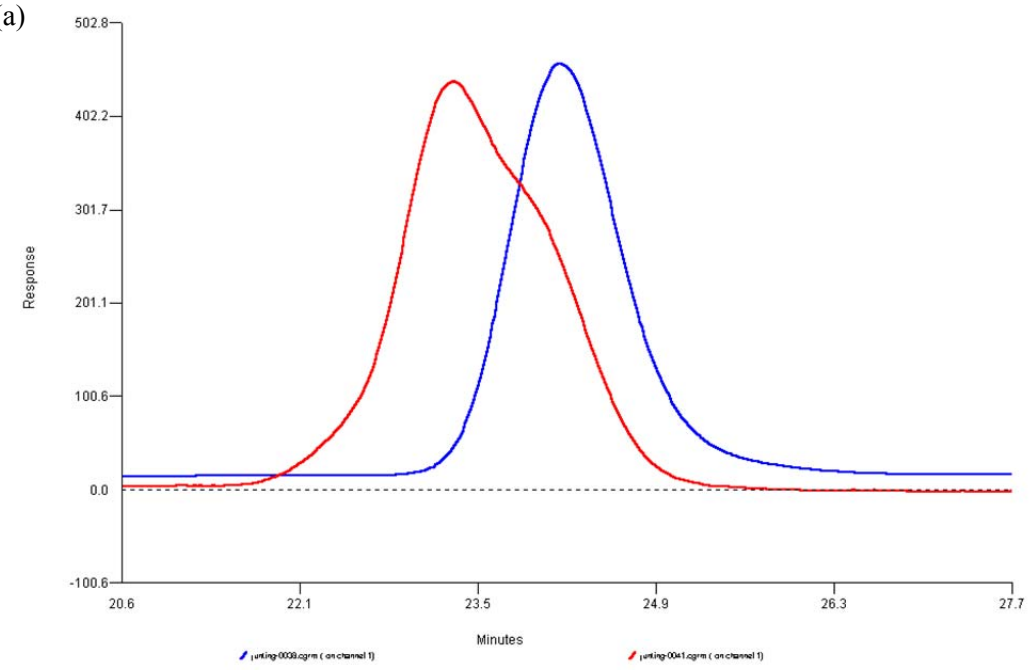

(b)

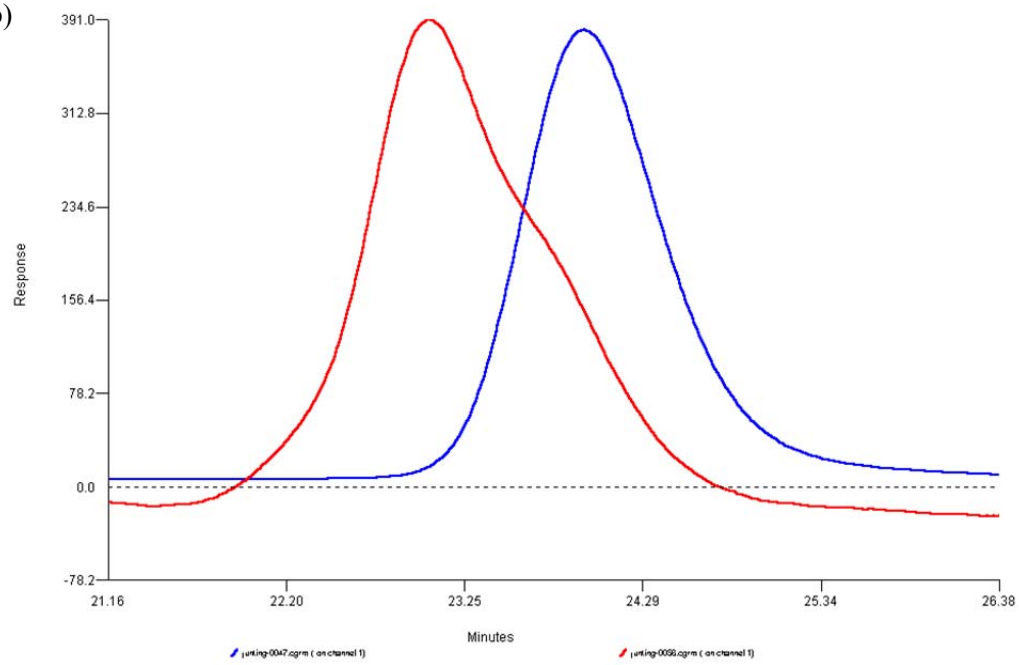
391.0
312.8
234.6
156.4
78.2
0.0
-78.2
Response
21.16
22.20
23.25
24.29
25.34
26.38
Minutes

(c)

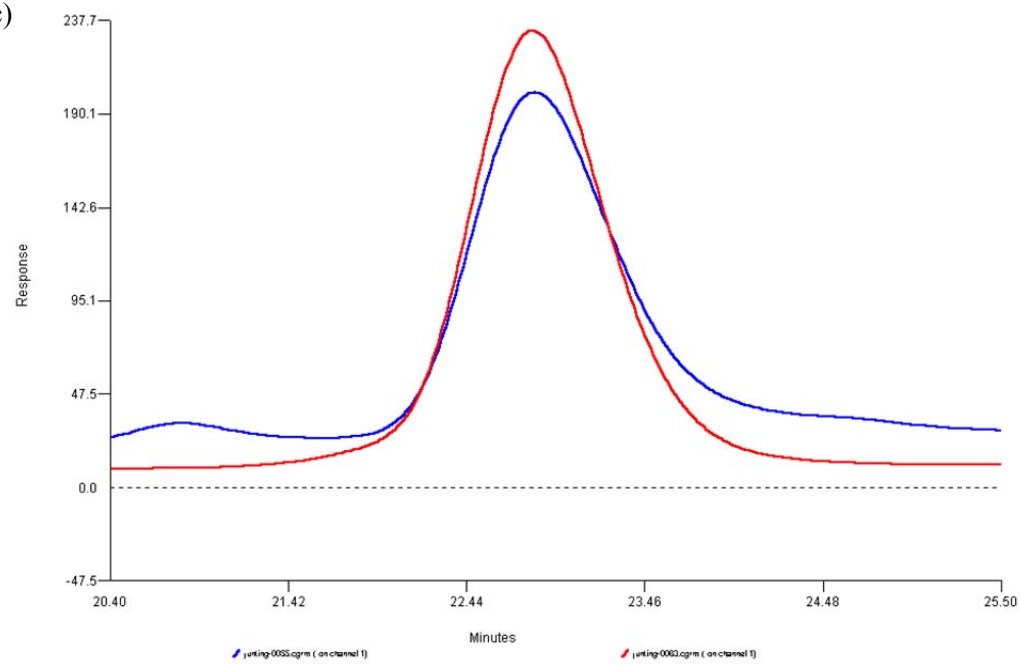
237.7
190.1
142.6
95.1
47.5
0.0
-47.5
Response
20.40
21.42
22.44
23.46
24.48
25.50
Minutes

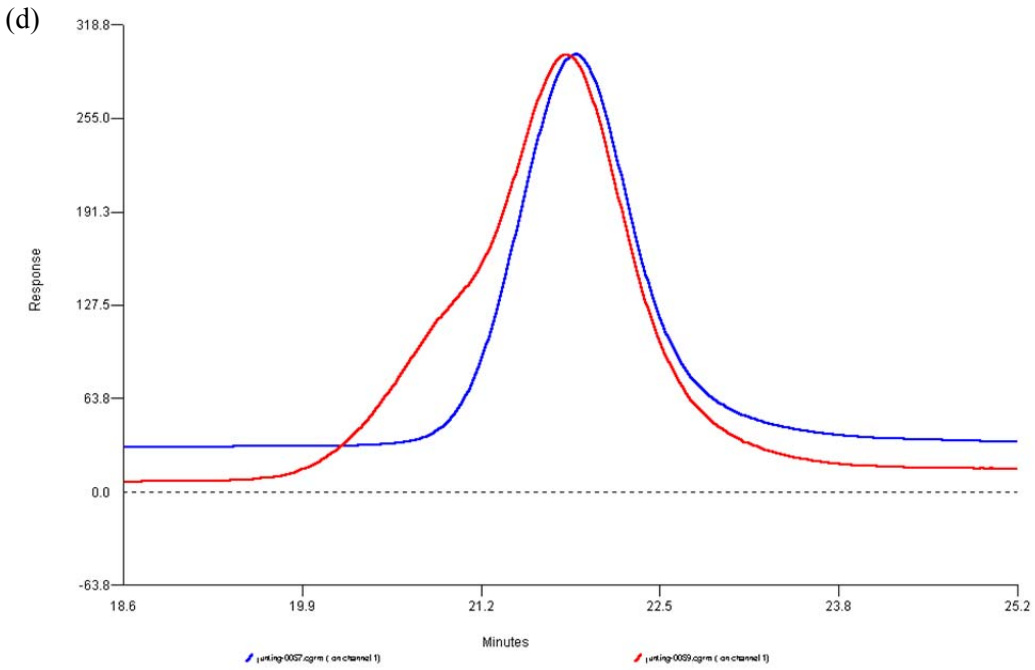

Figure 2.15 GPC traces of three groups of polymers before (blue) and after (red) click reaction: (a) blue – M_n = 9900, PDI = 1.14; red – M_n = 16,900, PDI = 1.22; (b) blue – M_n = 11,100, PDI = 1.13; red – M_n = 20,200, PDI = 1.21; (c) blue – M_n = 25,400, PDI = 1.16; red – M_n = 28,500, PDI = 1.12; and (d) blue – M_n = 54,700, PDI = 1.19; red – M_n = 66,400, PDI = 1.34.

2.3.7 Interactions between TFP and graphene

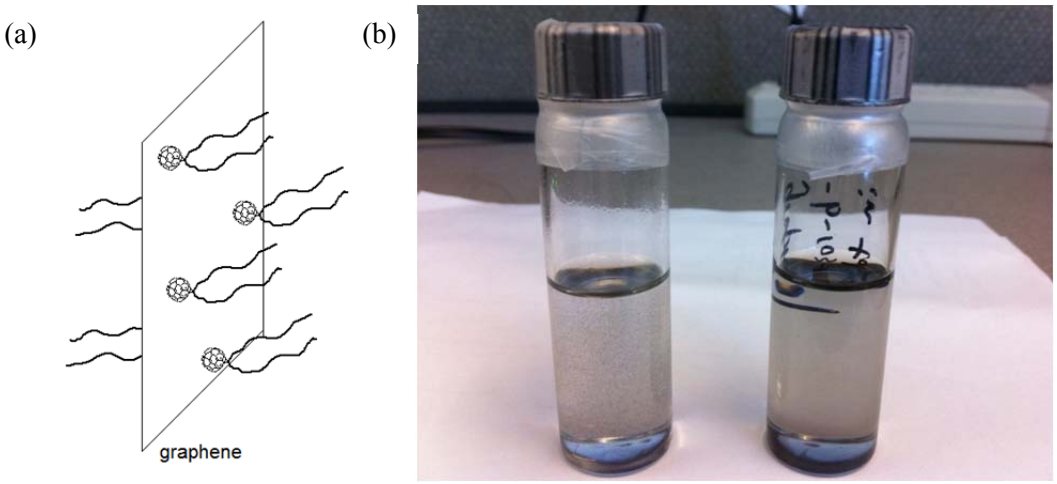

Figure 2.16 (a) Illustrative diagram of interactions between the TFP's and graphene. (b) Images of graphene (0.2 mg) in toluene (left) and graphene (0.2 mg) mixed with TFP (M_n = 20,200, PDI = 1.21) in toluene (right)

Experiments were conducted using mixed mono- and di-substituted TFP samples to test their ability to solubilize graphene via π-π stacking interactions (Figure 2.16a). In Figure 2.16b, it can be clearly observed by naked eyes that the solubility of graphene was greatly ameliorated when mixed with TFP having molecular weight around 20k and sonicated for 2 minutes. However, with higher molecular weight TFP's, the stabilizing effect of the TFP's for graphene was weakened. A possible explanation is that the polymeric tails were long enough to cover the fullerene moiety, and thus prevented contact of the fullerene head with the graphene. Further studies were necessary to investigate the interactions and binding of the TFP onto graphene through UV-vis and FT-IR analyses.

Figure 2.17a shows the UV-vis spectra of graphene, TFP and TFP-graphene complex, respectively. Generally, graphene only displayed an enhanced baseline in the whole range from 200 nm to 700 nm. The TFP sample showed a strong absorption at a nearly identical peak of approximately 282 nm, while the TFP-graphene complex had an absorption at 283.5 nm with slight differences in the peak characteristics. A series of titration-like experiments were considered to separate the fullerene-graphene interactions from other factors, such as concentration effects of the individual components.

Since the cuvettes for UV-vis spectroscopy cannot be sonicated without sustaining damage, a suspension of TFP-graphene complex was prepared first, and then added dropwise into a cuvette containing a TFP solution (Figure 2.17b). With the gradual addition of the TFP/graphene suspension, a peak around 290 nm appeared and eventually merged with the original TFP absorption to form a smooth peak. To exclude the possibility that the changes of the UV-vis absorption may result from the variation of the

TFP concentration, a controlled experiment was carried out as shown in Figure 2.17c. In the absence of graphene, the absorption peaks were always sharp and did not shift regardless of the TFP concentration, although the signals became stronger with higher concentrations. Additionally, if graphene was added into the TFP solution without sonication (obvious solids could be seen in the cuvette), there was no influence on the absorption peak, except the increase of the base line (Figure 2.17d). Consequently, we can conclude that an interaction between TFP and graphene occurred after sonication, and is the reason for the improvement of the solubility of graphene.

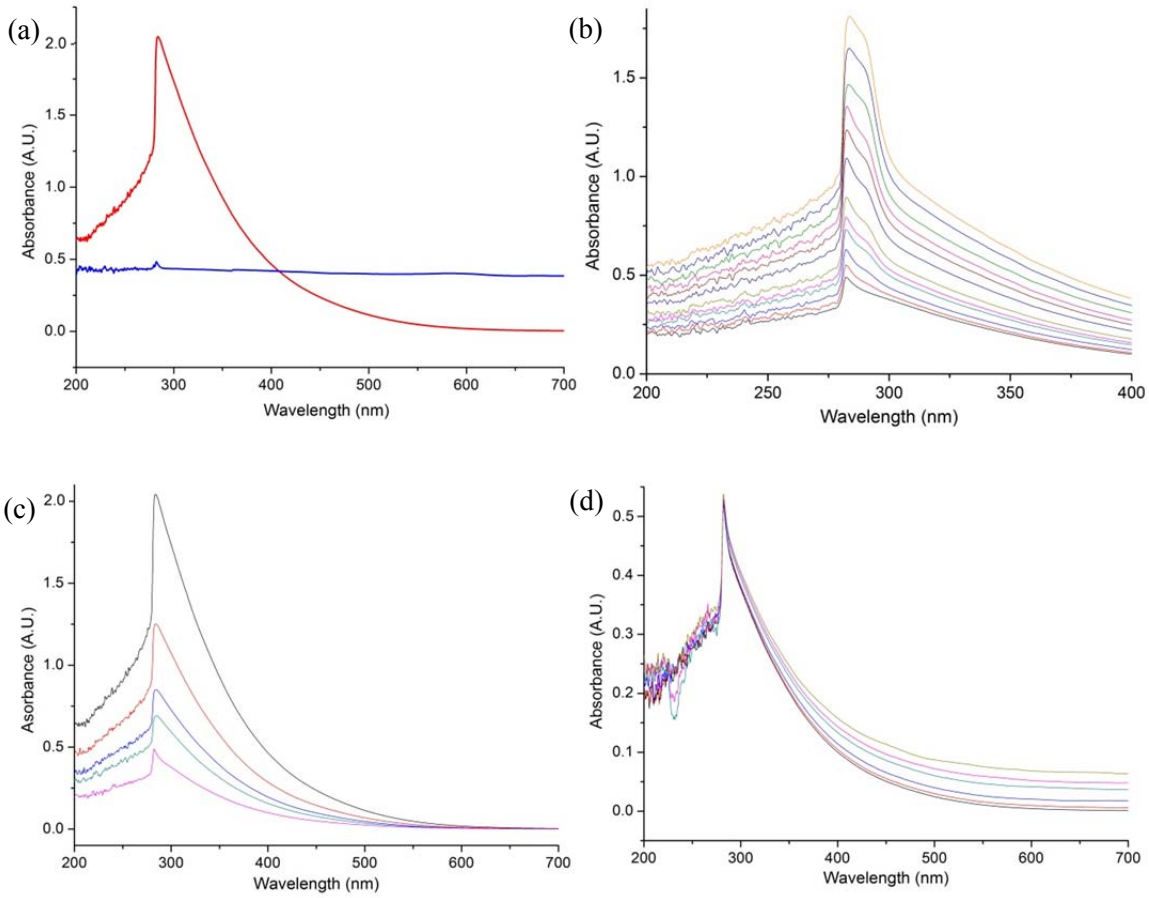

Figure 2.17 UV-vis spectra of (a) TFP (M_n = 20,200, PDI = 1.21) (red) and graphene (blue) in toluene; TFP solution in toluene with (b) gradual addition of graphene suspension; (c) gradual addition of TFP/graphene suspension; and (d) different concentrations.

Moreover, FT-IR spectra displayed more dramatic changes between TFP and TFP/graphene composites (Figure 2.18). In contrast with TFP, the carbonyl absorption of the composites was much weaker but the alkyl absorption became stronger, and this provided additional evidence for the interactions between TFP and graphene.

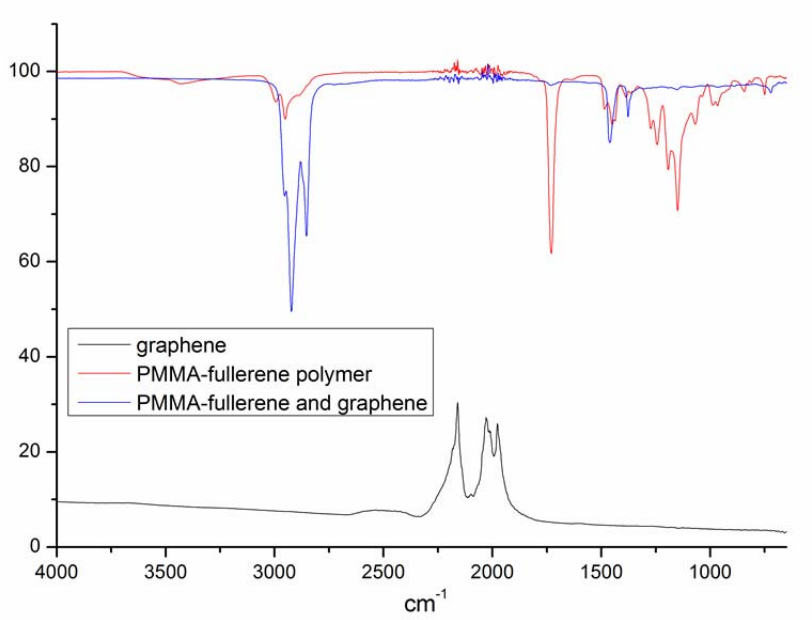

Figure 2.18 FT-IR spectra of graphene (black), TFP (M_n = 20,200, PDI = 1.21) (red) and TFP/graphene composites (blue).

The dispersion of the TFP/graphene composites in diverse solvents was studied using TEM (Figure 2.19). With the suspension in THF, many obvious aggregations of the TFP can be detected and they were not uniformly dispersed. In toluene and DMF, the TFP assembled into nanoparticles with diameters of 10 nm – 20 nm. These nanoparticles spread both on the surface of graphene sheets and the TEM grid, and the nanoparticles formed by the DMF sample had better dispersion on the graphene sheets than that of the toluene sample. Actually, the solubility of the composites in these solvents was also consistent with this sequence – the solubility in DMF was better than that in toluene, and

better than that in THF. Therefore, it is clear that the dispersion of TPF on the graphene surface is a very important factor influencing the solubility of graphene.

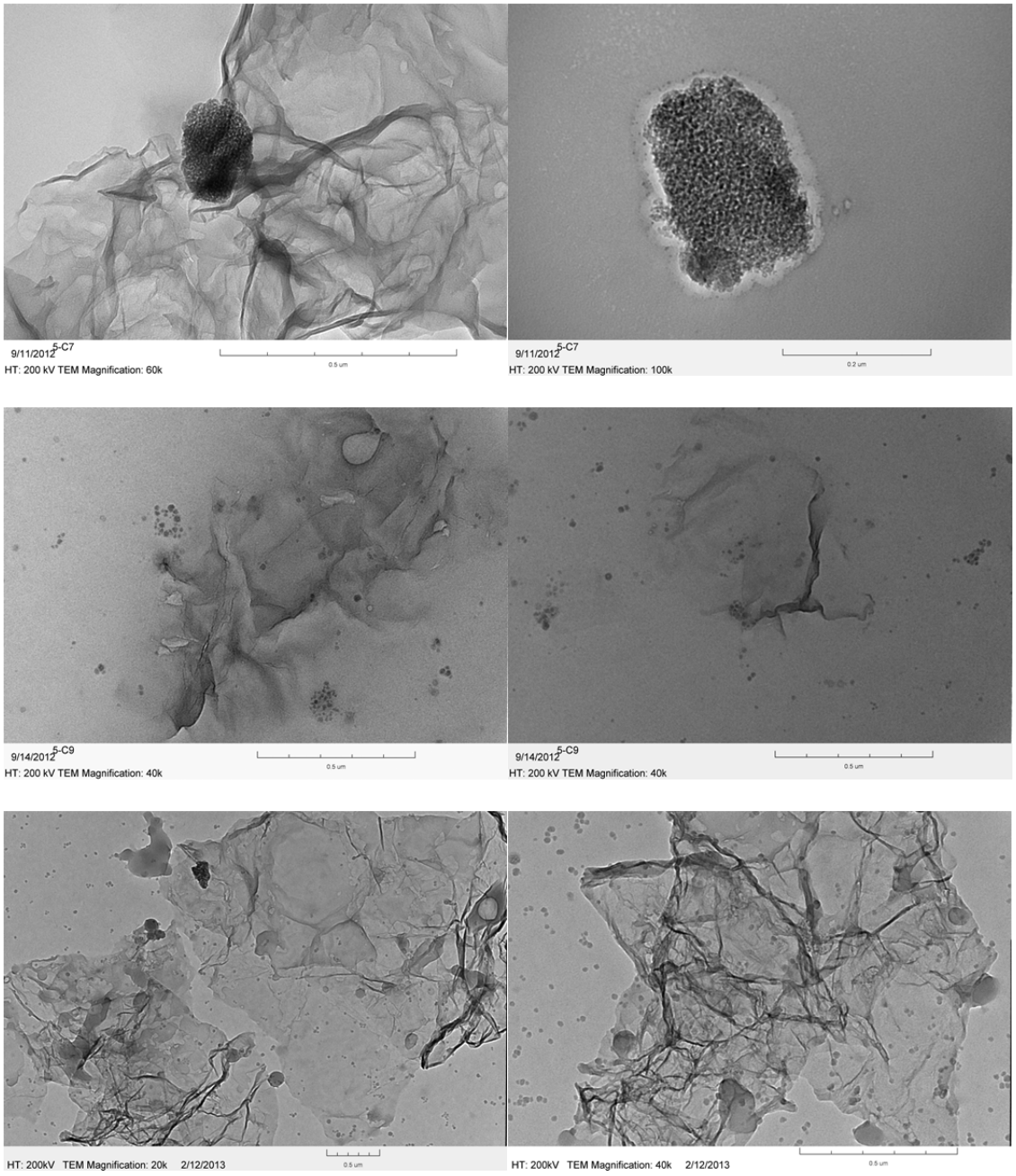

Figure 2.19 TEM images of the TFP (M_n = 20,200, PDI = 1.21) / graphene composites in diverse solvents: THF (top), toluene (middle) and DMF (bottom).

2.4 Conclusions

In this work, the precise synthesis of a mono-alkynyl functionalized fullerene derivative starting with pristine C_{60} has been reported. Combining RAFT polymerization and copper-mediated click reactions, we have successfully prepared a series of well-defined SFP's with variable molecular weights and fullerene contents. The RAFT polymerization proceeded with good control over the molecular weight and copolymer composition, and the click reaction reached high conversions despite the steric hindrance. Due to the great efficiency of this method, we are able to achieve a very high fullerene loading for the SFP's (up to 78 C_{60} moieties per chain on average from UV-vis calculation, which have not been reported before). Additionally, we have studied the self-aggregation behaviors of these SFP's both in solution and on silicon wafers, and found that the morphology of the supramolecular architectures varied depending on the polymer chain lengths and fullerene contents of the samples. Using the control over these two molecular variables, different morphologies were observes that ranged from individual nanoparticles to nanoparticle strings, sheets and crystalline-like structures. This type of self-aggregation may find applications on the design of new functional materials in the future.

In further investigations of fullerene-polymer molecular architectures, a type of PMMA-based TFP was successfully synthesized via RAFT polymerization and click reaction. The effect of the TFP has been demonstrated to significantly improve the solubility of graphene, and stabilize it in solution. This effect is solvent dependent, which has been further confirmed by TEM analysis in THF, toluene and DMF. The non-covalent interactions between graphene and fullerene polymers have been verified via UV-vis and FT-IR spectroscopies. Future work will focus on synthesizing TFP with

various functionalized polymeric tails and studying the morphology of the graphene-fullerene polymer composites in polymer matrices, which is believed to be a promising approach to produce polymer nanocomposites with well-dispersed graphene fillers.

2.5 Refereneces

1. Giacalone, F.; Martin, N. *Chem. Rev.* **2006**, *106*, 5136-5190.

2. Wang, C.; Guo, Z-X.; Fu, S.; Wu, W.; Zhu, D. *Prog. Polym. Sci. 2004*, *29*, 1079-1141.

3. Hiorns, R.; Cloutet, E.; Ibarboure, E.; Vignau, L.; Lematre, N.; Guillerez, S.; Absalon, C.; Cramail, H. *Macromolecules* **2009**, *42*, 3549-3558.

4. Natori, I.; Natori, S. *J. Polym. Sci., Part A: Polym. Chem.* **2008**, *46*, 3282-3293.

5. Dardel, B.; Guillon, D.; Heinrich, B.; Deschenaux, R. *J. Mater. Chem.* **2001**, *11*, 2814-2831.

6. Kim, J.; Yun, M. H.; Lee, J.; Kim, J. Y.; Wudl, F.; Yang, C. *Chem. Commun.* **2011**, *47*, 3078-3080.

7. Munoz, A.; Illescas, B. M.; Sanchez-Navarro, M.; Rojo, J.; Martin, N. *J. Am. Chem. Soc.* **2011**, *133*, 16758-16761.

8. Shi, S.; Khemanikc, K. C.; Li, Q. C.; Wudl, F. *J. Am. Chem. Soc.* **1992**, *114*, 10656-10657.

9. Yang, C.; Lee, J. K.; Heeger, A. J.; Wudl, F. *J. Mater. Chem.* **2009**, *19*, 5416-5423.

10. Lee, J. U.; Cirpan, A.; Emrick, T.; Russell, T. P.; Jo, W. H. *J. Mater. Chem.* **2009**, *19*, 1483-1489.

11. a) Stalmach, U.; de Boer, B.; Videlot, C.; van Hutten P. F.; Hadziioannou, G. *J. Am. Chem. Soc.* **2000**, *122*, 5464-5472. b) de Boer,B.; Stalmach, U.; van Hutten, P. F.; Melzer, C.; Krasnikov, V. V.; Hadziioannou, G. *Polymer* **2001**, *42*, 9097-9109.

12. a) van der Veen, M. H.; de Boer, B.; Stalmach, U.; van de Wetering, K. I.; Hadziioannou, G. *Macromolecules* **2004**, *37*, 3673-3684. b) Barrau, S.; Heiser, T.; Richard, F.; Brochon, C.; Ngov, C.; van de Wetering, K.; Hadziioannou, G.; Anokhin, D. V.; Ivanov, D. A. *Macromolecules* **2008**, *41*, 2701-2710.

13. Celli, A.; Marchese, P.; Vannini, M.; Berti, C.; Fortunati, I.; Signorini, R.; Bozio, R. *Reactive & Functional Polymers* **2011**, *71*, 641-647.

14. Li, M.; Xu, P.; Yang, J.; Yang, S. *J. Mater. Chem.* **2010**, *20*, 3953-3960.

15. Rusen, E.; Marculescu, B.; Preda, N.; Mihut, L. *J. Polym. Res.* **2008**, *15*, 447-451.

16. a) Kawauchi, T.; Kumaki, J.; Yashima, E. *J. Am. Chem. Soc.* **2006**, *128*, 10560-10567. b) Kawauchi, T.; Kumaki, J.; Kitaura, A.; Okoshi, K.; Kusanagi, H.; Kobayashi, K.; Shinahara, H.; Yashima, E. *Angew. Chem. Int. Ed.* **2008**, *47*, 515-519.

17. Wang, M.; Pramoda, K. P.; Goh, S. H. *Macromolecules* **2006**, *39*, 4932-4934.

18. Badamshina, E.; Gafurova, M. *J. Mater. Chem.* **2012**, *22*, 9427-9438.

19. Bonifazi, D.; Enger, O.; Diederich, F.; *Chem. Soc. Rev.* **2006**, *36*, 390-414.

20. Sanchez, L.; Otero, R.; Gallego, J. M.; Miranda, R.; Martin, N. *Chem. Rev.* **2009**, *109*, 2081-2091.

21. Babu, S. S.; Mohwald, H.; Nakanishi, T. *Chem. Soc. Rev.* **2010**, *39*, 4021-4035.

22. Schade, B.; Ludwig, K.; Bottcher, C.; Hartnagel, U.; Hirsch, A. *Angew. Chem. Int. Ed.* **2007**, *46*, 4393-4396.

23. Yu, X.; Zhang, W-B.; Yue, K.; Li, X.; Liu, H.; Xin, Y.; Wang, C-L.; Wesdemiotis, C.; Cheng, S. Z. D. *J. Am. Chem. Soc.* **2012**, *134*, 7780-7788.

24. Zhou, G.; He, J.; Harruna, I. I.; Geckeler, K. E. *J. Mater. Chem.* **2008**, *18*, 5492-5501.

25. Yao, Z. L.; Tam, K. C. *Langmuir* **2011**, *27*, 6668-6673.

26. Tang, Q.; Zhou, Z.; Chen, Z. *Nanoscale* **2013**, Advance Article.

27. Liu, J.; Yang, W.; Tao, L.; Li, D.; Boyer, C.; Davis, T. P. *J. Polym. Sci., Part A: Polym. Chem.* **2009**, *48*, 425-433.

28. Zhang, X.; Huang Y.; Wang, Y.; Ma, Y.; Liu Z.; Chen, Y. *Carbon* **2008**, *47*, 313-347.

29. Yu, D.; Park, K.; Durstock, M.; Dai, L. *J. Phys. Chem. Lett.* **2011**, *2*, 1113-1118.

30. Felder, D.; Nierengarten, H.; Gisselbrecht, J-P.; Boudon, C.; Leize, E.; Nicoud, J-F.; Gross, M.; van Dorsselaer, A.; Nierengarten, J-F. *New J. Chem.* **2000**, *24*, 687-695.

31. Iehl, J.; de *Freitas*, R. P.; Nierengarten, J-F. *Tetrahedron Lett.* **2008**, *49*, 4063-4066.

32. Li, Y.; Benicewicz, B. C. *Macromolecules* **2008**, *41*, 7986-7992.

33. Bingel, C. *Chemische Berichte* **1993**, *126*, 1957-1959.

34. Ruoff, R. S.; Tse, D. S.; Lorents, D. C. *J. Phys. Chem.* **1993**, *97*, 3379-3383.

35. Li, Y.; Yang, J.; Benicewicz, B. C. *J. Polym. Sci., Part A: Polym. Chem.* **2007**, *45*, 4300-4308.

36. Djojo, F.; Herzog, A.; Lamparth, I.; Hampel, F.; Hirsch, A. *Chem. Eur. J.* **1996**, *2*, 1537-1547.

37. Kim, H.; Bedrov, D.; Smith, G. D. *J. Chem. Theory Comput.* **2008,** *4*, 335-340.

38. Chu, C.; Tsai, Y.; Hsiao, L.; Wang, L. *Macromolecules* **2011**, *44*, 7056-7061.

39. Runge, M. B.; Dutta, S.; Bowden, N. B. *Macromolecules* **2006**, *39*, 498-508.

40. Yusa, S-I.; Awa, S.; Ito, M.; Kawase, T.; Takada, T.; Makashima, K.; Liu, D.; Yamago, S.; Morishima, Y. *J. Polym. Sci., Part A: Polym. Chem.* **2011**, *49*, 2761-2770.

41. Wang, J.; Shen, Y.; Kessel, S.; Fernandes, P.; Yoshida, K.; Yagai, S.; Kurth, D. G.; Mohwald, H.; Nakanishi, T. *Angew. Chem., Int. Ed.* **2009**, *48*, 2166-2170.

CHAPTER 3

SYNTHESIS OF POLYMER-GRAFTED JANUS NANOPARTICLES VIA COMBINATION OF REVERSIBLE CLICK REACTION AND "GRAFTING TO" STRATEGIES

3.1 Introduction

Asymmetric particles (also named Janus particles), including spatially asymmetric particles [1-3] and spherical particles carrying asymmetric functionalities, impart anisotropic properties with unique self-assemblies and thus have many potential applications, such as phase-transfer or multistep catalysts, multi-targeted drug carriers and bio-imaging agents.[4,5] In this work, our discussion focuses on the synthesis of the latter type of Janus particles. A number of strategies have been developed starting with isotropic particles,[6] in which the most crucial step is temporarily or permanently masking a portion of their surface, either by biphasic interaction,[7,8] or by monolayer coating.[9,10] Three significant challenges need to be considered when producing Janus particles: (1) precise control on the geometry of the Janus particles, i.e., the relative areas of their two faces; (2) synthesis of Janus particles in large quantities; (3) scaling down Janus particles to "real" nano-scale dimensions (with diameters less than 100 nm). So far most of the reported synthetic routes cannot overcome all of these three challenges simultaneously. Granick's approach using wax micelles for the masking-unmasking process can simultaneously achieve both control of geometry and scale-up production.[7] However, this approach is only effective for micro-sized particles (with diameters greater than 800 nm). When the particles became smaller, entropy became the predominant driving force, and the particles tended

to disperse in a uniform phase rather than the interface of the two phases. Therefore, no nanoparticles (NP's) were detected on the surface of the wax micelles when we tried to prepare 15 nm Janus NP's using Granick's approach.

Currently, modifying Janus particles with small molar mass ligands is still the most common synthetic route. In contrast, growing polymer brushes on inorganic NP's is of great interest, since polymers can have a more significant influence on the properties of NP's. By controlling the chemistry of the grafted polymers, graft densities and polymer chain lengths, the morphology of the NP's in matrices [11] and their mechanical properties [12] can be precisely tuned. The strategies for uniformly modifying NP's with polymer brushes can be categorized into "grafting from" [13-15] and "grafting to" [16]. However, it is still challenging to apply these strategies to produce Janus NP's, and only a few groups have reported successful syntheses of polymer-grafted Janus NP's.[17-19]

In this chapter, we describe our work on developing novel synthetic routes to prepare polymer-grafted Janus NP's with relatively high yields via a reversible masking-unmasking process. Our first approach includes chemically modifying silica particles, non-covalently or covalently fixing the particles on planar silicon wafers, and growing polymers on the uncovered face of the particles through a "grafting to" approach. Finally, sonication is applied to break the connections between the particles and the wafer, and release the obtained Janus particles to the solution.

With many new mechanophore structures developed in recent years, mechanochemistry has become a very powerful tool for organic synthesis and advanced material design,[20-24] because it enables many chemical transformations that cannot occur through thermal or photochemical stimuli, e.g., the cycloreversion of the triazole ring

formed by azide and alkyne in the copper-mediated click reaction, which has widely broadened the application of this classic reaction and made it an efficient pathway to reversible covalent connections.[25,26] However, the majority of these reactions to date have only relied on polymer materials to mechanically activate bond cleavages.

On the basis of the newly-developed chemistry, we designed another mechanochemically-driven and cyclic approach to the fabrication of polymer-grafted Janus NP's by combining the reversible click reaction and "grafting to" strategies. This approach harnesses mechanical forces to selectively "unclick" and cleave the particle-particle attachment, although the copper-mediated click reaction for NP connections has already been reported.[19]

3.2 Experimental Section

3.2.1 Materials

Double-side polished silicon wafers were purchased from Virginia Semiconductor Inc. Colloidal silica NP's of 30 wt% dispersed in methyl ethyl ketone were purchased from Nissan Chemical. The average particle diameter was 15 ± 4 nm as measured by TEM and 20 nm as measured by light scattering. 3-Aminopropyl-trimethoxysilane (APTES) (95%), 3-aminopropyldimethylethoxysilane (APDMES) (95%) and 3-bromopropyl-trimethoxysilane (BPTMS) (95%) were purchased from Gelest and used as received. Poly(ethylene glycol) methyl ether (PEG-OH) (M_n = 5,000) was purchased from SigmaAldrich and used as received. Tetrahydrofuran (THF) (99.9%, Acros) was dried over CaH_2 overnight and distilled before use. 4-Cyanopentanoic acid dithiobenzoate (CPDB) was purchased from Strem Chemical Inc. and used as received. Methyl methacrylate (MMA) (99%, Acros) was passed through a basic alumina column to remove inhibitors before use. 2,2'-Azobis(4-methoxy-2,4-dimethyl valeronitrile) (V-

70) was purchased from Wako Chemicals and used as received. Unless otherwise specified, all chemicals were purchased from Fisher Scientific and used as received.

3.2.2 Instrumentation

NMR spectra were recorded on Varian Mercury 300 and 400 spectrometers using $CDCl_3$ as solvent. To perform the static contact angle measurements, a VCA Optima Surface Analysis System from AST Products Ltd. was used. The static contact angles were measured by placing 0.25 ml droplets of DI water on the substrate surfaces. FT-IR spectra were recorded using a PerkinElmer Spectrum 100 FT-IR Spectrometer. X-ray Photoelectron Spectroscopy (XPS) spectra were recorded on a Kratos Axis Ultra DLD instrument equipped with a monochromated Al Kα X-ray source. After peak fitting of the C 1s spectra, all the spectra were calibrated in reference to the aliphatic C 1s component at a binding energy of 285.0 eV. Molecular weights and polydispersity indices (PDI, M_w/M_n) were determined by GPC conducted on a Varian 390-LC system, equipped with refractive index detector, 3 × PLgel 10 μm mixed-B LS columns (300 × 7.5 mm), with THF as eluent at 30 °C and a flow rate of 1.0 mL/min. The GPC system was calibrated with poly(methyl methacrylate) (PMMA) from Polymer Laboratories. The ultrasound treatment was performed with a Branson 1510 sonicator. The thermal stability of the polymers was determined by thermogravimetric analysis (TGA) performed on dried polymer samples from 80 °C to 800 °C using a TA Instruments Q5000 with a nitrogen flow rate of 20 mL/min and heating rate of 10 °C/min. TEM images were recorded using a Hitachi H8000 Scanning Transmission Electron Microscope. Tapping mode AFM experiments were carried out using a Multimode Nanoscope III system (Digital Instruments, Santa Barbara, CA). The measurements were performed under ambient atmosphere using commercial Si cantilevers with a spring constant and resonance

frequency respectively equal to 40-60 N/m and 250-300 kHz, and the samples were prepared on silicon wafers by spin-coating at 3000 rpm. SEM images were recorded using a Zeiss Ultraplus Thermal Field Emission Scanning Electron Microscope.

3.2.3 Preparation of silica particles (500 nm)

500 nm silica particles were prepared through the Stober process: [28,29] Ammonia (29%, 10 mL), distilled water (11 mL) and ethanol (75 mL) were mixed in a round-bottom flask at first, and then tetraethyl orthosilicate (TEOS) was added all at once under stirring at 500 rpm. After overnight reaction, the resultant silica particles were collected by centrifugation at 3000 rpm for 10 minutes, and redispersed in 100 mL of ethanol, and centrifuged again. The dispersion-centrifugation process was repeated another two times in THF to remove all the small molecules. Finally, 1.77 g silica particles as white powders were obtained after drying in a vacuum oven at room temperature. The average diameter of the particles was 500 ± 50 nm as measured by TEM. FT-IR: 793 cm^{-1} (Si-O), 940 cm^{-1} (Si-O-H), 1055 cm^{-1} (Si-O-Si).

3.2.4 Preparation of carboxylic acid-functionalized silica particles

Silica NP's with average diameter of 15 nm were fed in to prepare amino-functionalized NP's using a previously reported procedure.[14b] The obtained NP's (0.3 amine/nm^2) were dissolved in 35 mL of THF, and 1 mL of succinic anhydride solution in DMF (1.0 M) was added under stirring. The NP's were poured in 200 mL of diethyl ether and collected by centrifugation at 3000 rpm for 15 minutes after an overnight reaction, and then redispersed in 50 mL of DMF. This centrifugation-dispersion process was repeated another two times to remove all the small molecules. In the final round, the carboxylic acid-functionalized NP's were redispersed in DMF to make a solution of 0.1 g/mL for the further use. A small amount of amino-functionalized silica NP's from the

same batch were functionalized by activated CPDB following the same procedure, and the graft density was estimated by UV-vis analysis,[3] which was assumed the same as that of alkynyl-functionalized NP's. Otherwise, silica particles with average diameters of 50 nm and 500 nm were also functionalized with carboxylic acid, and the ratios of the chemicals varied according to the size of the particles.

3.2.5 Preparation of monolayers of carboxylic-functionalized silica NP's on silicon wafers

Silicon wafers were cleaned in piranha solution (H_2SO_4/H_2O_2 = 7/3, *v*/*v*) for 3 hours at 90 °C, and then rinsed with water and acetone sequentially. The treated wafers were then immersed into the APTES solution (5.0 mM) in mixed solvent of acetone and water (5/1, *v*/*v*), and kept for 3 hours, followed by washing with acetone.[27] After drying in vacuum at room temperature, silicon wafers with amino-functionalized surface were obtained.

Two groups of carboxylic acid-functionalized silica particles solution in DMF were prepared (0.01 g/mL, 10 mL) – one with the addition of 1.5 g of dicyclohexylcarbodiimide (DCC) and 0.25 g of (dimethylamino)pyridine (DMAP) and the other without. Two amino-functionalized silicon wafers were placed into the solutions, respectively, for 1-2 days at room temperature depending on the graft density which was desired. After rinsing with DMF, water and acetone, monolayers of carboxylic acid functionalized NP's were assembled on silicon wafers.

3.2.6 Graft of PEG-OH on the carboxylic acid-functionalized silica NP's assembled on silicon wafers

PEG-OH (4.27 g), DCC (0.18 g) and DMAP (0.03 g) were dissolved in 20 mL of dichloromethane. The silicon wafers coated with monolayers of carboxylic acid

functionalized NP's were placed into the solution for 24 hours, and then washed with dichloromethane and acetone. The exposed surface of the NP's were thus grafted with PEG. Finally, ultrasound weas performed for 30 minutes to release the NP's from the silicon wafers.

3.2.7 Preparation of bromo-functionalized silica particles (500 nm)

500 nm silica particles (1.77 g) were added to a three-necked round-bottom flask with BPTMS (0.73 g, 3.0 mmol) and dried THF (300 mL). The reaction mixture was heated at 75 °C under nitrogen protection overnight and then cooled to room temperature. The product were precipitated by centrifugation at 3000 rpm for 10 minutes, and redispersed in 100 mL of THF. This centrifugation-dispersion process was repeated another three times to remove all the small molecules. In the last round, the bromo-functionalized silica particles were redispersed in 200 mL of DMF for the further use. FT-IR: 796 cm^{-1} (Si-O), 936 cm^{-1} (Si-O-H), 1071 cm^{-1} (Si-O-Si).

3.2.8 Preparation of azido-functionalized silica particles (500 nm)

The DMF solution of bromo-functionalized silica particles obtained in the last step were added to a three-necked round-bottom flask together with sodium azide (0.39 g, 6.0 mmol) and distilled water (15 mL). The reaction mixture was heated at 80 °C overnight and then cooled to room temperature. The product were precipitated by centrifugation at 5000 rpm for 10 minutes, and redispersed in 100 mL of DMF. This centrifugation-dispersion process was repeated another two times to remove all the small molecules. Finally, the particles were dispersed in DMF for the further use. FT-IR: 799 cm^{-1} (Si-O), 948 cm^{-1} (Si-O-H), 1091 cm^{-1} (Si-O-Si), 2120 (N_3).

3.2.9 Activation of 5-hexynoic acid by 2-mercaptothiazoline

5-Hexynoic acid (500 mg, 4.46 mmol), 2-mercaptothiazoline (532 mg, 4.46 mmol), and DCC (1.11 g, 5.35 mmol) were dissolved in 20 mL of dichloromethane. DMAP (54 mg, 0.45 mmol) in 5 mL of dichloromethane was added dropwise to the solution, which was stirred at room temperature for 6 hours. The solution was filtered to remove the salt. After removal of solvent and silica gel column chromatography (3:2 mixture of hexane and ethyl acetate), the product was obtained as light green oil (903 mg, 95% yield). ^{1}H NMR (400 MHz, $CDCl_3$): δ = 1.87-1.94 (m, 2H, $CH_2C\mathbf{H}_2CH_2$), 1.97 (t, J = 2.8 Hz, 1H, C≡C**H**), 2.26-2.30 (ddd, $J_{1,2} = J_{3,4} = J_{5,6}$ = 2.8 Hz, $J_{1,3} = J_{2,4} = J_{3,5} = J_{4,6}$ = 6.8 Hz, 2H, $C\mathbf{H}_2C{\equiv}CH$), 3.29 (t, J = 7.2 Hz, 2H, $NCH_2C\mathbf{H}_2S$), 3.37 (t, J = 7.2 Hz, 2H, $C\mathbf{H}_2C{=}O$), 4.57 (t, J = 7.2 Hz, 2H, $NC\mathbf{H}_2CH_2S$). ^{13}C NMR (400 MHz, $CDCl_3$): δ = 17.72, 23.47, 28.33, 37.35, 55.95, 69.21, 83.40, 174.07, 201.56. FT-IR: 1049 cm^{-1} (C=S), 1693 cm^{-1} (C=O), 3287 cm^{-1} (C≡CH). HRMS (EI): calcd. for $C_9H_{11}NOS_2$ $[M + H]^+$ 214.0360; found 214.0362.

3.2.10 Activation of 5-hexynoic acid by N-hydroxysuccinimide (NHS)

5-Hexynoic acid (500 mg, 4.46 mmol), NHS (513 mg, 4.46 mmol), and DMAP (54 mg, 0.45 mmol) were dissolved in 20 mL of THF. DCC (1.11 g, 5.35 mmol) in 10 mL of THF was added dropwise to the solution, which was stirred at room temperature for 6 hours. The solution was filtered to remove the salt. After removal of solvent and silica gel column chromatography (3:1 mixture of hexane and ethyl acetate), NHS-activated 5-hexynoic acid was obtained as colorless crystals (670 mg, 72% yield). ^{1}H NMR (300 MHz, $CDCl_3$): δ = 1.84-1.94 (m, 2H, $CH_2C\mathbf{H}_2CH_2$), 1.99 (t, J = 2.7 Hz, 1H, C≡C**H**), 2.24-2.31 (m, 2H, $C\mathbf{H}_2CO$), 2.67-2.73 (m, 2H, $C\mathbf{H}_2C{\equiv}CH$), 2.77 (s, 4H, $O{=}CC\mathbf{H}_2C\mathbf{H}_2C{=}O$). ^{13}C NMR (400 MHz, $CDCl_3$): δ = 17.49, 23.28, 23.39, 25.54, 29.59,

69.87, 82.46, 168.20, 169.29. IR ($CHCl_3$): 1730 cm^{-1} (C=O), 3285 cm^{-1} (C≡CH). HRMS (EI): calcd. for $C_{10}H_{11}NO_4$ $[M + H]^+$ 210.0766; found 210.0770.

3.2.11 Preparation of alkynyl-functionalized silica NP's (15 nm)

A THF solution (30 mL) of amino-functionalized silica NP's (2.70 g) was added dropwise to a THF solution (30 mL) of 2-mercaptothiazoline-activated 5-hexynoic acid (0.50 g, 2.3 mmol) or NHS-activated 5-hexynoic acid (0.48 g, 2.3 mmol) at room temperature. After complete addition, the solution was stirred for 6 hours. The reaction mixture was then precipitated into a large amount of 4:1 mixture of cyclohexane and ethyl ether (500 mL). The particles were recovered by centrifugation at 3000 rpm for 15 minutes. The particles were then redissolved in 30 mL of THF and reprecipitated in 4:1 mixture of cyclohexane and ethyl ether. This dissolution-precipitation procedure was repeated another two times. 2.91 g NP's as light-yellow powders were obtained after drying in a vacuum oven at room temperature. FT-IR: 800 cm^{-1} (Si-C), 1096 cm^{-1} (Si-O), 3323 cm^{-1} (C≡CH). A small amount of amino-functionalized silica NP's from the same batch were functionalized by activated CPDB following the same procedure, and the graft density was estimated by UV-vis analysis,[3] which was assumed the same as that of alkynyl-functionalized NP's.

3.2.12 Synthesis of 6-azidohexyl 4-cyano-4-(phenylcarbonothioylthio)pentanoate (azido-functionalized CPDB)

1-Azido-6-hydroxyhexane was synthesized according to the methods published previously.[30] CPDB (878 mg, 3.15 mmol), 1-azido-6-hydroxyhexane (500 mg, 3.49 mmol), and dicyclohexylcarbodiimide (DCC) (720 mg, 3.49 mmol) were dissolved in 30 mL of dichloromethane. (Dimethylamino)pyridine (DMAP) (128 mg, 1.05 mmol) in 5 mL of dichloromethane was added slowly to the solution, which was stirred at room

temperature overnight. The solution was filtered to remove the salt. After removal of solvent and silica gel column chromatography (10:1 mixture of hexane and ethyl acetate), azido-functionalized CPDB, was obtained as a dark red oil (798 mg, 63% yield). ^{1}H NMR (300 MHz, $CDCl_3$): δ = 1.35-1.39 (m, 4H, $N_3CH_2(C\mathbf{H}_2)_2$), 1.54-1.66 (m, 4H, $N_3(CH_2)_3(C\mathbf{H}_2)_2$), 1.91 (s, 3H, $C\mathbf{H}_3$), 2.36-2.69 (m, 4H, $C(C\mathbf{H}_2)_2(C{=}O)O$), 3.24 (t, J = 6.8 Hz, 2H, $C\mathbf{H}_2N_3$), 4.09 (t, J = 6.6 Hz, 2H, $C\mathbf{H}_2OC{=}O$), 7.37 (t, J = 7.8 Hz, 2H, Ar), 7.54 (t, J = 7.4 Hz, 1H, Ar), 7.88 (dd, $J_{1,2} = J_{3,4}$ = 1.2 Hz, $J_{1,3} = J_{2,4}$ = 8.4 Hz, 2H, Ar). ^{13}C NMR (400 MHz, $CDCl_3$): δ = 24.09, 25.48, 26.32, 28.39, 28.70, 29.79, 33.40, 45.75, 51.28, 64.94, 118.49, 126.66, 128.57, 133.06, 144.48, 171.54, 222.33. FT-IR: 1181 cm^{-1} (PhC=S), 1732 cm^{-1} (C=O), 2094 cm^{-1} (N_3). HRMS (EI): calcd. for $C_{19}H_{24}N_4O_2S_2$ $[M]^+$ 404.1341; found 404.1347.

3.2.13 Synthesis of azido-capped poly(methyl methacrylate) (N_3-PMMA)

A solution of MMA (1.0 g, 10 mmol), azido-functionalized CPDB (13.4 mg, 33 μmol), V-70 (3.3 μmol), and THF (1.0 mL) was prepared in a dried Schlenk tube. The mixture was degassed by three freeze-pump-thaw cycles, back filled with nitrogen, and then placed in an oil bath at 40 °C for 15 hours. The polymerization solution was quenched in ice water and the resultant azido-capped polymer was precipitated in hexane. Molecular weight characteristics were analyzed by GPC.

3.2.14 Preparation of Janus NP's via reversible click reaction

Azido-functionalized silica particles (500 nm, 0.4 g), alkynyl-functionalized silica NP's (15 nm, 80 mg) and N,N,N',N',N''-pentamethyldiethylenetriamine (PMDETA) (0.5 μL, 2 μmol) were dispersed/dissolved in DMF (50 mL). The mixture was degassed by flushing nitrogen for 30 min, and then CuBr (0.3 mg, 2 μmol) was added. After the click reaction under nitrogen protection at room temperature for one day, the suspension was

centrifuged at 5000 rpm for 10 minutes, and redispersed in DMF (50 mL). This centrifugaion-dispersion process was repeated another two times. The precipitated 500 nm particles with 15 nm NP's attached on the surface were collected, and the free unreacted alkynyl-functionalized NP's were removed together with the liquid phase. Afterwards, the particle complexes in DMF (50 mL) were added into a three-neck flask with azido-capped PMMA (7.2 μmol) and a trace amount of PMDETA. After 30 minutes of nitrogen flushing, a trace amount of CuBr was added for another one-day click reaction. Finally, the unreacted PMMA was removed by centrifugation at 5000 rpm, and the particle complexes were redispersed in THF. The suspension was ultrasonicated for one hour, and sequentially centrifuged at 3000 rpm for 15 minutes and filtered. The Janus NP's were obtained in the liquid phase. FT-IR: 802 cm^{-1} (Si-C), 1105 cm^{-1} (Si-O), 1733 cm^{-1} (C=O), 3360 cm^{-1} (C≡CH).

3.3 Results and Discussion

3.3.1 Approach I: anchoring silica NP's on silicon wafer by hydrogen bonding

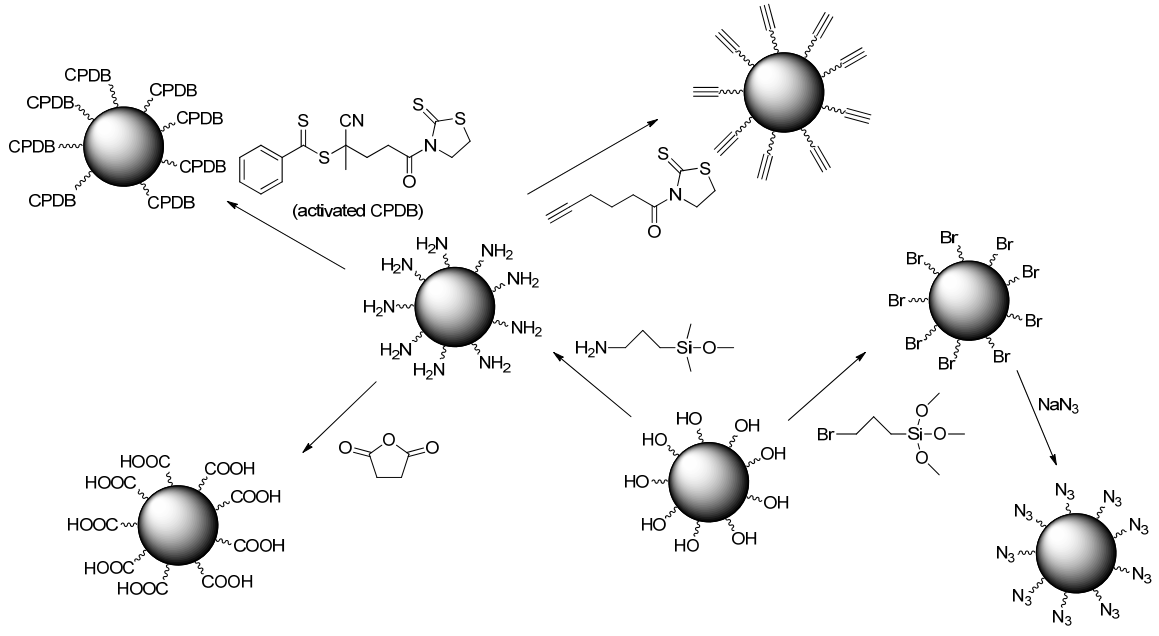

Scheme 3.1 Surface functionalization of silica particles.

Silica particles produced in a "sol-gel" process (the Stober synthesis) have hydroxyl groups uniformly spread over its surface (Si-OH),[28] which can readily react with silanes carrying diverse functional groups. Starting with the hydroxylated surface, silica particles with various functionalities have been facilely synthesized in a facile manner (Scheme 3.1). The synthetic strategies can be applied for particles with different diameters from 15 nm to 600 nm, and the graft density was achieved in a range from 0.01 to 0.7 units/nm^2. In this research, several types of the functionalized silica particles were selected from this pool to synthesize polymer-grafted Janus particles.

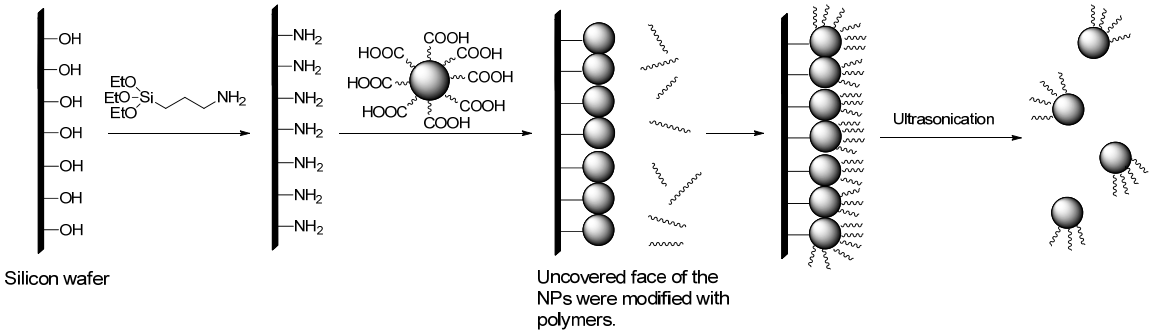

Figure 3.1 Synthetic route of PEG-grafted Janus particles using silicon wafers as substrates.

Initially, silica particles functionalized with carboxylic acids were immobilized on a planar amino-functionalized silicon wafer to partially protect their surface, which then allowed further modification of the uncovered faces of the particles with properly end-functionalized polymers. After grafting of the polymers on the unprotected surfaces, the silica particles were removed from the substrate to generate Janus architectures.

Silicon wafers were an ideal option as the solid substrate because they have well-defined surfaces due to the highly crystalized structures. Moreover, they possess similar surface chemistry to silica particles, so similar reactions can be applied to functionalize its surface. Figure 3.1 shows the general procedure using amine-acid coupling to

assemble a monolayer of silica particles on the surface of silicon wafers. Modifying the uncovered face of the particles with polymer can be performed using two approaches – "grafting to" and "grafting from". In comparison, the "grafting to" approach is more straightforward and easier to operate, so it was our preferential choice. Since carboxylic acids on the uncovered face of the particles were still reactive, the silicon wafer carrying particles was immersed into a solution of PEG-OH. Under the catalysis of DCC and DMAP, the hydroxyl groups covalently coupled with the acids on the particles to achieve the attachment. Because of the large size of PEG-OH (M_n = 5k), it was difficult for the polymer chains to attach on the covered face of the particles, which ensured the anisotropic architecture. Finally, the particles were removed from the wafer by sonication.

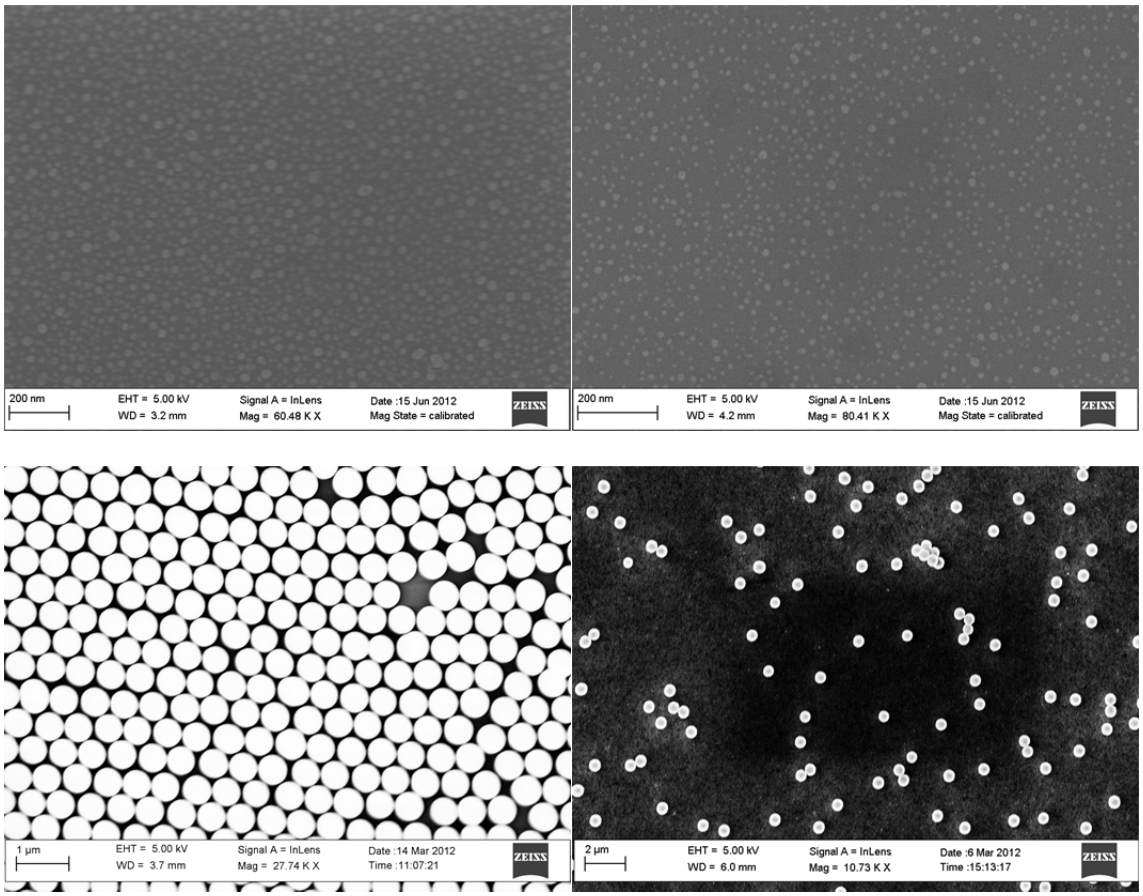

Figure 3.2 SEM images of different sizes of silica particles immobilized on silicon wafers with different densities: 15 nm NP's with high graft density (top left), 15 nm NP's with low graft density (top right), 500 nm particles with high graft density (bottom left) and 500 nm particles with low graft density (bottom right).

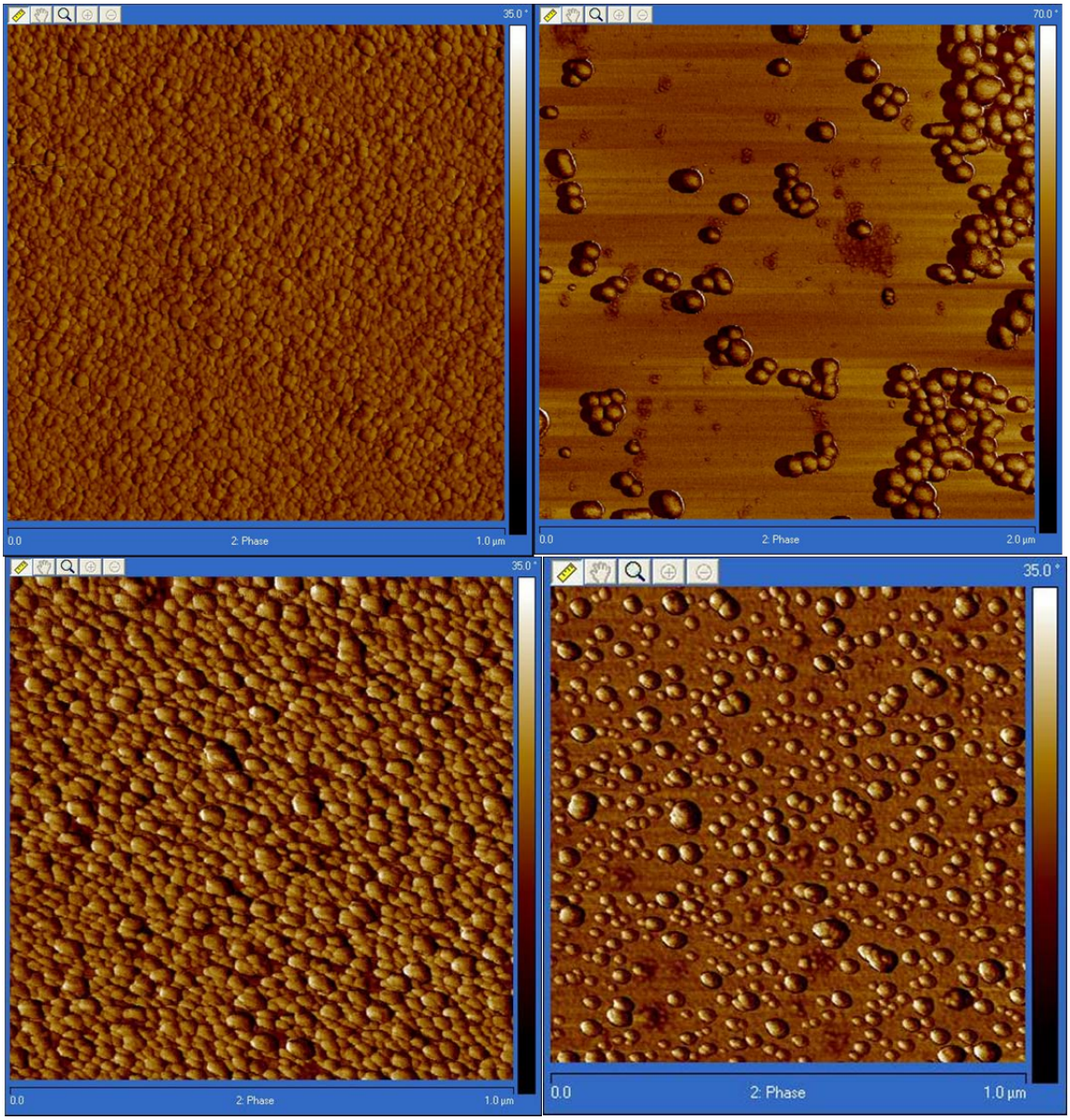

Figure 3.3 Phase images of different sizes of silica particles immobilized on silicon wafers with different densities captured by AFM: 15 nm NP's (top left), 500 nm particles (top right), 50 nm NP's with high graft density (bottom left) and 50 nm NP's with low graft density (bottom right).

Both SEM and AFM were applied to study the surface morphology of the silicon wafers after the silica particles were anchored (Figure 3.2 and 3.3). Particles with average

diameters of 15 nm, 50 nm and 500 nm were used to form monolayers on the wafers, and the attachment was achieved successfully for all the batches. Monolayers of particles on wafers were generated even without the addition of DCC and DMAP, and the graft density was similar to that with catalysts in the same reaction time, indicating that the particles can be effectively absorbed on the wafers by a surface layer of hydrogen bonding. In addition, it took less time of sonication (15 minutes) to remove the particles from the wafers for the hydrogen-bonding-attached samples than the covalent attached ones, and the larger particles were released easier than the smaller ones. It was also observed that the graft density of the particles on the wafers could be roughly tuned by adjusting the reaction time.

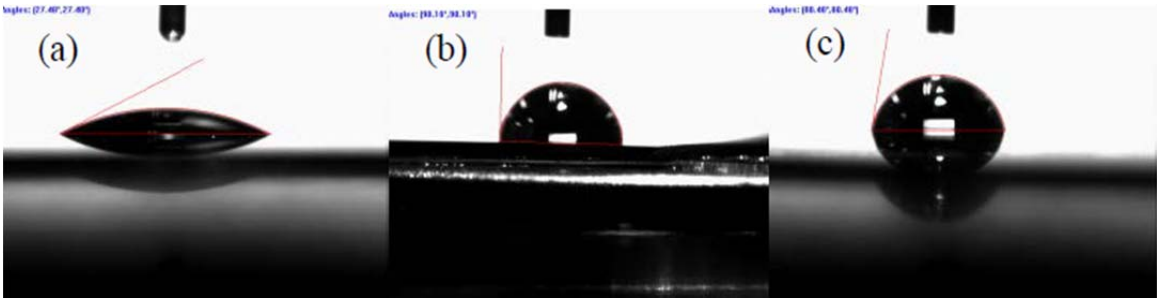

Figure 3.4 Contact angles of water on silicon wafers: (a) bare silicon wafer; (b) silicon wafer covered by silica NP's (15 nm); (c) silicon wafer b treated with PEG-OH.

Contact angles of water on different silicon wafers were measured to verify the changes of the surface properties after each step of modifications (Figure 3.4). In comparison with the bare silicon wafer (27.4°), the contact angle on the silicon wafer covered by silica NP's (90.1°) increased dramatically. This was mainly because the NP's distribution changed the morphology and increased the surface roughness of the wafer. Subsequently, the decrease of the contact angle (80.4°) after PEG-OH treatment was attributed to the hydrophilic property of the polymer.

This initially appeared to be a very promising method to produce polymer-grafted Janus NP's due to the efficient reversible hydrogen bonding layers under mechanical force. However, it had a significant disadvantage – very low yields. About 20 cm^2 of silicon wafers were applied in the experiments. Because of the limit of the surface area per wafer, less than 10 mg of particles could be afforded even if they were fully collected after the modification. Additionally, many silica particles were absorbed on the wall of the glassware during the rotary evaporation process. Therefore, the final sample size collected was so small that there were even insufficient particles for TEM tests, and it was very necessary to design another approach with improved yields.

3.3.2 Approach II: reversible click reaction

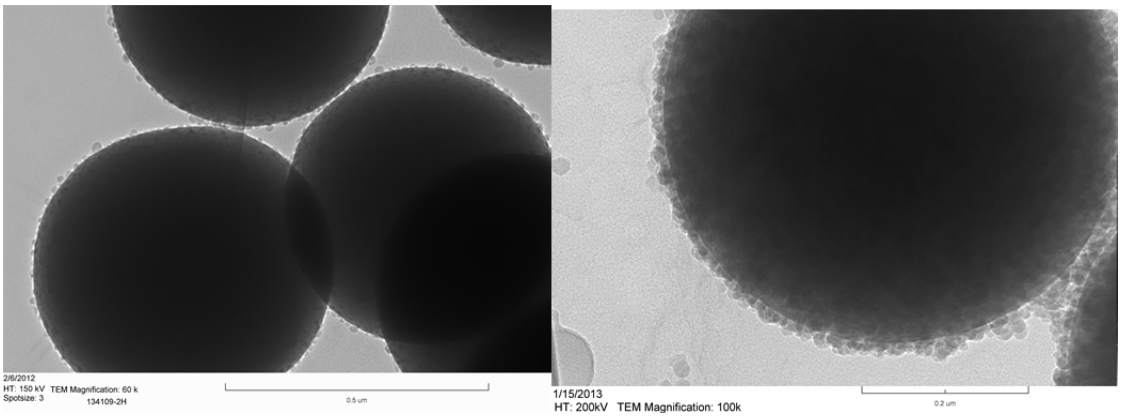

Figure 3.5 Attachment of 15 nm NP's on the surface of 500 nm particles by multiple hydrogen bonding (left) and click reaction (right).

In Approach II, silica particles with an average diameter of 500 nm were chosen as substrates to immobilize silica NP's with an average diameter of 15 nm on their surfaces. Considering the relatively small size, the 500 nm silica particles have much larger specific surface area than those planar substrates,[9,10,17] thus more NP's could be partially masked with the same volume of substrates. Moreover, they are easy to be synthesized, precipitated and redispersed in various solvents, and these properties simplified the

experimental operations. Two types of reversible chemistry were performed to anchor the 15 nm NP's on the 500 nm particles – hydrogen bonding by carboxylic acid-amine groups and the click reaction between an azide and alkyne. The assemblies of the particles through these two pathways are displayed in Figure 3.5 with the same concentrations of particles and similar graft densities of functional groups. As Figure 3.5 shows clearly, the latter approach could attained a much denser NP attachment, which was chosen for the further experiments.

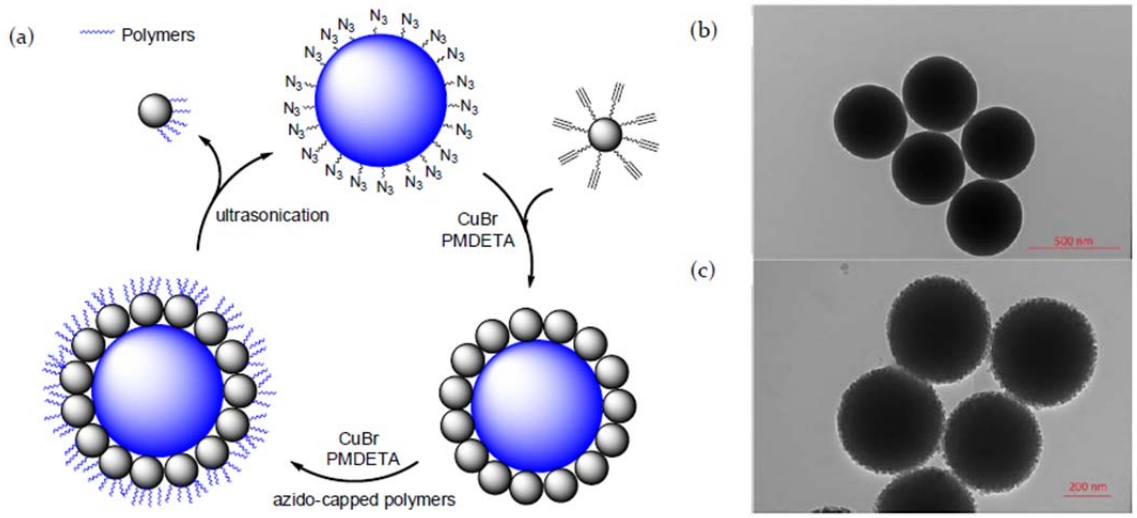

Figure 3.6 (a) Schematic illustration of the cyclic synthetic route for polymer-grafted Janus silica NP's by combining reversible click reaction and "grafting to" strategies. (b) TEM image of azido-functionalized 500 nm particles. (c) TEM image of 500 nm particles with 15 nm NP's attached.

The cyclic synthetic route is depicted in Figure 3.6a. First, the surfaces of 500 nm particles (Figure 3.6b) and 15 nm NP's were functionalized by azido and alkynyl groups, respectively. Then the 15 nm NP's were attached on the surface of the 500 nm particles via the copper-mediated click reaction (Figure 3.6c). All free 15 nm NP's were removed in a repeated centrifugation-dispersion process, noting that the 500 nm particles can be precipitated in DMF under centrifugation at 5000 rpm but the 15 nm NP's remain

suspended. Next, azido-capped poly(methyl methacrylate) (N_3-PMMA) was added into the suspension of the particle complexes in DMF, and the exposed surface of the 15 nm NP's was modified by N_3-PMMA through a click reaction again using a "grafting to" strategy. Finally, the PMMA-grafted Janus NP's were released under sonication, and the 500 nm particles could be recycled for another round of attachment.

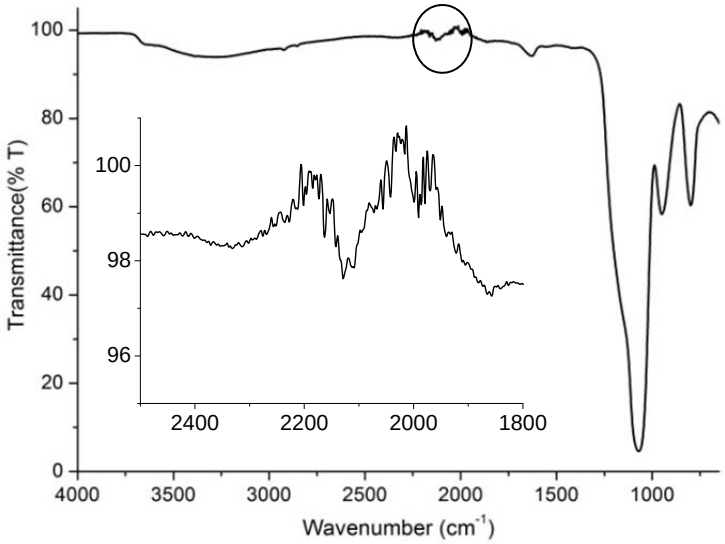

Figure 3.7 FT-IR spectra of azido-functionalized silica particles (500 nm).

Due to the low surface to volume ratio of the 500 nm particles, the surface functionalities were hardly detected through conventional methods, such as FT-IR and NMR, even though excess amounts of BPTMS and sodium azide were added in each step to maximize the graft densities. An azide absorption was displayed as a barely perceptible peak at 2120 cm^{-1} in the FT-IR spectrum of the azido-functionalized particles (Figure 3.7). Thus, X-ray photoelectron spectroscopy (XPS) was utilized to confirm the surface functionalities of the 500 nm particles. XPS analysis of the bromo-functionalized particles was verified by the presence of C 1s and Br 3d (Figure 3.8a and 3.8b). The C 1s region was observed as two overlapping peaks with binding energies of 286.7 eV and 285.0 eV which were assigned to C-Br and C-H/C-C groups, respectively. A more

distinctive bromine peak was observed at 70.8 eV consisting of Br $3d_{5/2}$ and Br $3d_{3/2}$ components. After the conversion of bromide to azide, the N 1s region appeared as two slightly merged peaks at 402.5 eV and 400.5 eV with an expected peak area ratio of 1:2 (Figure 3.8d), corresponding to the N^+ and N^- species of azide on the surface. The emergence of the two peaks was consistent with previous observations because of the degradation of azide under X-ray exposure.[31] In addition, both of the peaks of C-N (286.5 eV) and C-C/C-H (285.0 eV) were observed in the C 1s region (Figure 3.8c), and the other peak with binding energy of 288.7 eV was attributed to the degradation of azide. Therefore, the XPS analysis verified the functionalization and conversion of the groups on the surface of the 500 nm particles.

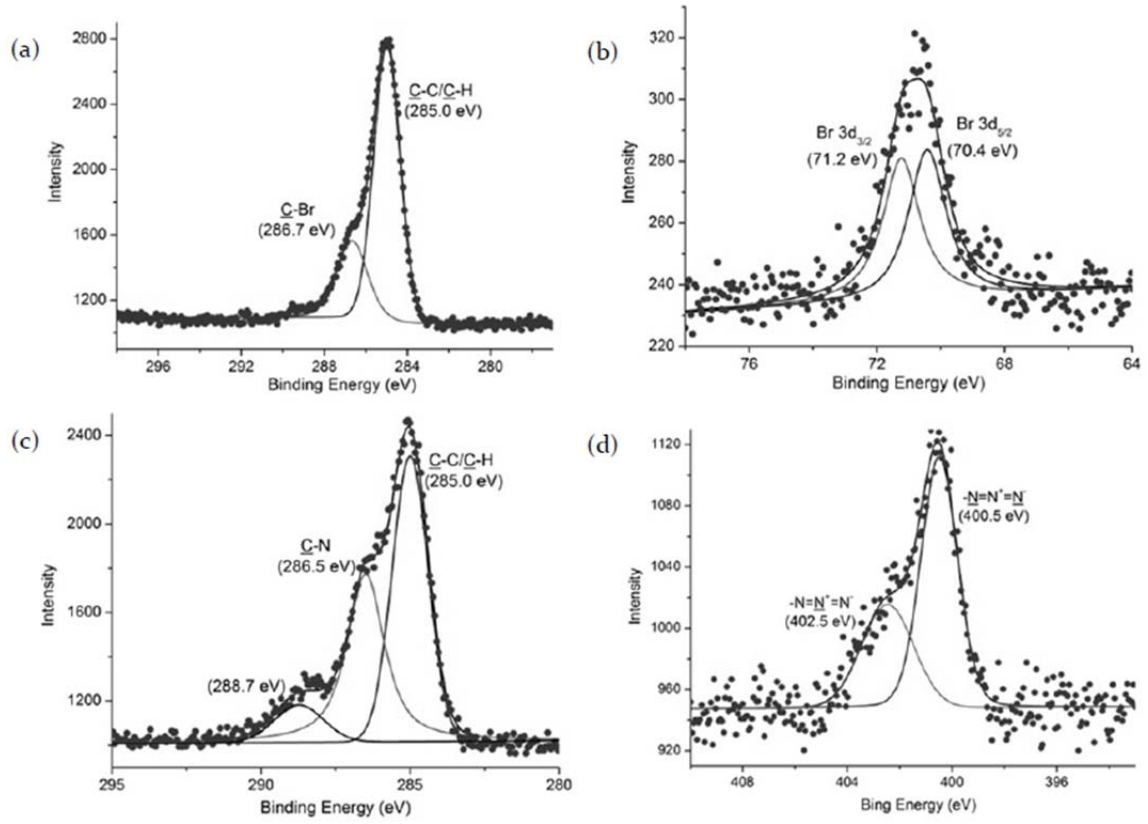

Figure 3.8 (a) C 1s and (b) Br 3d core level XPS spectra of bromo-functionalized 500 nm particles; (c) C 1s and (d) N 1s core level XPS spectra of azido-functionalized 500 nm particles. Binding energies are calibrated to aliphatic carbon at 285.0 eV.

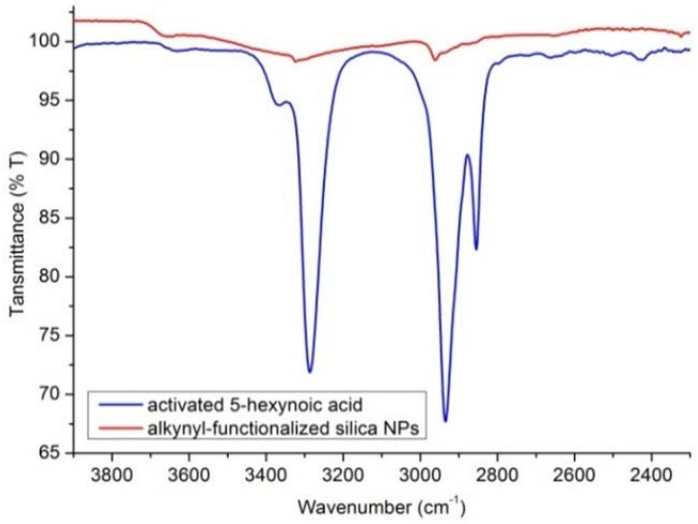

Figure 3.9 FT-IR spectra of activated 5-hexynoic acid and alkynyl-functionalized silica NP's (0.4 alkyne/nm^2) in a range of wavenumber from 2300 cm^{-1} to 3900 cm^{-1}.

In contrast, the alkynyl-functionalization of 15 nm NP's was easily verified by the absorption at 3323 cm^{-1} ascribed to C≡CH in the FT-IR spectrum (Figure 3.9), and UV-vis spectra were used to calculate the alkyne graft densities. 5-Hexynoic acid could react with the amino-functionalized NP's directly catalyzed by DCC and DMAP to attain the alkynyl-functionalization, but the efficiency was very low for this surface reaction. Moreover, the precipitates generated by DCC were difficult to be separated from the NP's resulting in a large loss of NP's. Therefore, 5-hexynoic acid was activated by 2-mercaptothiazoline or NHS first, and then coupled to the amino groups on the NP's surface with a higher reactivity. All small-molecular byproducts were washed away through the dissolution-precipitation procedure. In this experiment, silica NP's with high graft density (0.7 alkyne/nm^2) were synthesized. However, in the following step, it was difficult to break the attachment between these NP's and 500 nm azido-functionalized particles under sonication for more than one hour. It was hypothesized that, too many "triazole" linkages were formed between the surfaces attributed to the high graft

densities, and the ultrasound was not effective enough to cleave all the bonds. When NP's with graft density of 0.4 alkyne/nm^2 were used for the procedure, most of the resultant Janus NP's could be released after sonication for 30 min.

The click reaction generated covalent linkages between the particles, which were much stronger than non-covalent absorptions,[7,16] reducing the chance that the NP's might be washed away from the surface of the substrates during processing. A controlled reaction was carried out between the two sizes of particles without copper (I) bromide catalyst, which showed that attachment did not occur after overnight stirring. It was previously reported that chain scission of polymers through the mechanochemical "unclick" reaction was dependent on the molecular weights of the polymer blocks.[25] Thus, it is easier to break a 1,2,3-triazole ring if the masses on both sides of the ring are heavier. Because the particles used in this study were much heavier than individual polymer chains, the cleavage occurred readily. Additionally, collision and friction between the particles during sonication may have also assisted the cleavage. It is worth noting that after collection by centrifugation, the 500 nm particles were ready to react with alkynyl-functionalized NP's again without any further treatments, and similar particle complexes were obtained as observed in the first round, indicating that the azido groups on the particle surface had been recovered.

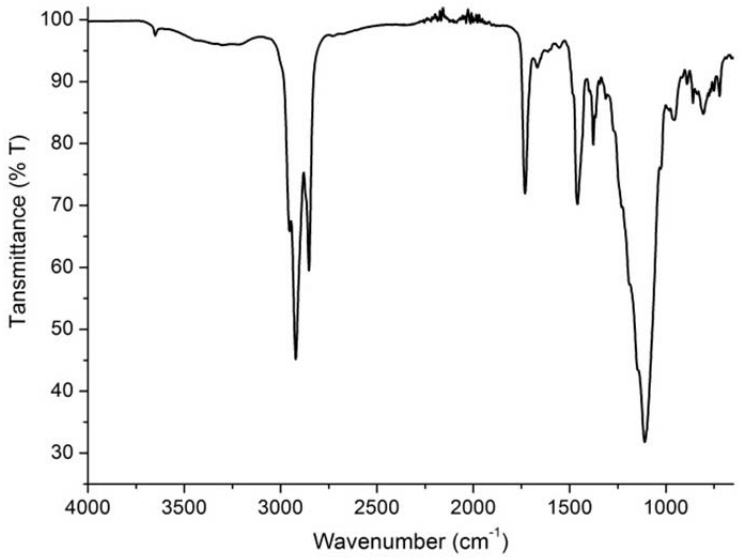

Figure 3.10 FT-IR spectra of PMMA-grafted Janus silica NP's (the initial graft density was 0.4 alkyne/nm^2).

The N_3-PMMA for Janus NP modification was synthesized via RAFT polymerization using an azido-functionalized chain transfer agent. To enhance the selectivity of the "unclick" reaction and prevent the risk that the grafted polymers might be removed from the surfaces during sonication, polymers with low molecular weights (PMMA: M_n = 13.3k, PDI = 1.11) and short ultrasound times (within one hour) were applied. After the treatment with azido-capped PMMA, the FT-IR spectrum of the PMMA-grafted Janus NP's revealed a characteristic absorption of PMMA (Figure 3.10, e.g., 1732 cm^{-1} ascribed to the carbonyl groups), which indicated the attachment of the polymer. TEM images also showed that there were significant changes on the surface of the particle complex (Figure 3.11). However, the asymmetric geometry of individual Janus NP cannot be observed by TEM due to their small size.

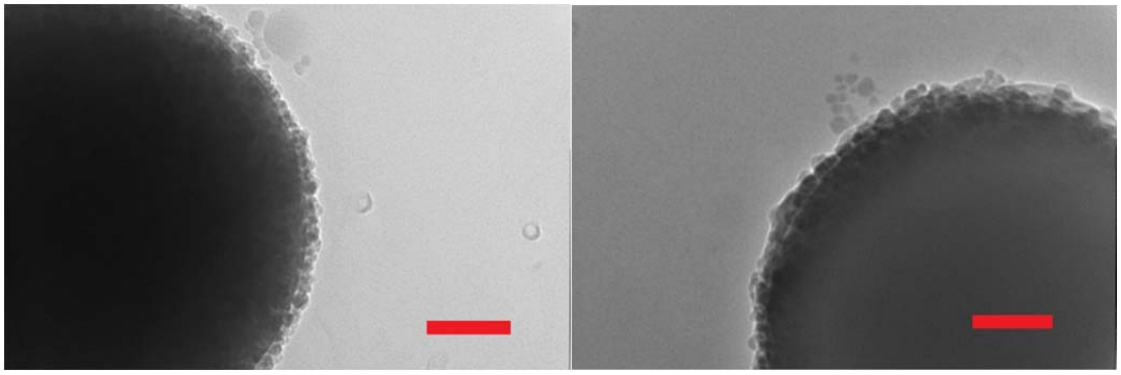

Figure 3.11 TEM images of 500 nm particles with 15 nm NP's attached before (left) and after (right) PMMA modification (PMMA: M_n = 13.3k, PDI = 1.11). The scale bars are 100 nm.

In addition, a contrast test was designed to demonstrate the partial functionalization of the Janus NP's: 500 nm particles having attachment of 15 nm NP's were used in one group, while free alkyne-functionalized NP's were in the other group with the same grafted density (0.4 alkyne/nm^2) and amount as the attached NP's. Both of them were treated with identical N_3-PMMA solution in DMF though the copper-mediated click reaction. After work-up, PMMA-functionalized Janus NP's and uniform NP's were produced, respectively. The NP's were subjected to TGA analysis, which showed that the Janus NP's exhibited an overall weight loss of 24% while the uniform NP's exhibited an overall weight loss of 35% (Figure 3.12). Considering the weights of the alkynyl-functionalization and other small molar mass impurities, the calculation indicated that the Janus NP's had about 16 wt% of PMMA grafted, and the uniform NP's had 26 wt% of PMMA. With the similar reaction conditions, the two groups of NP's should have similar polymer graft densities if all reaction sites were available. Accordingly, the explanation for the lower amount of PMMA on the Janus NP's was that its surface had only been partially modified.

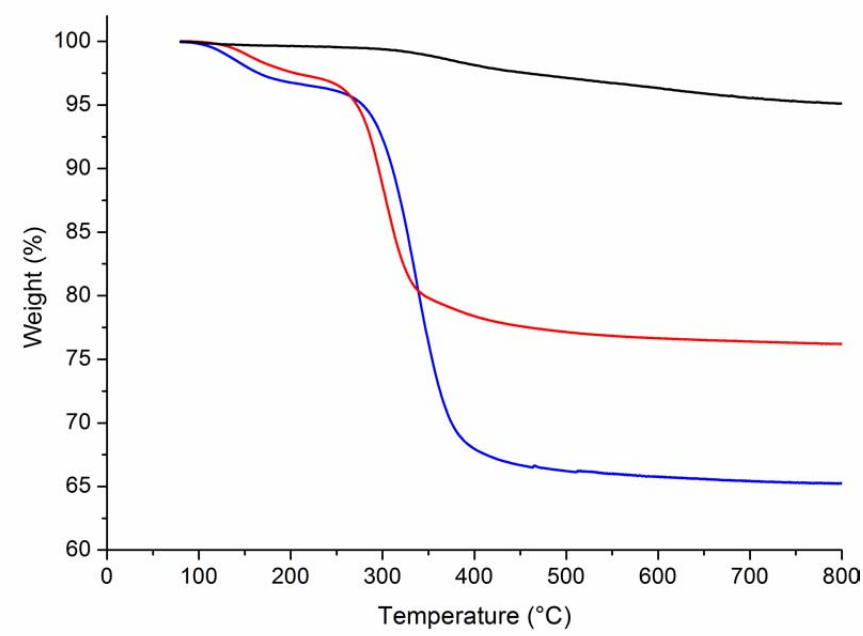

Figure 3.12 TGA scans of alkyne-functionalized NP's (black), PMMA-grafted Janus NP's (red) and PMMA-grafted uniform NP's (blue).

Although their anisotropic properties cannot be demonstrated by observing individual NP's, the PMMA-grafted Janus NP's dispersed with unique self-assembly behaviors which were investigated by TEM in different solvents and concentrations. Initially, when the sample was prepared with 3.1 mg/mL of PMMA-grafted NP's in THF, individual NP's were displayed in the TEM image (Figure 3.13a). Next, micelle-like structures in a range from 50 nm to 100 nm were detected when the solution was diluted to 0.62 mg/mL (Figure 3.13b), and this self-assembly was probably due to the different solubilities of the two faces of the Janus NP's. Since the PMMA-grafted Janus NP's have both solvophilic and solvophobic faces, it was logical to assume that they can act as nano-surfactants in solution. Nevertheless, unlike the critical micelle concentration of molecular surfactants, our observation implied that there was a maxmum limit of concentration for the Janus NP's beyond which micelles cannot be formed.

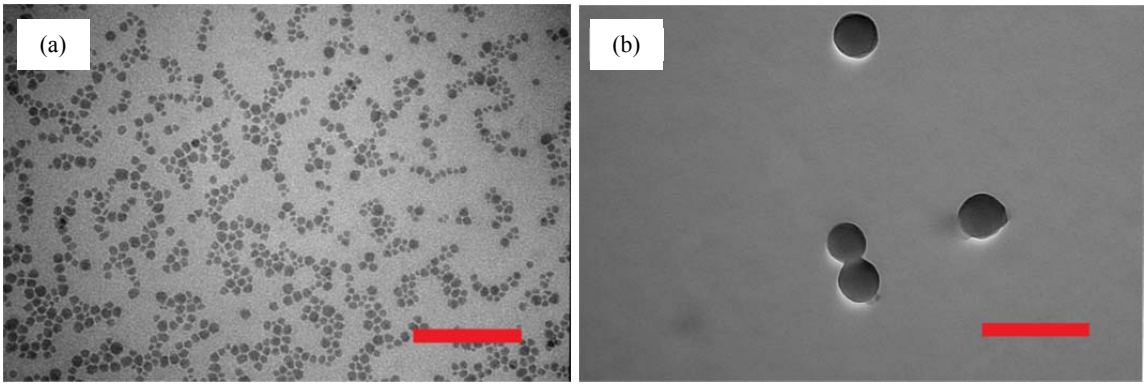

Figure 3.13 TEM images of (a) PMMA-grafted Janus NP's (15 nm) in THF (3.1 mg/mL); (b) PMMA-grafted Janus NP's (15 nm) in THF (0.62 mg/mL). The scale bars are 200 nm.

When samples of the PMMA-grafted Janus NP's were prepared in DMF, individual NP's could always be observed regardless of the concentrations. The different behaviors of the Janus NP's in THF and DMF were also verified by AFM analysis (Figure 3.14). The AFM image of the THF sample showed that the center of the round structures was thicker and softer, and their edge was thinner and harder, which were presumably deformed micelles resulting from the drying effect.

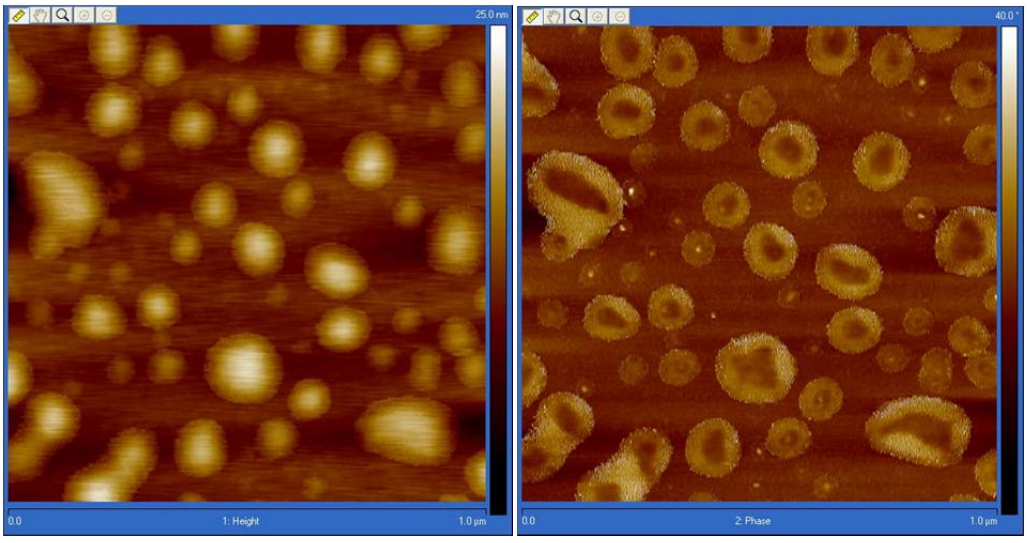

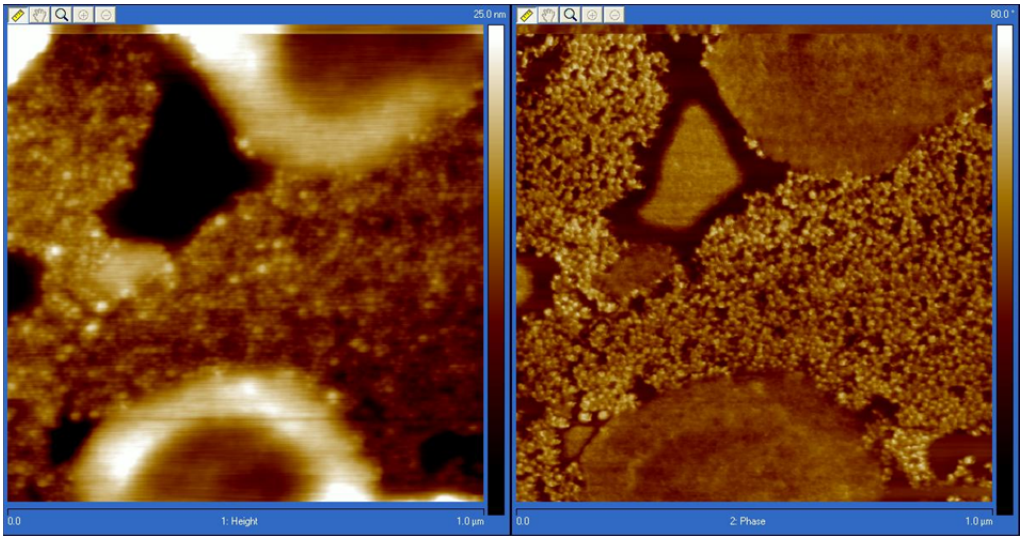

Figure 3.14 AFM studies on PMMA-grafted Janus NP's: top left – height image of Janus NP's prepared in THF; top right – phase image of Janus NP's prepared in THF; bottom left – height image of Janus NP's prepared in DMF; bottom right – phase image of Janus NP's prepared in DMF. All the samples were prepared by solutions with concentration of about 0.6 mg/mL.

Another experiment was conducted using both Janus and non-Janus NP's. When alkynyl-functionalized non-Janus NP's in DMF (0.4 alkyne/nm^2, 0.3 mg/mL) were gradually added into the solution of PMMA-grafted Janus NP's with the same concentration, a series of very interesting mutations of NP dispersion were displayed in the TEM analysis. Starting from the dispersion of pure Janus NP's (Figure 3.15a), micelle-like structures were generated immediately after addition of a few drops of the non-Janus NP's solution (Figure 3.15b). A reasonable explanation is that the Janus NP's behaved as nano-surfactants and covered the non-Janus NP's to form micelles ascribed to their better solubility and asymmetric properties. Then the micelle-like structures disappeared with the sample containing about 15% of the non-Janus NP's. Instead, the NP's were arranged around a few cyclical areas (Figure 3.15c). This dispersion might attributed to collapse of the unstable micelles, since not enough Janus NP's were available to cover the whole surface when more non-Janus NP's were added. Eventually,

when the proportion of the non-Janus NP's was high enough (> 50%), the NP rings vanished completely, and only single NP's and NP clusters could be detected (Figure 3.15d), which was similar to the dispersion of pure Janus NP's.

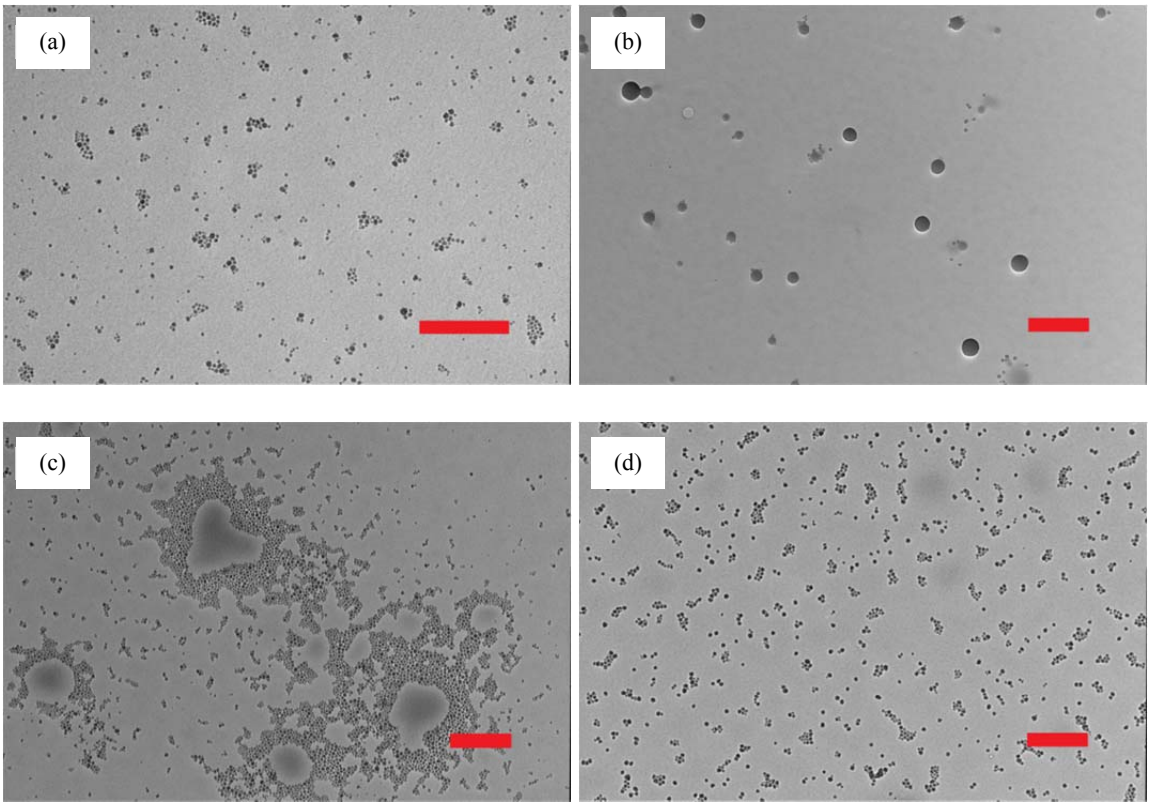

Figure 3.15 TEM images showing the dispersion changes (a→d) of the PMMA-grafted Janus NP's in DMF (0.3 mg/mL) with a gradual addition of alkynyl-functionalized NP's (0.3 mg/mL). The scale bars are 500 nm.

3.4 Conclusions

In this effort, we evaluated different routes to synthesize polymer-grafted Janus NP's. First, the Granick procedure failed due to the size limitation of this technique. Then we developed an approach with planar silicon wafers as the face-blocking substrates, which provided very low yields inherent in the low surface to volume ratio of the substrates. Eventually, we designed a facile and cyclic method involving the reversible click reaction. A novel mechanochemical approach was introduced into the particle

interactions to selectively achieve the protection-deprotection process of NP's, and used in combination with polymer modification of the unprotected surfaces of the NP's by a "grafting to" strategy. Although silica NP's were used as a template in the current experiments, this approach appears universal and can be performed on NP's of various materials to introduce asymmetric surface coverage as long as their surfaces are properly functionalized. Moreover, our research demonstrated that NP's could be another type of material suitable for mechanochemistry in addition to polymers. Preliminary investigations of the unique self-assembly behaviors of the polymer-grafted Janus NP's were conducted by TEM and AFM in different solvents and concentrations, implying their potential applications as nano-surfactants.

3.5 Refereneces

1. Reculusa, S.; Poncet-Legrand, C.; Perro, A.; Duguet, E.; Bourgeat-Lami, E.; Mingotaud, C.; Ravaine, S. *Chem. Mater.* **2005**, *17*, 3338-3344.

2. (a) Chen, Y.; Liang, F.; Yang, H.; Zhang, C.; Wang, Q.; Qu, X.; Li, J.; Cai, Y.; Qiu, D.; Yang, Z. *Macromolecules* **2012**, *45*, 1460-1467. (b) Liu, B.; Liu, J.; Liang, F.; Wang, Q.; Zhang, C.; Qu, X.; Li, J.; Qiu, D.; Yang, Z. *Macromolecules* **2012**, *45*, 5176-5184. (c) Tang, C.; Zhang, C.; Sun, Y.; Liang, F.; Wang, Q.; Li, J.; Qu, X.; Yang, Z. *Macromolecules* online.

3. Jia, L.; Zhou, F.; Liu, W. *Chem. Commun.* **2012**, *48*, 12112-12114.

4. de Gennes, P-G. *Angew. Chem., Int. Ed.* **1992**, *31*, 842-845.

5. Jiang, S.; Chen, Q.; Tripathy, M.; Luijten, E.; Schweizer, K. S.; Granick; S. *Adv. Mater.* **2010**, *22*, 1060-1071.

6. Perro, A.; Reculusa, S.; Ravaine, S.; Bourgeat-Lami, E.; Duguet, Etienne. *J. Mater. Chem.* **2005**, *15*, 3745-3760.

7. (a) Hong, L.; Jiang, S.; Granick, S. *Langmuir* **2006,** *22,* 9495-9499. (b) Jiang, S.; Granick, S. *Langmuir* **2008,** *24,* 2438-2445. (c) Jiang, S.; Schultz, M. J.; Chen, Q.; Moore, J. S.; Granick, S. *Langmuir* **2008**, *24*, 10073-10077.

8. Wang, F.; Phonthammachai, N.; Mya, K. Y.; Tjiua, W. W.; He, C. *Chem. Commun.* **2011**, *47*, 767-769.

9. Zhao, Z.; Shi, Z.; Yu, Y.; Zhang, G. *Langmuir* **2012**, *28*, 2382-2386.

10. Tang, J. L.; Schoenwald, K.; Potter, D.; White, D.; Sulchek, T. *Langmuir* **2012**, *28*, 10033-10039.

11. (a) Akcora, P.; Liu, H.; Kumar, S. K.; Moll, J.; Li, Y.; Benicewicz, B. C.; Schadler, L. S.; Acehan, D.; Panagiotopoulos, A. Z.; Pryamitsyn, V.; Ganesan, V.; Ilavsky, J.; Thiyagarajan, P.; Colby, R. H.; Douglas, J. F. *Nature Materials* **2009**, *8*, 354-359. (b) Dukes, D.; Li, Y.; Lewis, S.; Benicewicz, B. C.; Schadler, L. S.; Kumar, S. K. *Macromolecules* **2010**, *43*, 1564-1570. (c) Akcora, P.; Kumar, S. K.; Sakai, V. G.; Li, Y.; Benicewicz, B. C.; Schadler, L. S. *Macromolecules* **2010**, *43*, 8275-8281. (d) Maillard, D.; Kumar, S. K. Rungta, A.; Benicewicz, B. C.; Prud'homme, R. E. *Nano letters* **2011**, *11*, 4569-4573.

12. (a) Khan, J.; Harton, S. E.; Akcora, P.; Benicewicz, B. C.; Kumar, S. K. *Macromolecules* **2009**, *42*, 5741-5744. (b) Akcora, P.; Kumar, S. K.; Moll, J.; Lewis, S.; Schadler, L. S.; Li, Y.; Benicewicz, B. C.; Sandy, A.; Narayanan, S.; Ilavsky, J.; Thiyagarajan, P.; Colby, R. H.; Douglas, J. F. *Macromolecules* **2010**, *43*, 1003-1010. (c) Gao, J.; Li, J.; Benicewicz, B. C.; Zhao, S.; Hillorg, H.; Schadler, L. S. *Polymers* **2012**, *4*, 187-210.

13. Pyun, J.; Jia, S.; Kowalewski, T.; Patterson, G. D.; Matyjaszewski, K. *Macromolecules* **2003,** *36,* 5094-5104.

14. (a) Li, C.; Benicewicz, B. C. *Macromolecules* **2005,** *38,* 5929-5936. (b) Li, C.; Han, J.; Ryu, C. Y.; Benicewicz, B. C. *Macromolecules* **2006,** *39,* 3175-3183. (c) Huang, X.; Appelhans, D.; Formanek, P.; Simon, F.; Voit, B. *Macromolecules* **2011**, *44*, 8351-8360. (d) Ohno, K.; Ma, Y.; Huang, Y.; Mori, C.; Yahata, Y.; Tsujii, Y.; Maschmeyer, T.; Moraes, J.; Perrier, S. *Macromolecules* **2011**, *44*, 8944-8953. (e) Cash, B. M.; Wang, L.; Benicewicz, B. C. *J. Polym. Sci. Part A: Polym. Chem.* **2012**, *50*, 2533-2540.

15. Li, D.; Sheng, X.; Zhao, B. *J. Am. Chem. Soc.* **2005**, *127*, 6248-6256. (b) Zhao, B.; Zhu, L. *Macromolecules* **2009**, *42*, 9369-9383. (c) Horton, J. M.; Tang, S.; Bao, C.; Tang, P.; Qiu, F.; Zhu, L.; Zhao B. *ACS Macro Lett.* **2012**, *1*, 1061-1065.

16. Lupitskyy, R.; Motornov, M.; Minko, S. *Langmuir* **2008**, *24*, 8976.

17. Lattuada, M.; Hatton, T. A. *J. Am. Chem. Soc.* **2007**, *129*, 12878-12889.

18. (a) Wang, B.; Li, B.; Zhao, B.; Li, C. Y. *J. Am. Chem. Soc.* **2008**, *130*, 11594-11595. (b) Wang, B.; Li, B.; Ferrier, Jr., R. C. M.; Li, C. Y. *Macromol. Rapid Commun.* **2010**, *31*, 169-175.

19. Zhang, S.; Li, Z.; Samarajeewa, S.; Sun, G.; Yang, C.; Wooley, K. L. *J. Am. Chem. Soc.* **2011**, 133, 11046-11049.

20. Diesendruck, C. E.; Steinberg, B. D.; Sugai, N.; Silberstein, M. N.; Sottos, N. R.; White, S. R.; Braun, P. V.; Moore, J. S. *J. Am. Chem. Soc.* **2012**, *134*, 12446-12449.

21. Wiggins, K. M.; Brantley, J. N.; Bielawski, C. W. *ACS Macro Lett.* **2012**, *1*, 623-626.

22. Groote, R.; Jakobs, R. T. M.; Sijbesma, R. P. *ACS Macro Lett.* **2012**, *1*, 1012-1015.

23. (a) Kean, Z. S.; Craig. S. L. *Polymer* **2012**, *53*, 1035-1048. (b) Kean, Z. S.; Black Ramirez, A. L.; Craig. S. L. *J. Polym. Sci. Part A: Polym. Chem.* **2012**, *50*, 3481-3484. (c) Kean, Z. S.; Black Ramirez, A. L.; Yan, Y.; Craig. S. L. *J. Am. Chem. Soc.* **2012**, *134*, 12939-12942.

24. Cravotto, G.; Cintas, P. *Chem. Sci.* **2012**, *3*, 295-307.

25. Brantley, J. N.; Wiggins, K. M.; Bielawski, C. W. *Science* **2011**, *333*, 1606-1609.

26. Leibfarth, F. A.; Hawker, C. J. *Science* **2011**, *333*, 1582-1583.

27. An, Y.; Chen, M.; Xue, Q.; Liu, W. *J. Colloid. Interf. Sci.* **2007**, *311*, 507-513.

28. Stöber, W.; Fink, A.; Bohn, E. *J. Colloid Interface Sci.* **1968**, *26*, 62-69.

29. Nozawa, K.; Gailhanou, H.; Raison, L.; Panizza, P.; Ushiki, H.; Sellier, E.; Delville, J. P.; Delville, M. H. *Langmuir* **2005,** *21,* 1516-1523.

30. Li, Y.; Benicewicz, B. C. *Macromolecules* **2008**, *41*, 7986-7992.

31. Hansen, T. S.; Larsen, N. B. *Macromolecules* **2008**, *41*, 4321-4327.

CHAPTER 4

SURFACE-INITIATED RAFT POLYMERIZATION ON SILICA NANOPARTICLES WITH VARIOUS FUNCTIONAL MONOMERS

4.1 Introduction

Since inorganic nanoparticles (NP's) are typically immiscible with an organic phase, it is very challenging to control their dispersion in polymer matrices and its crucial influence on the properties of the polymer nanocomposites. An effective strategy to overcome the difficulty is growing polymer brushes, which are compatible with the matrices, on the surface of NP's. In this context, both graft density and molecular weight of the polymer brushes need to be precisely adjusted. If the graft density is too high, the polymer brushes may not be able to interact with the polymer matrices effectively because of the unfavorable enthalpy; on the other hand, if the graft density is too low and the polymer brushes are too short, the "shielding effect" would not be significant enough to prevent the core-core attractions. Overall, NP's can be well-dispersed in polymer matrices only when the enthalpy and entropy of the system are considered.[1, 2]

As mentioned in the previous chapters, our group has successfully performed surface-initiated RAFT polymerization on 15 nm silica NP's with good control over the graft density and molecular weight of polymers attached to the NP surface.[3-5] On the basis of the former work, we extended this concept by exploring more functional monomers, different sizes of NP's, and designing diverse architectures of the polymer brushes for potential applications.

The first type of polymer-grafted NP's was designed for epoxy modification. Rubber filled epoxy can exhibit greatly improved toughness and ductility compared to unfilled epoxy. However, these improvements are typically accompanied by a large and undesirable decrease in the T_g and modulus. A ternary mixture of micro-size rubber particles, silica NP's and epoxy has been shown to alleviate the decrease in modulus and strength.[6] Herein, we combined these two fillers by creating a controlled geometry of rubber surrounding each silica NP for epoxy matrix modification. More specifically, multi-layers of poly(hexyl methacrylate) (PHMA) and poly(glycidyl methacrylate) (PGMA) were prepared on 15 nm silica NP's in which PHMA functioned as the rubbery inner block, and PGMA was in the outer layer to make the NP's compatible with the epoxy matrix.

In addition, stearyl methacrylate (SMA), which is derived from renewable plant oils, can form very useful polymeric materials. Random copolymers containing SMA displayed microphase separations involving semi-crystalline structures ascribed to its side chains.[7, 8] Copolymers of SMA and other hydrophilic monomers are able to self-assemble into various nano-structures in solution.[9-13] Moreover, SMA can be used as a reactive costabilizer for miniemulsion polymerization.[14] In industrial applications, copolymers containing SMA are coated on material surfaces to improve water repellency and soil resistance,[15] or function as oil-absorptive polymers resulting from their hydrophobic properties.[16] Otherwise, poly(stearyl methacrylate) (PSMA) and their mixtures with olefinic copolymers, and styrene based copolymers are used extensively as viscosity index improvers and pour-point depressants for lubricating oil because of their superior viscosity index character, their structural diversity, ease of modification and economic

considerations.[17] So far most of the PSMA polymers reported were produced by conventional free radical polymerization. ATRP is the most mature living radical polymerization for PSMA preparation,[13, 18, 19] and molecular weights up to 160k were reached with relatively good control.[20] In contrast, synthesis of PSMA through RAFT polymerization has been rarely reported and only low molecular weights of a few thousands were obtained.[11] Surface-initiated polymerization of SMA has not been reported so far. In this research, we performed kinetics studies on RAFT polymerizations of SMA both in solution and on silica NP's. Also, PSMA-grafted silica NP's with different graft densities were prepared to investigate their distribution in polypropylene (PP) matrices. Transparent PP films were afforded with NP loadings up to 2 wt%.

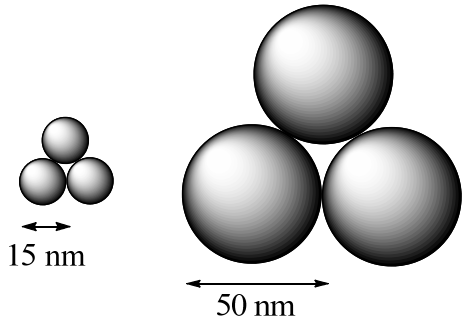

Figure 4.1 Illustrative diagram showing that NP's with a diameter of 50 nm have larger cavities than that of NP's with a diameter of 15 nm.

In the last part, we describe our work on surface-initiated RAFT polymerization on 50 nm silica NP's to study a more significant cavitation effect compared to 15 nm NP's which are more commonly used in our group (Figure 4.1). If it is assumed that the NP's are uniform with a diameter of 50 nm, the mean size of the interstitial cavities is $(3^{0.5}-1)*D=36.6$ nm when they form crystals. There would be an empty space created in the center of this NP arrangement if the graft brushes are too short to fill, which is energetically unfavorable. Therefore, when such a grafted NP crystal contacts a short-

chain matrix, the matrix polymers would intercalate into the cavity. Otherwise a phase separation would occur. Alternatively, when graft brushes are long enough that brushes from the opposite side can touch each other, an energetic gain is not achieved by the matrix polymer penetration unless the matrix likes to wet the brushes. Similar procedures were applied to functionalize the surface of the NP's with chain transfer agents (CTA's), and kinetics studies of the polymerizations of poly(methyl methacrylate) (PMMA) and polystyrene (PS) in THF were explored.

4.2 Experimental Section

4.2.1 Materials

Colloidal silica particles of 30 wt % dispersed in methyl ethyl ketone were purchased from Nissan Chemical with average diameters of 15 nm and 50 nm, respectively. 3-Aminopropyldimethylethoxysilane (APDMES) (95%) was purchased from Gelest and used as received. 4-Cyanopentanoic acid dithiobenzoate (CPDB) was purchased from Strem Chemical Inc. and used as received. Activated CPDB was prepared according to the previous literature.[3] n-Hexyl methacrylate (HMA) (98%, TCI) and glycidyl methacrylate (GMA) (97%, Acros) were passed through a neutral alumina column to remove inhibitors before the polymerization. Methyl methacrylate (MMA) (99%, Acros) and styrene (99%, Acros) were passed through a basic alumina column to remove inhibitors before use. SMA (95%, TCI) and azobisisobutyronitrile (AIBN) (98%, SigmaAldrich) were recrystallized from hexane and ethanol, respectively. Syndiotactic polypropylene (M_n = 75,000, Mw = 174, 000) was purchased from SigmaAldrich and used as received. Unless otherwise specified, all chemicals were purchased from Fisher Scientific and used as received.

4.2.2 Instrumentation

NMR spectra were recorded on Varian Mercury 300 spectrometers using $CDCl_3$ as the solvent. UV-vis absorption spectra were taken on a Perkin-Elmer Lamda 4C UV/vis spectrophotometer. Molecular weights and polydispersity indices (PDI = M_w/M_n) were determined using a Waters gel permeation chromatograph equipped with a 515 HPLC pump, a 2410 refractive index detector, and three Styragel columns (HR1, HR3, HR4 in the effective molecular weight range of 100-5000, 500-30 000, and 5000-500 000, respectively) with THF as the eluent at 30 °C and a flow rate of 1.0 mL/min. The GPC system was calibrated with both poly(methyl methacrylate) and polystyrene standards from Polymer Laboratories.

4.2.3 Preparation of CTA-Anchored Silica NP's

The process of modifying 15 nm silica NP's with CTA's has been reported in the previous literature.[3] Functionalization of 50 nm silica NP's were performed via the similar procedure, and is briefly described below.

A suspension (8 g) of 30 wt % colloidal silica NP's (50 nm) was added to a three-necked round-bottom flask with APDMES (0.37 g, 2.3 mmol) and dried THF (80 mL). The reaction mixture was heated at 75 °C under N_2 protection overnight and then cooled to room temperature. The reaction mixture was precipitated into a large amount of hexanes (400 mL, ACS Reagent). The particles were recovered by centrifugation at 3000 rpm for 5 minutes. The particles were then redissolved in 60 mL of acetone and reprecipitated in 300 mL of hexanes. The amino-functionalized NP's were dispersed directly into 50 mL of THF for subsequent use. Amino-functionalized NP's with a lower surface density was also prepared similarly using 8 g of silica NP suspension and APDMES (62 mg, 0.38 mmol).

A THF solution (50 mL) of the high surface density amino-functionalized NP's was added dropwise to a THF solution (50 mL) of activated CPDB (0.96 g, 2.5 mmol) at room temperature. After complete addition, the solution was stirred for 6 hours. The reaction mixture was then precipitated into a large amount of 4:1 mixture of cyclohexane and ethyl ether (500 mL). The NP's were recovered by centrifugation at 3000 rpm for 5 minutes. The NP's were then redissolved in 50 mL of THF and reprecipitated in 4:1 mixture of cyclohexane and ethyl ether (250 mL). This dissolution-precipitation procedure was repeated another two times until the supernatant layer after centrifugation was colorless. The high surface density CPDB anchored silica NP's were dried at room temperature (2.1 g, 88% yield). The low surface density CTA-anchored NP's were prepared (1.8 g, 75% yiled) similarly using a THF solution (50 mL) of the low surface density amino-functionalized NP's and activated CPDB (0.17 g, 0.46 mmol). The graft densities of CTA were 0.43 chains/nm^2 and 0.14 chains/nm^2, respectively, which were measured and calculated by UV-vis analysis with a modified equation according to the different diameter.[21]

4.2.4 RAFT polymerization of HMA (and/or GMA) on 15 nm silica NP's

Typically, the CTA-anchored NP's were dissolved in THF, and added to a dried Schlenk tube together with monomer (HMA or GMA) and AIBN. The mixture was degassed by three freeze-pump-thaw cycles, backfilled with nitrogen, and then placed in an oil bath at 60 °C for various intervals. The ratios of the reactants were varied to investigate their influence on the polymerization. In the case of large-scale production, the CTA-anchored NP's were dissolved in THF, and added to a three-necked round-bottom flask together with monomer (HMA or GMA) and AIBN. The flask was flushed

by nitrogen for half an hour, and then placed in an oil bath at 60 °C under the protection of nitrogen for various intervals. The polymerizations were quenched in ice water.

A sample of grafted chains was cleaved from the surface using hydrofluoric acid (HF). Typically, about 40 mg of nanoparticles was mixed with 4 mL of THF and 0.5 mL of HF (48%-51% in water), and the solution was allowed to stir at room temperature overnight, and then dried for GPC tests. If the polymers contained GMA repeat units, approximately 40 mg of nanoparticles were dissolved in 4 mL of methylene chloride, and then 4 mL of water, 0.5 mL of HF and one drop of Aliquot® 336 were added. After stirring overnight, the organic layer was taken out and evaporated for GPC tests. The rest of the polymer-grafted NP's were precipitated in methanol to remove unreacted monomers, and then either re-dispersed in THF to polymerize another block, or re-dispersed in methylene chloride.

4.2.5 RAFT polymerization of SMA in solution

SMA (1.0 g, 3.0 mmol) was dissolved in 2 mL of THF, and added in a dried Schlenk tube together with CPDB (2.8 mg, 10 μmol) and AIBN (0.16 mg, 1.0 μmol). The mixture was degassed by three freeze-pump-thaw cycles, back filled with nitrogen, and then placed in an oil bath at 60 °C for various intervals. The polymerizations were quenched in ice water. Monomer conversion was determined by ^{1}H NMR, and molecular weight characteristics were analyzed by GPC.

4.2.6 RAFT polymerization of SMA on 15 nm silica NP's

CTA-anchored NP's (10 mg, 0.10 mmol/g), THF (3 mL), and SMA (1.13 g, 3.3 mmol) were added to a 15 mL Schlenk tube followed by sonication until a transparent solution was obtained, and then AIBN (10 μL of 10mM THF solution) was added. The

tubes were subjected to three cycles of freeze-pump-thaw to remove oxygen. The tubes were then placed in an oil bath preset to 60 °C for various intervals. The polymerizations were stopped by quenching the tubes in ice water. The ratios of the reactants were varied for different graft density NP's. Monomer conversion was determined by ^{1}H NMR, and polymer brushes were cleaved from the NP's for GPC test following the same procedure as the description in **4.2.4**.

4.2.7 RAFT polymerization of MMA on 50 nm silica NP's

CTA-anchored NP's (125 mg, 13.3 μmol/g) were dissolved in 1.06 mL of THF, and added to a dried Schlenk tube together with MMA (1.06 ml, 10.0 mmol) and AIBN (16.5 μL, 10 mM). The mixture was degassed by three freeze-pump-thaw cycles, backfilled with nitrogen, and then placed in an oil bath at 60 °C for various intervals. The polymerizations were stopped by quenching the tubes in ice water, and the polymerization mixtures were poured into an aluminum boat to evaporate the solvent in a fume hood. The aluminum boat was then transferred to a vacuum oven to remove traces of solvent and monomer at 30 °C overnight to determine the monomer conversions via gravimetric analysis. Polymer brushes were cleaved from the NP's for GPC test following the same procedure as the description in **4.2.4**. The ratios of the reactants were varied according to the graft density of the NP's.

4.2.8 RAFT polymerization of styrene on 50 nm silica NP's

CTA-anchored NP's (63 mg, 13.3 μmol/g) were dissolved in 0.635 mL of THF, and added to a dried Schlenk tube together with styrene (0.635 mL, 5.8 mmol) and AIBN (8.3 μL, 10 mM). The mixture was degassed by three freeze-pump-thaw cycles, backfilled with nitrogen, and then placed in an oil bath at 60 °C for various intervals. The

polymerizations were stopped by quenching the tubes in ice water, and the polymerization mixtures were poured into an aluminum boat to evaporate the solvent in a fume hood. The aluminum boat was then transferred to a vacuum oven to remove traces of solvent and monomer at 30 °C overnight to determine the monomer conversions via gravimetric analysis. Polymer brushes were cleaved from the NP's for GPC testing following the same procedure as the description in **4.2.4**. The ratios of the reactants were varied according to the graft density of the NP's.

4.3 Results and Discussion

4.3.1 Grafting block copolymers of HMA and GMA on 15 nm silica NP's

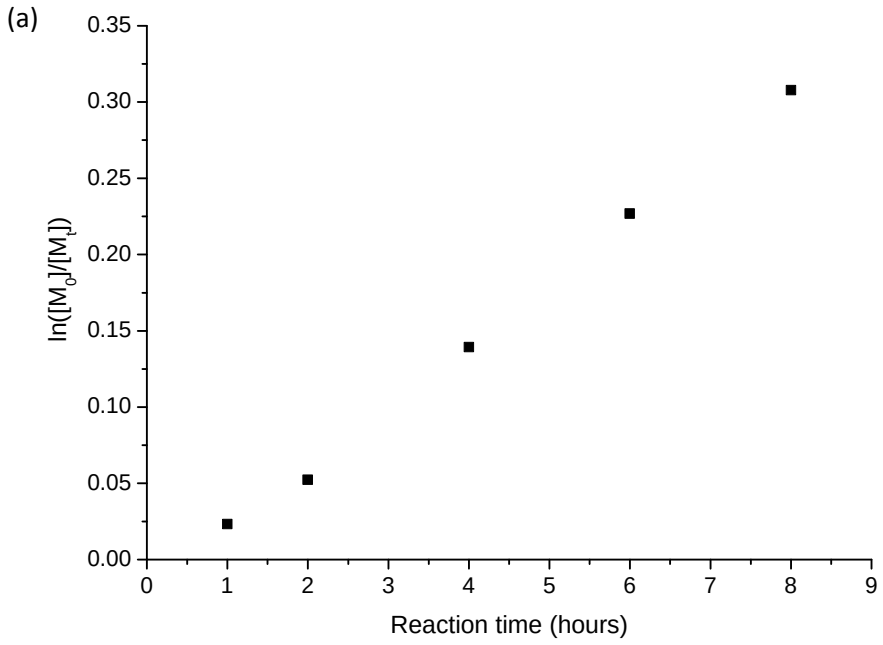

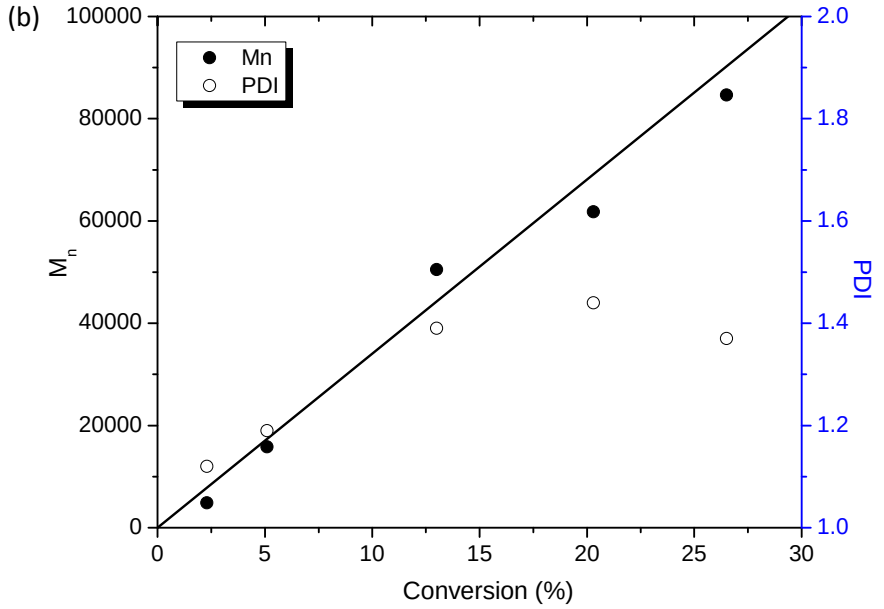

Figure 4.2 (a) Kinetics plot and (b) dependence of M_n and polydispersity on the conversion for the RAFT polymerization of HMA on silica NP's (graft density of the NP's is 0.3 chains/nm^2, [monomer]: [CPDB]: [AIBN] = 2000:1:0.1, [monomer] = 50 vol% in THF, 60 °C). The solid line represents the theoretical M_n.

The surface-initiated RAFT polymerization of each monomer on silica NP's was studied separately prior to block copolymer formation. Kinetic studies on the polymerization of HMA are displayed in Figure 4.2 with a ratio of CTA to monomer of 1/2000, which was commonly applied in our previous studies with other similar monomers.[3, 4] Although the pseudo-first-order kinetics plot indicated a constant free radical concentration in the polymerization process (Figure 4.2a) and the number average molecular weights (M_n) increased linearly with monomer conversion in agreement with the predictions (Figure 4.2b), the polymerization was not under precise control. First, silica NP's were not compatible with HMA, which could be considered as a bad solvent for the NP's. When HMA was poured into the NP solution in THF, the mixture became cloudy immediately. Therefore, the first stage was actually a heterogeneous

polymerization containing NP aggregates. Obvious shoulders were observed on the GPC traces before 2 hours (Figure 4.3), which was probably because of free radical polymerization in the solution at the beginning of the polymerization while most of the CTA's could not effectively parcipitate in the reaction. After 2 hours, the suspension became gradually transparent and there were no shoulders detected on the GPC traces. However, a second problem was observed, i.e., the solution became very viscous leading to relatively broad polydispersities of the polymer brushes. Figure 4.2b shows that PDI increased from about 1.2 to 1.4 in this period.

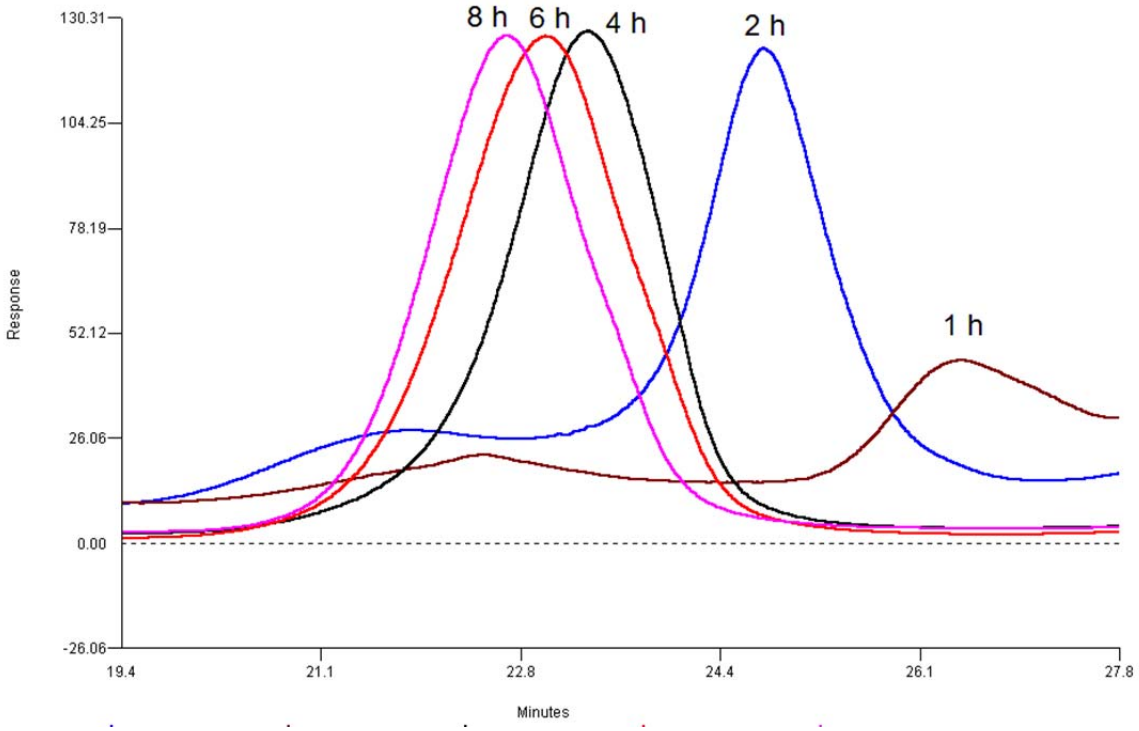

Figure 4.3 GPC traces of PHMA for kinetic studies.

To prevent the heterogeneous polymerization and reduce the viscosity of the solution in the later stage, more THF could be added as it is good solvent for both silica NP's and HMA. However, the concentration of HMA would be lower as well, resulting in a slower polymerization. Hence, to overcome the issues without sacrificing the reaction rate, both

the amount of THF and HMA were increased on equal scales. In this way, the NP's were diluted to form transparent solutions with HMA. Since the CTA's were anchored on the surface of NP's, the local concentration of CTA was not significantly influenced by the dilution. The results of the RAFT polymerization of HMA are shown in Figure 4.4a with a ratio of CTA to monomer of 1/30,000. In this case, the PDI's were approxmately 1.2 up to molecular weights of 55 kg/mol with lower viscosities, and the polymerization was even faster than that with the higher ratio. In addition, Figure 4.4b also shows that the M_n of PGMA increased almost linearly with the reaction time in a predictable manner in the same conditions as PHMA, which had slightly higher PDI's.

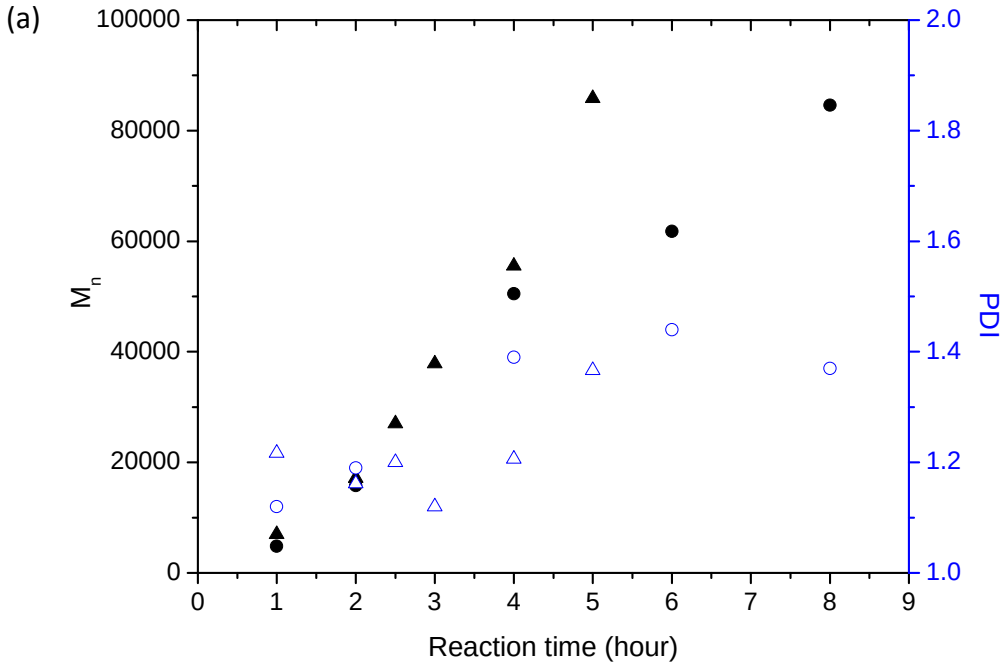

(b)

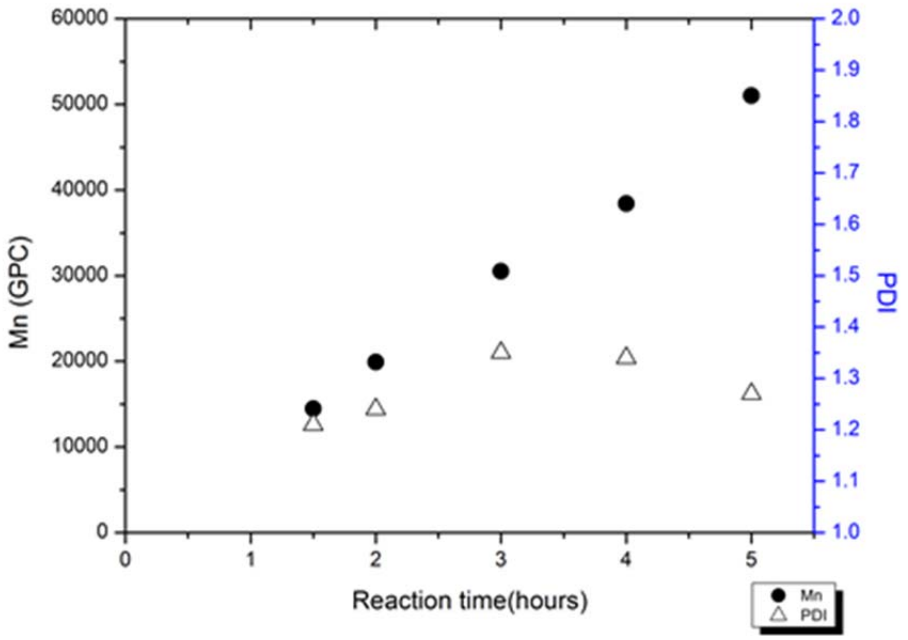

Figure 4.4 Dependences of molecular weight and PDI on reaction time for the RAFT polymerization of (a) HMA (50 vol% in THF) at 60 °C with different ratios of CTA to monomer: 1/2000 (circle) and 1:30,000(triangle); and (b) GMA (50 vol% in THF) at 60 °C with AIBN as initiator (1.5×10^{-5} M) mediated with CTA anchored silica NP's (1.5×10^{-4} M; 0.6 chains/nm^2).

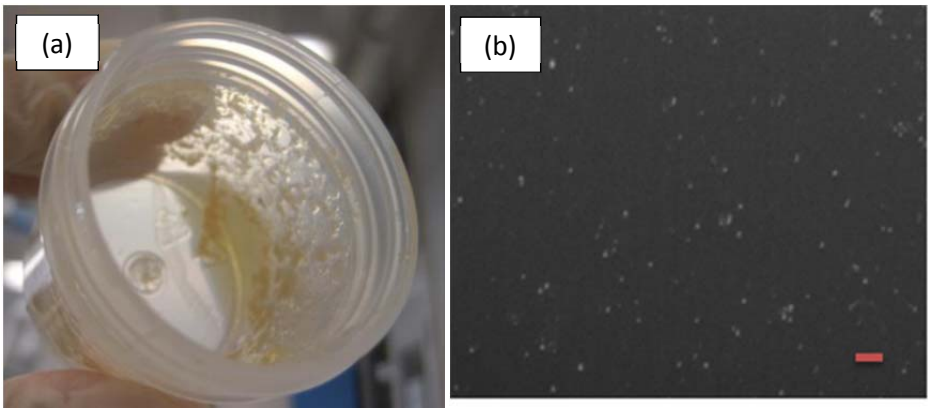

Figure 4.5 (a) The precipitation of 20 kg/mol PHMA grafted NP's with graft density of 0.6 chains/nm^2 in epoxy resin. (b) TEM image of PGMA-SiO_2/epoxy nanocomposites (20 kg/mol PGMA, 0.6 chains/nm^2).

It was observed that PHMA-grafted NP's (PHMA-SiO_2) were completely incompatible with epoxy resin. The PHMA-SiO_2 would precipitate immediately after

mixing with epoxy resin even with solvent added (Figure 4.5a). On the other hand, PGMA-SiO_2 mixed with epoxy resin very well (Figure 4.5b), indicating that PGMA would be a good choice as an epoxy compatible layer for the copolymer grafted NP's.

Three different architectures were designed on the surface of NP's for the epoxy modification. The most straightforward one was block copolymer brushes – PGMA-*b*-PHMA-SiO_2 (Figure 4.6a), which was synthesized by sequential RAFT polymerizations of HMA and GMA. To study the effects of the interface structure on the compatibility of the NP's in epoxy matrices, alternate interfaces between PGMA and PHMA layers were investigated. At first, we planned to synthesize a gradient copolymer poly(HMA-*grad*-GMA) instead of a block copolymer to make the interface more "diffuse". Typically, with two monomers having similar reactivity ratios close to 1, gradient copolymers can be formed through gradual addition of the second type of monomer to a reaction vessel containing the first kind of monomer when they are almost consumed. However, unlike the "free" polymerization in solution, the concentration of HMA did not decrease significantly during the process of the surface-initiated polymerization on NP's. Since HMA was in excess during the first polymerzation, GMA would have to be added at least ten times higher than the original concentration of HMA, which means that hundreds milliliters of GMA would be required only for the polymerization of 0.5 g NP's. Obviously, this was not feasible. Instead, we prepared the random copolymer PGMA-*r*-PHMA as the second block (Figure 4.6b) by adding the equivalent amounts of HMA and GMA. According to the ^{1}H NMR analysis, the ratios of HMA and GMA repeat units in the random copolymers were also 1/1. Additionally, we also synthesized a "pseudo-gradient" copolymer on the NP's (Figure 4.6c). The procedure followed up the synthetic

steps to prepare NP's (**b**). After building up the random block and removing all free monomers, another round of RAFT polymerization was performed to add PGMA as the third block. Table 4.1 shows some samples of NP's grafted by these different block copolymers. Even after twice precipitations and three separate polymerizations, the polymer brushes were still obtained with relatively low polydispersity (PDI = 1.46), demonstrating that the polymer chains on the NP's were "living" due the existence of the CTA and could be repeatedly initiated for polymerization.

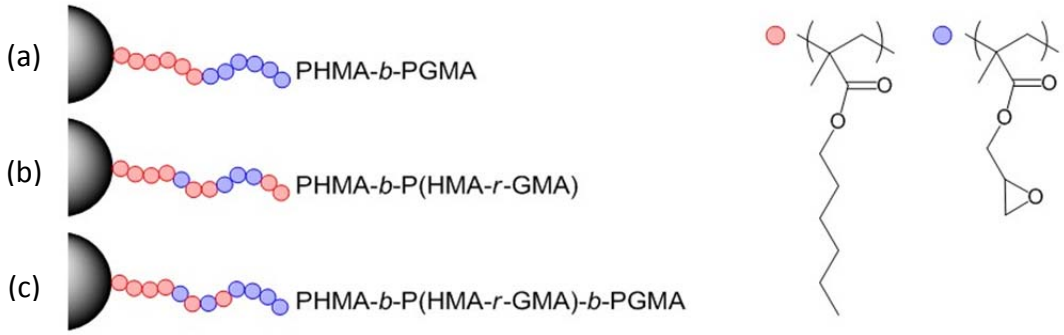

Figure 4.6 Designs of different rubbery interfaces on silica NP's.

Table 4.1 Samples of block copolymer grafted NP's consisting of HMA and GMA (graft density = 0.6 chains/nm^2).

Samples	First block	Second block	Third block
1	PHMA, Mn=17,119, PDI=1.16	PGMA, Mn=35,551, PDI=1.32	_
2	PHMA, Mn=16,869, PDI=1.23	PHMA-r-GMA, Mn=27,029, PDI=1.24	PGMA, Mn=70,707, PDI=1.46
3	PHMA, Mn=19,021, PDI=1.10	PHMA-r-GMA, Mn=38,096, PDI=1.12	_

We observed that only the NP's (**a**) and (**c**) could be easily mixed with the epoxy resin. Figure 4.7 compares the distributions of NP's (**a**) and (**b**) in the epoxy matrices.

The graft densities of the samples were both 0.6 chains/nm^2, and M_n of each block of the polymer brushes was approximately 20 kg/mol. Unlike the uniform distribution of NP's in (**a**), phase separations were observed in the TEM image of NP's in (**b**), and NP's could only be found in certain regions, although no NP aggregates were formed due to the high graft density of polymer brushes. Therefore, HMA should be avoided in the outer layer of the NP's to prepare compatible fillers for epoxy resin.

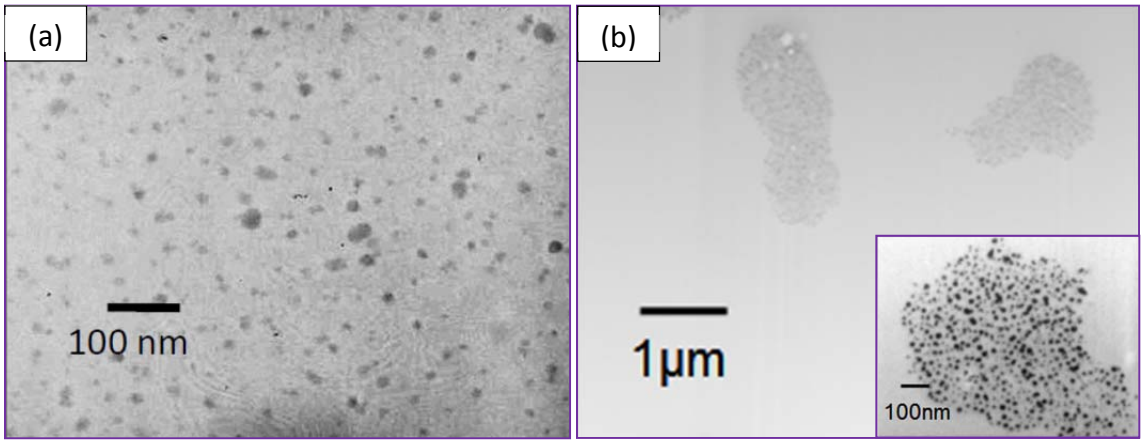

Figure 4.7 (a) TEM image of 1vol% PHMA-*b*-PGMA-SiO_2 (20k20k, 0.6 chains/nm^2) / epoxy nanocomposite. (b) TEM image of 1vol% PHMA-*b*-(PGMA-*r*-PHMA)-SiO_2 (20k20k, 0.6 chains/nm^2) / epoxy nanocomposites.

The mechanical tests of epoxy resin mixed with the rubbery block copolymer grafted NP's having diverse molecular weights and graft densities were conducted by Dr. Schadler's group at Rensselaer Polytechnic Institute.[22] The test results demonstrated that the copolymer grafted silica NP's enhanced the ductility (maximum 60 % improvement), fracture toughness (maximum 300 % improvement) and fatigue crack growth resistance of the epoxy matrix while maintaining the modulus at loadings of less than 2 vol% of silica core. The PHMA block induced plastic void growth and shear banding as the major mechanisms for the toughening. At lower graft density and larger molecular weight of the PHMA block, the nanocomposites exhibited simultaneous improvements in fracture

toughness and tensile modulus. Overall, adding rubbery copolymer grafted rigid particles is a promising method to toughen glassy polymers. These particles can also improve modulus and maintain tensile strength, a combination cannot be achieved by conventional rubber particles.

4.3.2 RAFT polymerization of stearyl methacylate in solution and on nanoparticles

As discussed in the Introduction, PSMA is a very useful material for many applications, but its preparation through RAFT polymerization has been rarely studied. In this research, RAFT polymerization of SMA in THF was investigated first. The results of the kinetic studies are displayed in Figure 4.8, which indicated that the polymerization did not proceed in a well-controlled manner. It is observed from Figure 4.8a that an induction period of approximately 2 hours occurred and the polymer chain growth began after this time. Although $ln\,[M_0]/[M]$ remained almost linear with the reaction time, indicating a constant free radical concentration in this process, the molecular weight did not exhibit a significant growth after reaching approximately 35 kg/mol. A reasonable explanation is that the long side chains of the polymer/monomer blocked radical chain ends from reacting with monomers (or CTA's), and retarded the propagation (it did show a slower polymerization rate than MMA in similar conditions according to our previous work). The retardation became more severe with an increase of the molecular weight ascribed to tangling and coiling of the polymer chains, which may increase chances for chain transfer reactions and suppression of the propagation. Additionally, the first three points in Figure 4.8b were higher than the theoretical predictions probably because of the error of GPC using PMMA samples as standards.

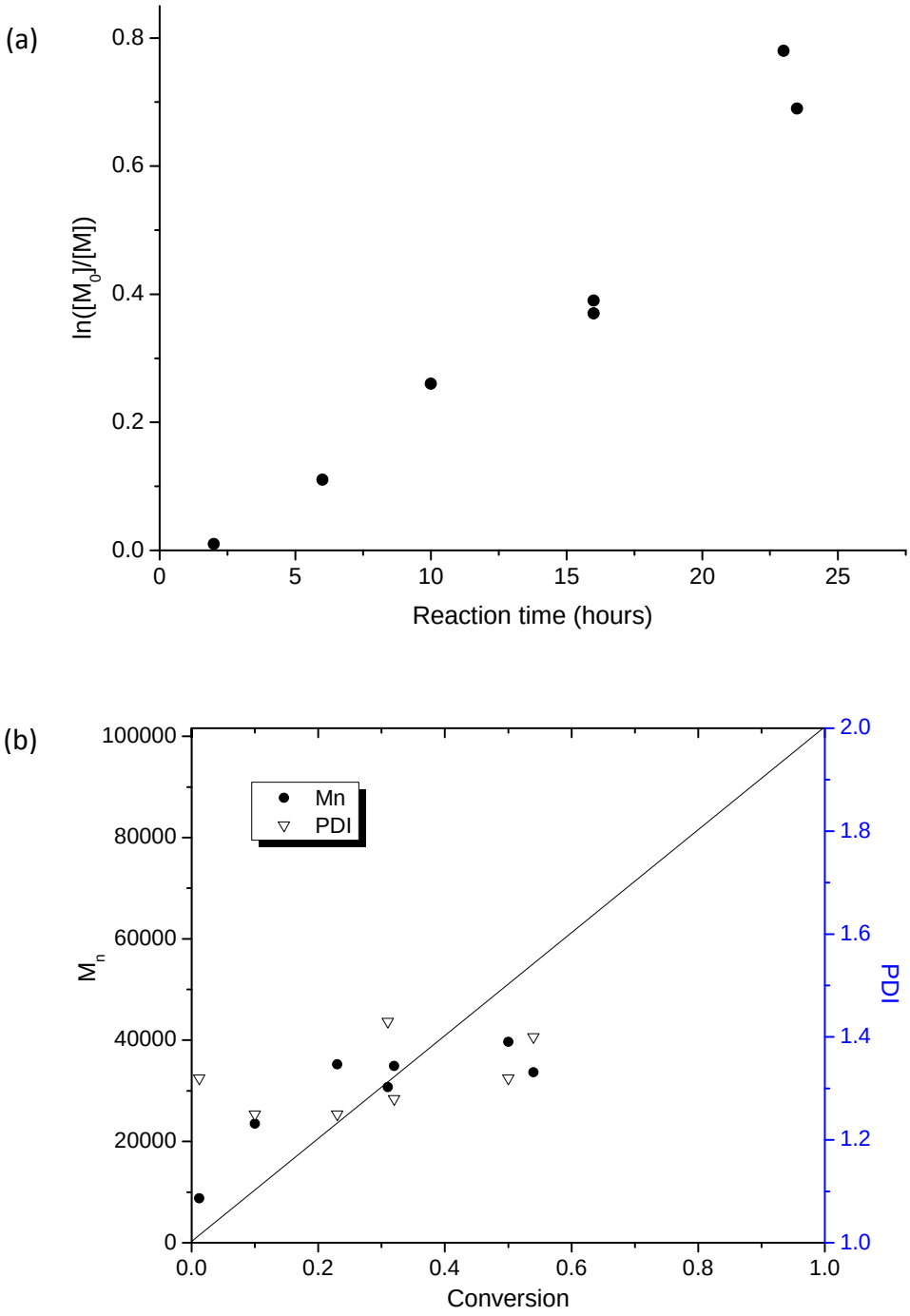

Figure 4.8 (a) Kinetics plot and (b) dependence of M_n and polydispersity on the conversion for the RAFT polymerization of SMA in THF ([monomer]: [CPDB]: [AIBN] = 300:1:0.1, 60 °C). The solid line represents the theoretical M_n.

Kinetic studies on RAFT polymerization of SMA were then performed on silica NP's with a graft density of 0.4 chains/nm^2 (Figure 4.9). Similarly, it was found that the

polymerization on NP's also had a molecular weight limit. After reaching this point, the molecular weights remain relatively constant. However, the limit in the range of 130k-140k (Figure 4.9b) was higher than that of the solution polymerization at around 35 k, and it was presumably because polymers on the surfaces were highly stretched with less tangle and coiling, and retardation would not become significant until the polymer chains got very long and behaved the same as free chains. Moreover, the kinetics plot shows that polymer chains on NP's started to become inactive over the molecular weight limit, as the propagation was seriously retarded at this moment and the chain end radicals were quenched by each other due to the high local concentration of radicals. Otherwise, the concentration of SMA had an important influence on the polydispersity of the resultant polymers. When the monomer concentration was diluted from 0.38 mg/mL to 0.19 mg/mL while other conditions were kept the same, the PDI's of the polymer brushes (M_n = 140k) decreased from 1.8 to 1.4.

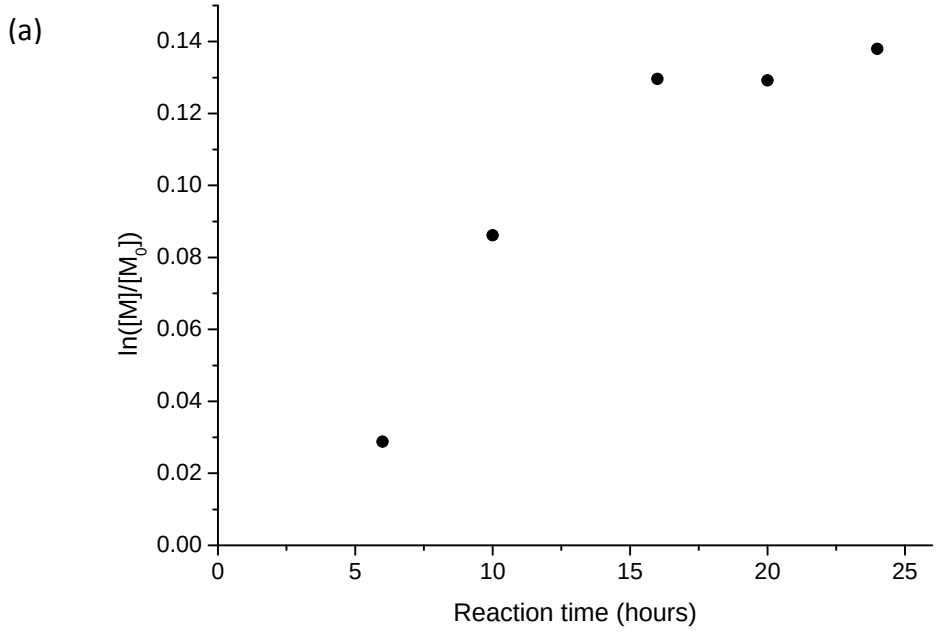

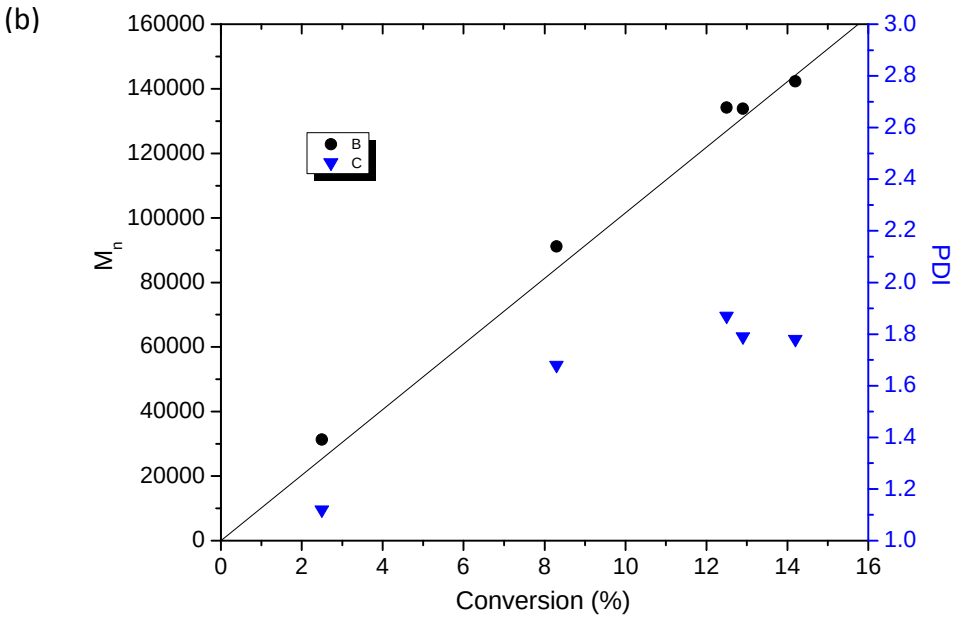

Figure 4.9 (a) Kinetics plot and (b) dependence of M_n and polydispersity on the conversion for the RAFT polymerization of SMA on silica NP's (0.4 chains/nm^2) in THF ([monomer]: [CPDB]: [AIBN] = 3000:1:0.1, 60 °C). The solid line represents the theoretical M_n.

Two samples of PSMA-grafted silica NP's (Table 4.2) were mixed with syndiotactic polypropylene (PP), since the side chains of PSMA may enhance the compatibility with PP matrices. Both PSMA-NPs and polypropylene were dissolved in toluene (10 mg/mL, respectively) at 90 °C, and then opaque films were cast with different NP loadings. After 30 minutes of annealing at 110 °C and cooling to room temperature, transparent films were obtained for all the samples (Figure 4.10), indicating that PSMA-NPs were miscible in PP matrices without agglomeration.

Table 4.2 Samples of PSMA-grafted silica NP's for PP modification.

	Mn	**PDI**	**Graft density**
PSMA-NP 1	138,047	1.37	0.68 chains/nm^2
PSMA-NP 2	111,453	1.40	0.03 chains/nm^2

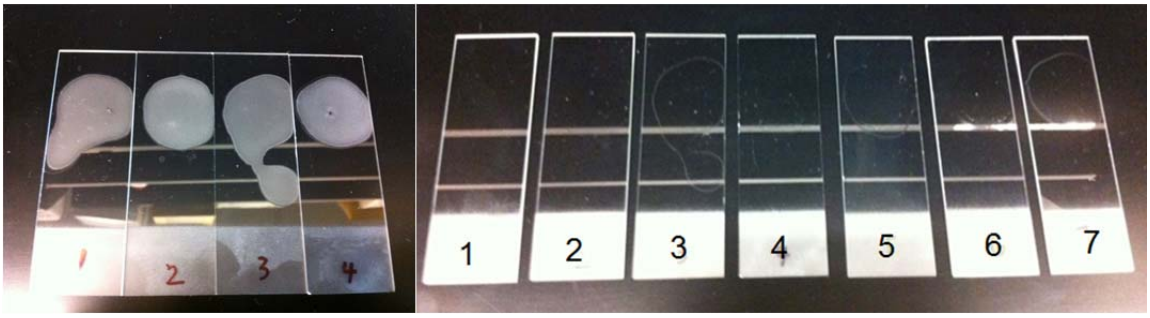

Figure 4.10 PP films before (left) and after (right) annealing. (film 1: Neat PP; film 2: PP with 1 wt% PSMA-NP 1; film 3: PP with 1 wt% PSMA-NP 2; film 4: PP with 2 wt% PSMA-NP 1; film 5: PP with 2 wt% PSMA-NP 2; film 6: PP with 5 wt% PSMA-NP 1; film 7: PP with 5 wt% PSMA-NP 2.)

4.3.3 Surface-initiated RAFT polymer on 50 nm silica NP's

Functionalization of 50 nm silica NP's with CPDB was conducted using similar procedures to that with 15 nm NP's. Graft densities as high as 0.45 chains/nm^2 were achieved, which is slightly lower than 0.7 chain/nm^2 for the 15 nm NP's probably because of their smaller curvature. For the preparation of low-density CPDB-anchored 15 nm NP's, dimethylmethoxy-n-octylsilane was usually added together with the amino silane to prevent aggregation of the NP's.[23] However, this step was not necessary for the 50 nm NP's, since they were much easier to redisperse even after they were completely dried due to their larger cavitation effect.

Surface-initiated polymerization of MMA was conducted from CPDB anchored 50 nm silica NP's having a graft density of 0.14 chains/nm^2. The kinetic studies are displayed in Figure 4.11. A pseudo first-order kinetics plot and a linear relationship between M_n and monomer conversion was observed with PDI's at or below 1.2. Overall, the polymerization exhibited relatively good control over M_n and PDI.

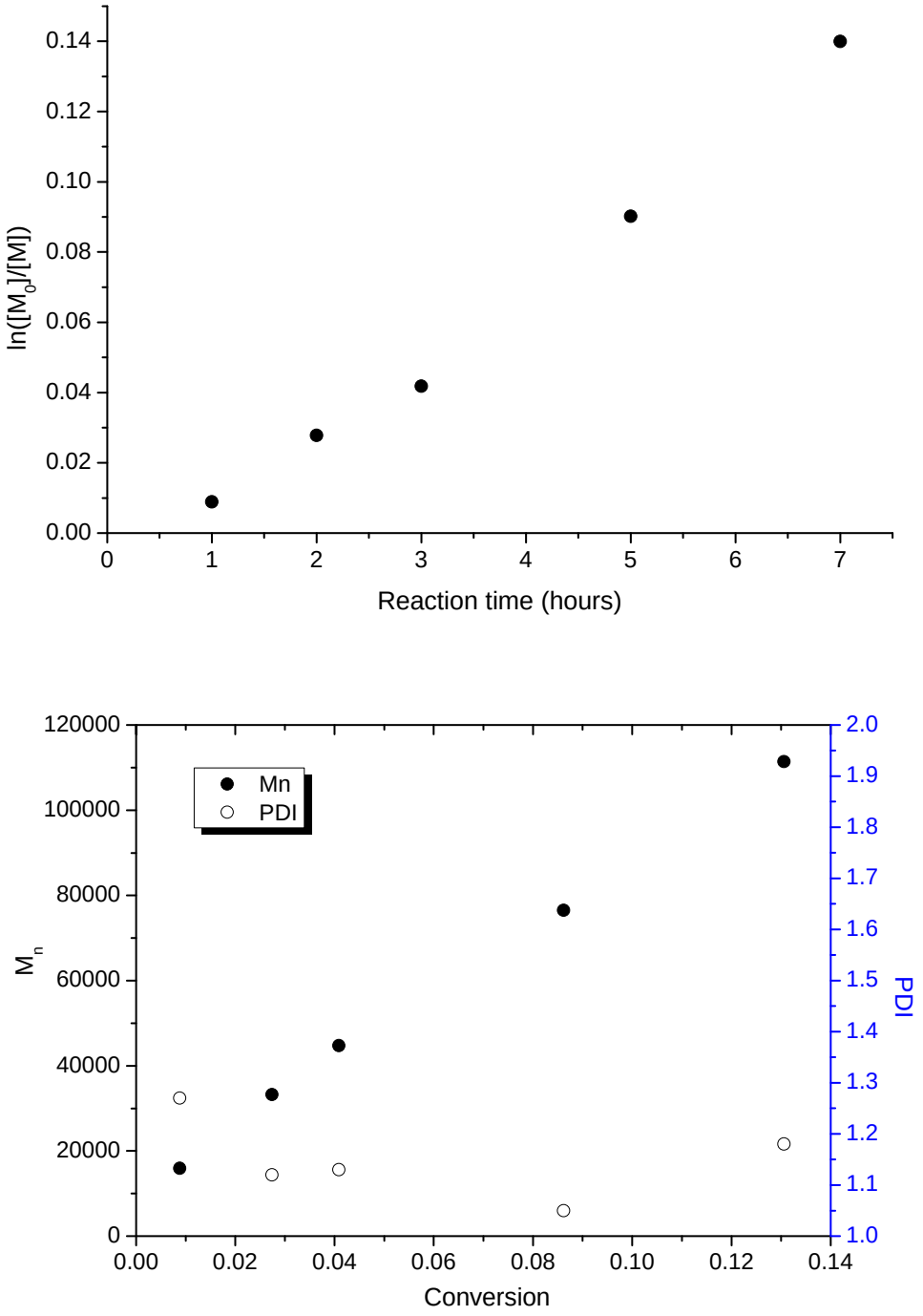

Figure 4.11 (a) Kinetics plot and (b) dependence of M_n and polydispersity on the conversion for the RAFT polymerization of MMA on 50 nm silica NP's (0.14 chains/nm^2) in THF ([MMA]: [CPDB]: [AIBN] = 3000:1:0.1, [MMA] = 50 vol%, 60 °C).

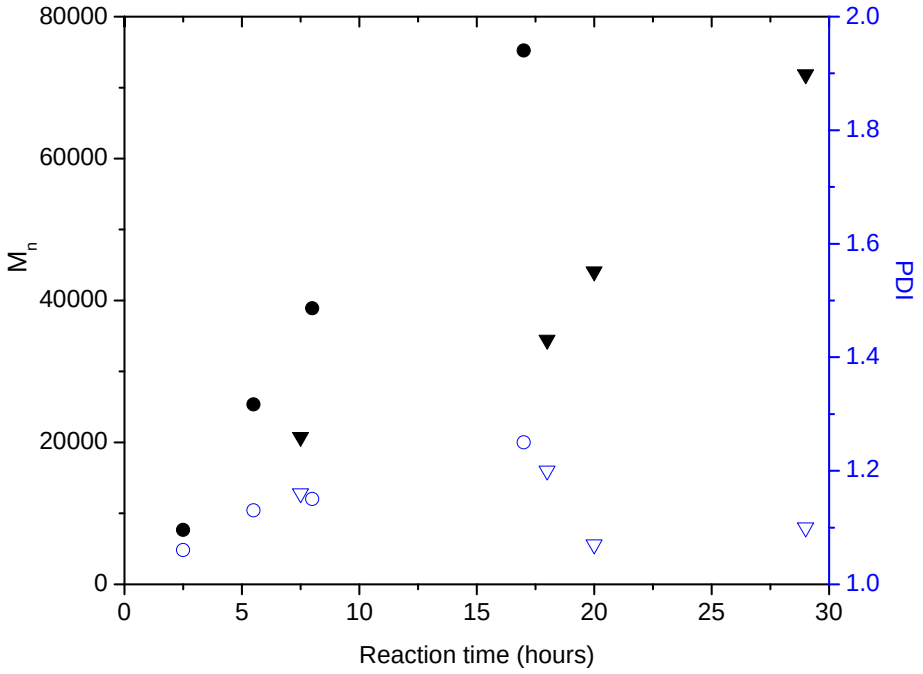

Figure 4.12 Dependence of molecular weight and PDI on reaction time for the RAFT polymerization of styrene on CTA anchored silica NP's (circle: 0.08 chains/nm^2, triangle: 0.14 chains/nm^2) in THF ([styrene]: [CPDB]: [AIBN] = 13000:1:0.1, [styrene] = 50 vol%, 60 °C).

Additionally, the polymerization of styrene was studied on 50 nm silica NP's. Figure 4.12 shows that the Mn increased with reaction time in a controlled manner, and PDI's were generally below 1.2. Apparently, under the same reaction conditions polymer brushes on lower-graft-density NP's grew faster than that on higher-graft-density NP's due to the "surface radical migration" effect,[24] and this phenomenon was consistent with our previous observation.[4] Additionally, it was observed that the suspensions of 50 nm NP's for styrene polymerization were optically much clearer than the suspensions for MMA polymerization. Following this observation, we found that solvents containing aromatic structures can actually improve the solubility of 50 nm NP's when mixed with THF, such as benzene or toluene, although these solvents cannot dissolve the NP's by themselves.

4.4 Conclusions

In this research, we studied the polymerization of different kinds of functional monomers on silica NP's with diverse sizes. It was observed that polymer brushes grew on the NP's through surface-initiated RAFT polymerization with all the monomers, and most of their polymerizations were performed under good control. Through sequential RAFT polymerizations, we designed a facile approach to graft multilayer block copolymer on silica NP's (up to three layers with relatively low polydispersities). The designed rubbery NP's displayed good dispersion in epoxy matrices, and showed a significant effect on toughening the epoxy resin. The surface-initiated polymerization of SMA achieved molecular weights greater than 100k, and such high values have not been reported before by RAFT even in solution. It was also found there were molecular weight limits for the polymerizations, probably because the resultant PSMA was not highly compatible with the solvent. Kinetic studies of SMA in less-polar solvents are in process, which may lead to better control of the polymerization. Additionally, the morphology studies on the relationship between the cavitation effect and the distribution of 50 nm PS-grafted NP's in PS matrices are being conducted by our collaborators at Columbia University and are still in process.

4.5 Reference

1. Bansal, A.; Yang, H.; Li, C.; Benicewicz, B. C.; Kumar, S. K.; Schadler, L. S. *J. Polym. Sci., Part B: Polym. Phys.* **2006,** *44*, 2944-2950.

2. Akcora, P.; Liu, H.; Kumar, S. K.; Moll, J.; Li, Y.; Benicewicz, B. C.; Schadler, L. S.; Acehan, D.; Panagiotopoulos, A. Z.; Pryamitsyn, V.; Ganesan, V.; Ilavsky, J.; Thiyagarajan, P.; Colby, R. H.; Douglas, J. F. *Nat. Mater.* **2009,** *8*, 354-359.

3. Li, C.; Han, J.; Ryu, C. Y.; Benicewicz, B. C. *Macromolecules* **2006,** *39*, 3175-3183.

4. Li, C. Z.; Benicewicz, B. C. *Macromolecules* **2005,** *38*, 5929-5936.

5. Li, Y.; Benicewicz, B. C. *Macromolecules* **2008,** *41*, 7986-7992.

6. Kinloch, A. J.; Mohammed, R. D.; Taylor, A. C.; Eger, C.; Sprenger, S.; Egan, D. *J. Mater. Sci.* **2005,** *40*, 5083-5086.

7. Shang, S. R.; Huang, S. J.; Weiss, R. A. *Polymer* **2009,** *50*, 3119-3127.

8. Shang, S. R.; Huang, S. J.; Weiss, R. A. *Polymer* **2011,** *52*, 2764-2771.

9. Yu, H. J.; Wang, L.; Zhou, J. F.; Dong, X. C.; Jiang, G. H. *J. Appl. Polym. Sci.* **2007,** *105*, 1156-1161.

10. Zhou, J. F.; Wang, L.; Yang, Q.; Dong, X. C.; Yu, H. J. *Colloid Polym. Sci.* **2007,** *285*, 1369-1376.

11. Liu, C. C.; Ni, P. H.; Fang, X.; Zhou, X. D. *Colloid Polym. Sci.* **2009,** *287*, 45-55.

12. Sun, G. X.; Zhang, M. Z.; He, J. L.; Ni, P. H. *J. Polym. Sci. Pol. Chem.* **2009,** *47*, 4670-4684.

13. Zhou, J. F.; Wang, L.; Dong, X. C.; Yang, Q.; Wang, J. J.; Yu, H. J.; Chen, X. *Eur. Polym. J.* **2007,** *43*, 1736-1743.

14. Lin, C. T.; Shiau, F. T.; Chern, C. S. *Colloid Polym. Sci.* **2009,** *287*, 1139-1144.

15. Saihi, D.; El-Achari, A.; Ghenaim, A.; Caze, C. *Polym. Test* **2002,** *21*, 607-612.

16. Kim, S. H.; Chung, I. D.; Ha, C. S.; Kim, K. J.; Cho, W. J. *J. Appl. Polym. Sci.* **1999,** *73*, 2349-2357.

17. Torres, E.; Dutta, N.; Choudhury, N. R.; Matisons, J. *Polym. Eng. Sci.* **2004,** *44*, 736-748.

18. Zhou, J. F.; Wang, L.; Dong, X. C.; Yang, Q.; Deng, L.; Huo, J.; Tan, Q. H.; Liu, Q. Q. *J. Appl. Polym. Sci.* **2008,** *108*, 2010-2016.

19. Saikia, P. J.; Goswami, A.; Baruah, S. D. *J. Appl. Polym. Sci.* **2002,** *86*, 386-394.

20. Saikia, P. J.; Goswami, A.; Baruah, S. D. *J. Appl. Polym. Sci.* **2002,** *85*, 1236-1245.

21. Pyun, J.; Jia, S. J.; Kowalewski, T.; Patterson, G. D.; Matyjaszewski, K. *Macromolecules* **2003,** *36*, 5094-5104.

22. Gao, J.; Li, J.; Benicewicz, B. C.; Zhao, S.; Hillborg, H.; Schadler, L. S. *Polymers* **2012,** *4*, 187-210.

23. Cash, B. M.; Wang, L.; Benicewicz, B. C. *J. Polym. Sci., Part A: Polym. Chem.* **2012**, *50*, 2533-2540.

24. Tsujii, Y.; Ejaz, M.; Sato, K.; Goto, A.; Fukuda, T. *Macromolecules* **2001**, *34*, 8872-8878.

CONCLUSIONS

Both side-chain fullerene polymers (SFP's) and PMMA-grafted "tadpole-like" fullerene polymers (TFP's) were synthesized via a combination of RAFT polymerization and the copper-catalyzed click reaction. Due to the high efficiency of the two techniques, the fullerene loading, molecular weight and polymer architecture of the SFP's were simultaneously controlled with as high as 78 C_{60} moieties per chain on average, which have not been reported before. Additionally, the self-assembly behaviors of these SFP's were studied both in solution and on silicon wafers, and it was found that the formation of the supramolecular architectures varied depending on the polymer chain lengths and fullerene contents of the samples. Using the control over these two molecular variables, different morphologies were observes that ranged from individual nanoparticles to nanoparticle strings, sheets and crystalline-like structures. On the other hand, the stabilization of graphene with the TFP's via π-π stacking interactions shows very promising data. The solubility of graphene was significantly improved in certain solvents with the binding of the TFP's. This effect is solvent dependent, which has been further confirmed by TEM analysis in THF, toluene and DMF. The non-covalent interactions between the TFP's and graphene were verified by UV-vis and FT-IR analyses.

In the aspect of Janus nanoparticle (NP) synthesis, we evaluated different routes to synthesize polymer-grafted Janus NP's. First, the Granick's procedure failed due to the size limitation of this technique. Then we developed an approach with planar silicon as

wafers the face-blocking substrates, which provided very low yields inherent in the low surface to volume ratio of the substrates. Eventually, we designed a facile and cyclic method involving the reversible click reaction. A novel mechanochemical approach was introduced into the particle interactions to selectively achieve the protection-deprotection process of NP's, and used in combination with polymer modification of the unprotected surfaces of the NP's by a "grafting to" strategy. Preliminary investigations of the unique self-assembly behaviors of the polymer-grafted Janus NP's were conducted by TEM and AFM in different solvents and concentrations, implying their potential applications as nano-surfactants.

Finally, we studied the polymerization of different kinds of functional monomers on silica NP's with diverse sizes. It was observed that polymer brushes grew on the NP's through surface-initiated RAFT polymerization with all the monomers in the experiments. Through sequential RAFT polymerizations, we designed a facile approach to graft multilayer block copolymer on silica NP's (up to three layers with relatively low polydispersities). The designed rubbery NP's displayed good dispersion in epoxy matrices, and showed a significant effect on toughening the epoxy resin. The surface-initiated polymerization of SMA achieved molecular weights greater than 100k, and such high values have not been reported before by RAFT even in solution. It was also found there were molecular weight limits for the polymerizations of SMA, probably because the resultant PSMA was not highly compatible with the solvent.

FUTURE WORK

Based on the highly efficient click reaction, more complicated fullerene-containing polymers can be prepared through post-functionalization. For example, the SFP can further be converted to a "double-cable" block copolymer by connecting to another chain of polythiophene, which would be very useful in the field of solar cell; or fullerene star polymers can be prepared with C_{60} as the cores by creating multi-functionalized fullerene and followed by a click reaction, in this way the fullerene would be treated as nanoparticles with many potential applications, such as biomedicine, electronic or optic materials, depending on what kinds of polymers would be grafted to. Additionally, the dispersion of TFP-stabilized graphene can be further studied in diverse polymer matrices, and graphene filled polymer nonocomposites may display very interesting mechanical and photoelectric properties.

In the aspect of Janus NP synthesis, the most important and challenging work so far is to develop a method to characterize the different morphologies on the two hemispheres of the Janus NP's. It would be more convincing if we can tell the anisotropy by observing individual particles. Otherwise, a "grafting from" strategy can be performed by functionalized the exposed surface of the NP's with CTA's after the partial protection. Therefore, the polymer chains would be more adjustable without concerns about the molecular weight limit, and also, with longer polymer brushes the asymmetrical structures may be easier to detect under microscopes. Moreover, a lot of further

investigations could to be conducted in the future, such as controlling the geometry of the Janus NP's, developing new chemistry to functionalize both sides of the particles and exploring more applications with the Janus NP's.

Surface-initiated RAFT polymerization is a very universal method to tune the surface chemistry of substrates. In the future, more novel and functional monomers can be polymerized from the surface of NP's in a controlled manner by optimizing the reaction conditions. For example, kinetic studies of SMA in less-polar solvents than THF are in process, which are expected to achieve a better control of the polymerization. Additionally, by designing different architectures on the NP surface, such as block copolymer brushes and binary polymer brushes, and adjusting the graft densities and core radii of NP's, we will have opportunities to better understand the relationship between the NP structures and their dispersion in polymer nanocomposites.

Although the copper-catalyzed click reaction has been widely used in our post-functionalization, there are more facile and efficient reactions developed in recent years, and with the addition of these chemical tools we can design more flexible and diverse synthetic routes. For example, the "thio-ene" and "thio-yne" reactions are two types of photo-initiated click reactions with no need of catalyst, which are very convenient for our chain-end functionalization or "graft to" strategies since the CTA can be easily converted to a thiol group.

BIBLIOGRAPHY

1. Jenkins, A. D.; Jones, R. G.; Moad, G. *Pure Appl. Chem.* **2010,** *82*, 483-491.

2. Hrsic, E.; Zografou, I.; Schulte, B.; Pich, A.; Keul, H.; Moller, M. *Polymer* **2013,** *54*, 495-504.

3. Quek, J. Y.; Roth, P. J.; Evans, R. A.; Davis, T. P.; Lowe, A. B. *J. Polym. Sci. Pol. Chem.* **2013,** *51*, 394-404.

4. Xu, J. X.; Xiao, X.; Zhang, Y. Y.; Zhang, W. Q.; Sun, P. C. *J. Polym. Sci. Pol. Chem.* **2013,** *51*, 1147-1161.

5. Moad, G.; Chiefari, J.; Chong, Y. K.; Krstina, J.; Mayadunne, R. T. A.; Postma, A.; Rizzardo, E.; Thang, S. H. *Polym. Int.* **2000,** *49*, 993-1001.

6. Keddie, D. J.; Moad, G.; Rizzardo, E.; Thang, S. H. *Macromolecules* **2012,** *45*, 5321-5342.

7. Kolb, H. C.; Finn, M. G.; Sharpless, K. B. *Angew. Chem. Int. Edit.* **2001,** *40*, 2004-2021.

8. Bock, V. D.; Hiemstra, H.; van Maarseveen, J. H. *Eur. J. Org. Chem.* **2005**, 51-68.

9. Lowe, A. B. *Polym. Chem.* **2010,** *1*, 17-36.

10. Kotsuchibashi, Y.; Ebara, M.; Aoyagi, T.; Narain, R. *Polym. Chem.* **2012,** *3*, 2545-2550.

11. Fairbanks, B. D.; Sims, E. A.; Anseth, K. S.; Bowman, C. N. *Macromolecules* **2010,** *43*, 4113-4119.

12. Blackman, M. L.; Royzen, M.; Fox, J. M. *J. Am. Chem. Soc.* **2008,** *130*, 13518-13519.

13. Lutz, J.-F. *Angew. Chem. Int. Edit.* **2007,** *46*, 1018-1025.

14. Chernykh, A.; Agag, T.; Ishida, H. *Polymer* **2009,** *50*, 382-390.

15. Li, Y.; Yang, J.; Benicewicz, B. C. *J. Polym. Sci. Pol. Chem.* **2007,** *45*, 4300-4308.

16. Opsteen, J. A.; van Hest, J. C. M. *Chem. Commun.* **2005**, 57-59.

17. Wu, P.; Feldman, A. K.; Nugent, A. K.; Hawker, C. J.; Scheel, A.; Voit, B.; Pyun, J.; Frechet, J. M. J.; Sharpless, K. B.; Fokin, V. V. *Angew. Chem. Int. Edit.* **2004,** *43*, 3928-3932.

18. Chen, J. C.; Xiang, J. M.; Cai, Z. W.; Yong, H.; Wang, H. D.; Zhang, L. H.; Luo, W. Q.; Min, H. *J. Macromol. Sci. Part A-Pure Appl. Chem.* **2010,** *47*, 655-662.

19. An, Z.; Tang, W.; Wu, M.; Jiao, Z.; Stucky, G. D. *Chem. Commun.* **2008**, 6501-6503.

20. Liu, J.; Nie, Z.; Gao, Y.; Adronov, A.; Li, H. *J. Polym. Sci. Pol. Chem.* **2008,** *46*, 7187-7199.

21. Brantley, J. N.; Wiggins, K. M.; Bielawski, C. W. *Science* **2011,** *333*, 1606-1609.

22. Leibfarth, F. A.; Hawker, C. J. *Science* **2011,** *333*, 1582-1583.

23. Kroto, H. W.; Heath, J. R.; O'Brien, S. C.; Curl, R. F.; Smalley, R. E. *Nature* **1985,** *318*, 162-163.

24. Kratschmer, W.; Lamb, L. D.; Fostiropoulos, K.; Huffman, D. R. *Nature* **1990,** *347*, 354-358.

25. Thompson, B. C.; Frechet, J. M. J. *Angew. Chem. Int. Edit.* **2008,** *47*, 58-77.

26. Giacalone, F.; Martin, N. *Chem. Rev.* **2006,** *106*, 5136-5190.

27. Wang, C. C.; Guo, Z. X.; Fu, S. K.; Wu, W.; Zhu, D. B. *Prog. Polym. Sci.* **2004,** *29*, 1079-1141.

28. Mamo, M. A.; Freitas, F. S.; Forbes, R. P.; Black, R. S.; Nogueira, A. F.; van Otterlo, W. A. L.; Coville, N. J. *Fuller. Nanotub. Carbon Nanostruct.* **2013,** *21*, 198-212.

29. de Boer, B.; Stalmach, U.; van Hutten, P. F.; Melzer, C.; Krasnikov, V. V.; Hadziioannou, G. *Polymer* **2001,** *42*, 9097-9109.

30. Barrau, S.; Heiser, T.; Richard, F.; Brochon, C.; Ngov, C.; van de Wetering, K.; Hadziioannou, G.; Anokhin, D. V.; Ivanov, D. A. *Macromolecules* **2008,** *41*, 2701-2710.

31. Iskin, B.; Yilmaz, G.; Yagci, Y. *Chem.-Eur. J.* **2012,** *18*, 10254-10257.

32. Natori, I.; Natori, S. *J. Polym. Sci. Pol. Chem.* **2008,** *46*, 3282-3293.

33. Kim, J.; Yun, M. H.; Lee, J.; Kim, J. Y.; Wudl, F.; Yang, C. *Chem. Commun.* **2011,** *47*, 3078-3080.

34. Munoz, A.; Illescas, B. M.; Sanchez-Navarro, M.; Rojo, J.; Martin, N. *J. Am. Chem. Soc.* **2011,** *133*, 16758-16761.

35. Lanzi, M.; Paganin, L.; Errani, F. *Polymer* **2012,** *53*, 2134-2145.

36. Miyanishi, S.; Zhang, Y.; Hashimoto, K.; Tajima, K. *Macromolecules* **2012,** *45*, 6424-6437.

37. Heuken, M.; Komber, H.; Erdmann, T.; Senkoyskyy, V.; Kiriy, A.; Voit, B. *Macromolecules* **2012,** *45*, 4101-4114.

38. Bicciocchi, E.; Chen, M.; Rizzardo, E.; Ghiggino, K. P. *Polym.Chem.* **2013,** *4*, 53-56.

39. Lin, I. C.; Liang, M. T.; Liu, T. Y.; Jia, Z. F.; Monteiro, M. J.; Toth, I. *Bioorg. Med. Chem.* **2012,** *20*, 6862-6869.

40. Park, J. T.; Roh, D. K.; Patel, R.; Kim, E.; Ryu, D. Y.; Kim, J. H. *J. Mater. Chem.* **2010,** *20*, 8521-8530.

41. Shi, H. Y.; Yuan, L.; Wu, Y. F.; Liu, S. Q. *Biosens. Bioelectron.* **2011,** *26*, 3788-3793.

42. Tao, P.; Li, Y.; Rungta, A.; Viswanath, A.; Gao, J. N.; Benicewicz, B. C.; Siegel, R. W.; Schadler, L. S. *J. Mater. Chem.* **2011,** *21*, 18623-18629.

43. Yang, J.; Deng, L. H.; Han, C. R.; Duan, J. F.; Ma, M. G.; Zhang, X. M.; Xu, F.; Sun, R. C. *Soft Matter* **2013,** *9*, 1220-1230.

44. Lowe, A. B.; Sumerlin, B. S.; Donovan, M. S.; McCormick, C. L. *J. Am. Chem. Soc.* **2002,** *124*, 11562-11563.

45. Lupitskyy, R.; Motornov, M.; Minko, S. *Langmuir* **2008,** *24*, 8976-8980.

46. Feng, L. B.; He, L.; Ma, Y. X.; Wang, W. *Mater. Chem. Phys.* **2009,** *116*, 158-163.

47. Thong-On, B.; Rutnakornpituk, B.; Wichai, U.; Rutnakornpituk, M. *J. Nanopart. Res.* **2012,** *14*.

48. Wang, Y. Z.; Fan, D. Q.; He, J. P.; Yang, Y. L. *Colloid Polym. Sci.* **2011,** *289*, 1885-1894.

49. Bartholome, C.; Beyou, E.; Bourgeat-Lami, E.; Chaumont, P.; Zydowicz, N. *Macromolecules* **2003,** *36*, 7946-7952.

50. Li, C. Z.; Benicewicz, B. C. *Macromolecules* **2005,** *38*, 5929-5936.

51. Pyun, J.; Jia, S. J.; Kowalewski, T.; Patterson, G. D.; Matyjaszewski, K. *Macromolecules* **2003,** *36*, 5094-5104.

52. Rutot-Houze, D.; Fris, W.; Degee, P.; Dubois, P. *J. Macromol. Sci. Pure* **2004,** *A41*, 697-711.

53. Raula, J.; Shan, J.; Nuopponen, M.; Niskanen, A.; Jiang, H.; Kauppinen, E. I.; Tenhu, H. *Langmuir* **2003,** *19*, 3499-3504.

54. Stenzel, M. H.; Zhang, L.; Huck, W. T. S. *Macromol. Rapid Commun.* **2006,** *27*, 1121-1126.

55. Zhao, Y.; Perrier, S. *Macromolecules* **2006,** *39*, 8603-8608.

56. Li, C.; Han, J.; Ryu, C. Y.; Benicewicz, B. C. *Macromolecules* **2006,** *39*, 3175-3183.

57. Ohno, K.; Ma, Y.; Huang, Y.; Mori, C.; Yahata, Y.; Tsujii, Y.; Maschmeyer, T.; Moraes, J.; Perrier, S. *Macromolecules* **2011,** *44*, 8944-8953.

58. Rungta, A.; Natarajan, B.; Neely, T.; Dukes, D.; Schadler, L. S.; Benicewicz, B. C. *Macromolecules* **2012,** *45*, 9303-9311.

59. Zhao, B.; He, T. *Macromolecules* **2003,** *36*, 8599-8602.

60. Vaia, R. A.; Wagner, H. D. *Mater. Today* **2004,** *7*, 32-37.

61. Zhang, Z. L.; Glotzer, S. C. *Nano Letters* **2004,** *4*, 1407-1413.

62. Vanakaras, A. G. *Langmuir* **2006,** *22*, 88-93.

63. Degennes, P. G. *Angew. Chem. Int. Edit.* **1992,** *31*, 842-845.

64. Perro, A.; Reculusa, S.; Ravaine, S.; Bourgeat-Lami, E. B.; Duguet, E. *J. Mater. Chem.* **2005,** *15*, 3745-3760.

65. Wang, F.; Phonthammachai, N.; Mya, K. Y.; Tjiu, W. W.; He, C. *Chem. Commun.* **2011,** *47*, 767-769.

66. Paunov, V. N.; Cayre, O. J. *Adv. Mater.* **2004,** *16*, 788-791.

67. Tang, J. L.; Schoenwald, K.; Potter, D.; White, D.; Sulchek, T. *Langmuir* **2012,** *28*, 10033-10039.

68. Hong, L.; Jiang, S.; Granick, S. *Langmuir* **2006,** *22*, 9495-9499.

69. Jiang, S.; Granick, S. *Langmuir* **2008,** *24*, 2438-2445.

70. Jiang, S.; Granick, S. *Langmuir* **2009,** *25*, 8915-8918.

71. Li, Y.; Benicewicz, B. C. *Macromolecules* **2008,** *41*, 7986-7992.

72. Giacalone, F.; Martin, N. *Chem. Rev.* **2006**, *106*, 5136-5190.

73. Wang, C.; Guo, Z-X.; Fu, S.; Wu, W.; Zhu, D. *Prog. Polym. Sci. 2004*, *29*, 1079-1141.

74. Hiorns, R.; Cloutet, E.; Ibarboure, E.; Vignau, L.; Lematre, N.; Guillerez, S.; Absalon, C.; Cramail, H. *Macromolecules* **2009**, *42*, 3549-3558.

75. Natori, I.; Natori, S. *J. Polym. Sci., Part A: Polym. Chem.* **2008**, *46*, 3282-3293.

76. Dardel, B.; Guillon, D.; Heinrich, B.; Deschenaux, R. *J. Mater. Chem.* **2001**, *11*, 2814-2831.

77. Kim, J.; Yun, M. H.; Lee, J.; Kim, J. Y.; Wudl, F.; Yang, C. *Chem. Commun.* **2011**, *47*, 3078-3080.

78. Munoz, A.; Illescas, B. M.; Sanchez-Navarro, M.; Rojo, J.; Martin, N. *J. Am. Chem. Soc.* **2011**, *133*, 16758-16761.

79. Shi, S.; Khemanikc, K. C.; Li, Q. C.; Wudl, F. *J. Am. Chem. Soc.* **1992**, *114*, 10656-10657.

80. Yang, C.; Lee, J. K.; Heeger, A. J.; Wudl, F. *J. Mater. Chem.* **2009**, *19*, 5416-5423.

81. Lee, J. U.; Cirpan, A.; Emrick, T.; Russell, T. P.; Jo, W. H. *J. Mater. Chem.* **2009**, *19*, 1483-1489.

82. a) Stalmach, U.; de Boer, B.; Videlot, C.; van Hutten P. F.; Hadziioannou, G. *J. Am. Chem. Soc.* **2000**, *122*, 5464-5472. b) de Boer,B.; Stalmach, U.; van Hutten, P. F.; Melzer, C.; Krasnikov, V. V.; Hadziioannou, G. *Polymer* **2001**, *42*, 9097-9109.

83. a) van der Veen, M. H.; de Boer, B.; Stalmach, U.; van de Wetering, K. I.; Hadziioannou, G. *Macromolecules* **2004**, *37*, 3673-3684. b) Barrau, S.; Heiser, T.; Richard, F.; Brochon, C.; Ngov, C.; van de Wetering, K.; Hadziioannou, G.; Anokhin, D. V.; Ivanov, D. A. *Macromolecules* **2008**, *41*, 2701-2710.

84. Celli, A.; Marchese, P.; Vannini, M.; Berti, C.; Fortunati, I.; Signorini, R.; Bozio, R. *Reactive & Functional Polymers* **2011**, *71*, 641-647.

85. Li, M.; Xu, P.; Yang, J.; Yang, S. *J. Mater. Chem.* **2010**, *20*, 3953-3960.

86. Rusen, E.; Marculescu, B.; Preda, N.; Mihut, L. *J. Polym. Res.* **2008**, *15*, 447-451.

87. a) Kawauchi, T.; Kumaki, J.; Yashima, E. *J. Am. Chem. Soc.* **2006**, *128*, 10560-10567. b) Kawauchi, T.; Kumaki, J.; Kitaura, A.; Okoshi, K.; Kusanagi, H.; Kobayashi, K.; Shinahara, H.; Yashima, E. *Angew. Chem. Int. Ed.* **2008**, *47*, 515-519.

88. Wang, M.; Pramoda, K. P.; Goh, S. H. *Macromolecules* **2006**, *39*, 4932-4934.

89. Badamshina, E.; Gafurova, M. *J. Mater. Chem.* **2012**, *22*, 9427-9438.

90. Bonifazi, D.; Enger, O.; Diederich, F.; *Chem. Soc. Rev.* **2006**, *36*, 390-414.

91. Sanchez, L.; Otero, R.; Gallego, J. M.; Miranda, R.; Martin, N. *Chem. Rev.* **2009**, *109*, 2081-2091.

92. Babu, S. S.; Mohwald, H.; Nakanishi, T. *Chem. Soc. Rev.* **2010**, *39*, 4021-4035.

93. Schade, B.; Ludwig, K.; Bottcher, C.; Hartnagel, U.; Hirsch, A. *Angew. Chem. Int. Ed.* **2007**, *46*, 4393-4396.

94. Yu, X.; Zhang, W-B.; Yue, K.; Li, X.; Liu, H.; Xin, Y.; Wang, C-L.; Wesdemiotis, C.; Cheng, S. Z. D. *J. Am. Chem. Soc.* **2012**, *134*, 7780-7788.

95. Zhou, G.; He, J.; Harruna, I. I.; Geckeler, K. E. *J. Mater. Chem.* **2008**, *18*, 5492-5501.

96. Yao, Z. L.; Tam, K. C. *Langmuir* **2011**, *27*, 6668-6673.

97. Tang, Q.; Zhou, Z.; Chen, Z. *Nanoscale* **2013**, Advance Article.

98. Liu, J.; Yang, W.; Tao, L.; Li, D.; Boyer, C.; Davis, T. P. *J. Polym. Sci., Part A: Polym. Chem.* **2009**, *48*, 425-433.

99. Zhang, X.; Huang Y.; Wang, Y.; Ma, Y.; Liu Z.; Chen, Y. *Carbon* **2008**, *47*, 313-347.

100. Yu, D.; Park, K.; Durstock, M.; Dai, L. *J. Phys. Chem. Lett.* **2011**, *2*, 1113-1118.

101. Felder, D.; Nierengarten, H.; Gisselbrecht, J-P.; Boudon, C.; Leize, E.; Nicoud, J-F.; Gross, M.; van Dorsselaer, A.; Nierengarten, J-F. *New J. Chem.* **2000**, *24*, 687-695.

102. Iehl, J.; de *Freitas*, R. P.; Nierengarten, J-F. *Tetrahedron Lett.* **2008**, *49*, 4063-4066.

103. Bingel, C. *Chemische Berichte* **1993**, *126*, 1957-1959.

104. Ruoff, R. S.; Tse, D. S.; Lorents, D. C. *J. Phys. Chem.* **1993**, *97*, 3379-3383.

105. Djojo, F.; Herzog, A.; Lamparth, I.; Hampel, F.; Hirsch, A. *Chem. Eur. J.* **1996**, *2*, 1537-1547.

106. Kim, H.; Bedrov, D.; Smith, G. D. *J. Chem. Theory Comput.* **2008,** *4*, 335-340.

107. Chu, C.; Tsai, Y.; Hsiao, L.; Wang, L. *Macromolecules* **2011**, *44*, 7056-7061.

108. Runge, M. B.; Dutta, S.; Bowden, N. B. *Macromolecules* **2006**, *39*, 498-508.

109. Yusa, S-I.; Awa, S.; Ito, M.; Kawase, T.; Takada, T.; Makashima, K.; Liu, D.; Yamago, S.; Morishima, Y. *J. Polym. Sci., Part A: Polym. Chem.* **2011**, *49*, 2761-2770.

110. Wang, J.; Shen, Y.; Kessel, S.; Fernandes, P.; Yoshida, K.; Yagai, S.; Kurth, D. G.; Mohwald, H.; Nakanishi, T. *Angew. Chem., Int. Ed.* **2009**, *48*, 2166-2170.

111. Reculusa, S.; Poncet-Legrand, C.; Perro, A.; Duguet, E.; Bourgeat-Lami, E.; Mingotaud, C.; Ravaine, S. *Chem. Mater.* **2005**, *17*, 3338-3344.

112. (a) Chen, Y.; Liang, F.; Yang, H.; Zhang, C.; Wang, Q.; Qu, X.; Li, J.; Cai, Y.; Qiu, D.; Yang, Z. *Macromolecules* **2012**, *45*, 1460-1467. (b) Liu, B.; Liu, J.; Liang, F.; Wang, Q.; Zhang, C.; Qu, X.; Li, J.; Qiu, D.; Yang, Z. *Macromolecules* **2012**, *45*, 5176-5184. (c) Tang, C.; Zhang, C.; Sun, Y.; Liang, F.; Wang, Q.; Li, J.; Qu, X.; Yang, Z. *Macromolecules* online.

113. Jia, L.; Zhou, F.; Liu, W. *Chem. Commun.* **2012**, *48*, 12112-12114.

114. de Gennes, P-G. *Angew. Chem., Int. Ed.* **1992**, *31*, 842-845.

115. Jiang, S.; Chen, Q.; Tripathy, M.; Luijten, E.; Schweizer, K. S.; Granick; S. *Adv. Mater.* **2010**, *22*, 1060-1071.

116. Perro, A.; Reculusa, S.; Ravaine, S.; Bourgeat-Lami, E.; Duguet, Etienne. *J. Mater. Chem.* **2005**, *15*, 3745-3760.

117. (a) Hong, L.; Jiang, S.; Granick, S. *Langmuir* **2006,** *22,* 9495-9499. (b) Jiang, S.; Granick, S. *Langmuir* **2008,** *24,* 2438-2445. (c) Jiang, S.; Schultz, M. J.; Chen, Q.; Moore, J. S.; Granick, S. *Langmuir* **2008**, *24*, 10073-10077.

118. Wang, F.; Phonthammachai, N.; Mya, K. Y.; Tjiua, W. W.; He, C. *Chem. Commun.* **2011**, *47*, 767-769.

119. Zhao, Z.; Shi, Z.; Yu, Y.; Zhang, G. *Langmuir* **2012**, *28*, 2382-2386.

120. Tang, J. L.; Schoenwald, K.; Potter, D.; White, D.; Sulchek, T. *Langmuir* **2012**, *28*, 10033-10039.

121. (a) Akcora, P.; Liu, H.; Kumar, S. K.; Moll, J.; Li, Y.; Benicewicz, B. C.; Schadler, L. S.; Acehan, D.; Panagiotopoulos, A. Z.; Pryamitsyn, V.; Ganesan, V.; Ilavsky, J.; Thiyagarajan, P.; Colby, R. H.; Douglas, J. F. *Nature Materials* **2009**, *8*, 354-359. (b) Dukes, D.; Li, Y.; Lewis, S.; Benicewicz, B. C.; Schadler, L. S.; Kumar, S. K. *Macromolecules* **2010**, *43*, 1564-1570. (c) Akcora, P.; Kumar, S. K.; Sakai, V. G.; Li, Y.; Benicewicz, B. C.; Schadler, L. S. *Macromolecules* **2010**, *43*, 8275-8281. (d) Maillard, D.; Kumar, S. K. Rungta, A.; Benicewicz, B. C.; Prud'homme, R. E. *Nano letters* **2011**, *11*, 4569-4573.

122. (a) Khan, J.; Harton, S. E.; Akcora, P.; Benicewicz, B. C.; Kumar, S. K. *Macromolecules* **2009**, *42*, 5741-5744. (b) Akcora, P.; Kumar, S. K.; Moll, J.; Lewis, S.; Schadler, L. S.; Li, Y.; Benicewicz, B. C.; Sandy, A.; Narayanan, S.; Ilavsky, J.; Thiyagarajan, P.; Colby, R. H.; Douglas, J. F. *Macromolecules* **2010**, *43*, 1003-1010. (c) Gao, J.; Li, J.; Benicewicz, B. C.; Zhao, S.; Hillorg, H.; Schadler, L. S. *Polymers* **2012**, *4*, 187-210.

123. Pyun, J.; Jia, S.; Kowalewski, T.; Patterson, G. D.; Matyjaszewski, K. *Macromolecules* **2003,** *36,* 5094-5104.

124. (a) Li, C.; Benicewicz, B. C. *Macromolecules* **2005,** *38,* 5929-5936. (b) Li, C.; Han, J.; Ryu, C. Y.; Benicewicz, B. C. *Macromolecules* **2006,** *39,* 3175-3183. (c) Huang, X.; Appelhans, D.; Formanek, P.; Simon, F.; Voit, B. *Macromolecules* **2011**, *44*, 8351-8360. (d) Ohno, K.; Ma, Y.; Huang, Y.; Mori, C.; Yahata, Y.; Tsujii, Y.; Maschmeyer, T.; Moraes, J.; Perrier, S. *Macromolecules* **2011**, *44*, 8944-8953. (e) Cash, B. M.; Wang, L.; Benicewicz, B. C. *J. Polym. Sci. Part A: Polym. Chem.* **2012**, *50*, 2533-2540.

125. Li, D.; Sheng, X.; Zhao, B. *J. Am. Chem. Soc.* **2005**, *127*, 6248-6256. (b) Zhao, B.; Zhu, L. *Macromolecules* **2009**, *42*, 9369-9383. (c) Horton, J. M.; Tang, S.; Bao, C.; Tang, P.; Qiu, F.; Zhu, L.; Zhao B. *ACS Macro Lett.* **2012**, *1*, 1061-1065.

126. Lupitskyy, R.; Motornov, M.; Minko, S. *Langmuir* **2008**, *24*, 8976.

127. Lattuada, M.; Hatton, T. A. *J. Am. Chem. Soc.* **2007**, *129*, 12878-12889.

128. (a) Wang, B.; Li, B.; Zhao, B.; Li, C. Y. *J. Am. Chem. Soc.* **2008**, *130*, 11594-11595. (b) Wang, B.; Li, B.; Ferrier, Jr., R. C. M.; Li, C. Y. *Macromol. Rapid Commun.* **2010**, *31*, 169-175.

129. Zhang, S.; Li, Z.; Samarajeewa, S.; Sun, G.; Yang, C.; Wooley, K. L. *J. Am. Chem. Soc.* **2011**, 133, 11046-11049.

130. Diesendruck, C. E.; Steinberg, B. D.; Sugai, N.; Silberstein, M. N.; Sottos, N. R.; White, S. R.; Braun, P. V.; Moore, J. S. *J. Am. Chem. Soc.* **2012**, *134*, 12446-12449.

131. Wiggins, K. M.; Brantley, J. N.; Bielawski, C. W. *ACS Macro Lett.* **2012**, *1*, 623-626.

132. Groote, R.; Jakobs, R. T. M.; Sijbesma, R. P. *ACS Macro Lett.* **2012**, *1*, 1012-1015.

133. (a) Kean, Z. S.; Craig. S. L. *Polymer* **2012**, *53*, 1035-1048. (b) Kean, Z. S.; Black Ramirez, A. L.; Craig. S. L. *J. Polym. Sci. Part A: Polym. Chem.* **2012**, *50*, 3481-3484. (c) Kean, Z. S.; Black Ramirez, A. L.; Yan, Y.; Craig. S. L. *J. Am. Chem. Soc.* **2012**, *134*, 12939-12942.

134. Cravotto, G.; Cintas, P. *Chem. Sci.* **2012**, *3*, 295-307.

135. Brantley, J. N.; Wiggins, K. M.; Bielawski, C. W. *Science* **2011**, *333*, 1606-1609.

136. Leibfarth, F. A.; Hawker, C. J. *Science* **2011**, *333*, 1582-1583.

137. An, Y.; Chen, M.; Xue, Q.; Liu, W. *J. Colloid. Interf. Sci.* **2007**, *311*, 507-513.

138. Stöber, W.; Fink, A.; Bohn, E. *J. Colloid Interface Sci.* **1968**, *26*, 62-69.

139. Nozawa, K.; Gailhanou, H.; Raison, L.; Panizza, P.; Ushiki, H.; Sellier, E.; Delville, J. P.; Delville, M. H. *Langmuir* **2005,** *21,* 1516-1523.

140. Hansen, T. S.; Larsen, N. B. *Macromolecules* **2008**, *41*, 4321-4327.

141. Bansal, A.; Yang, H.; Li, C.; Benicewicz, B. C.; Kumar, S. K.; Schadler, L. S. *J. Polym. Sci., Part B: Polym. Phys.* **2006**, *44*, 2944-2950.

142. Akcora, P.; Liu, H.; Kumar, S. K.; Moll, J.; Li, Y.; Benicewicz, B. C.; Schadler, L. S.; Acehan, D.; Panagiotopoulos, A. Z.; Pryamitsyn, V.; Ganesan, V.; Ilavsky, J.; Thiyagarajan, P.; Colby, R. H.; Douglas, J. F. *Nat. Mater.* **2009**, *8*, 354-359.

143. Kinloch, A. J.; Mohammed, R. D.; Taylor, A. C.; Eger, C.; Sprenger, S.; Egan, D. *J. Mater. Sci.* **2005**, *40*, 5083-5086.

144. Shang, S. R.; Huang, S. J.; Weiss, R. A. *Polymer* **2009**, *50*, 3119-3127.

145. Shang, S. R.; Huang, S. J.; Weiss, R. A. *Polymer* **2011**, *52*, 2764-2771.

146. Yu, H. J.; Wang, L.; Zhou, J. F.; Dong, X. C.; Jiang, G. H. *J. Appl. Polym. Sci.* **2007**, *105*, 1156-1161.

147. Zhou, J. F.; Wang, L.; Yang, Q.; Dong, X. C.; Yu, H. J. *Colloid Polym. Sci.* **2007**, *285*, 1369-1376.

148. Liu, C. C.; Ni, P. H.; Fang, X.; Zhou, X. D. *Colloid Polym. Sci.* **2009**, *287*, 45-55.

149. Sun, G. X.; Zhang, M. Z.; He, J. L.; Ni, P. H. *J. Polym. Sci. Pol. Chem.* **2009**, *47*, 4670-4684.

150. Zhou, J. F.; Wang, L.; Dong, X. C.; Yang, Q.; Wang, J. J.; Yu, H. J.; Chen, X. *Eur. Polym. J.* **2007**, *43*, 1736-1743.

151. Lin, C. T.; Shiau, F. T.; Chern, C. S. *Colloid Polym. Sci.* **2009**, *287*, 1139-1144.

152. Saihi, D.; El-Achari, A.; Ghenaim, A.; Caze, C. *Polym. Test* **2002**, *21*, 607-612.

153. Kim, S. H.; Chung, I. D.; Ha, C. S.; Kim, K. J.; Cho, W. J. *J. Appl. Polym. Sci.* **1999**, *73*, 2349-2357.

154. Torres, E.; Dutta, N.; Choudhury, N. R.; Matisons, *J. Polym. Eng. Sci.* **2004**, *44*, 736-748.

155. Zhou, J. F.; Wang, L.; Dong, X. C.; Yang, Q.; Deng, L.; Huo, J.; Tan, Q. H.; Liu, Q. Q. *J. Appl. Polym. Sci.* **2008**, *108*, 2010-2016.

156. Saikia, P. J.; Goswami, A.; Baruah, S. D. *J. Appl. Polym. Sci.* **2002**, *86*, 386-394.

157. Saikia, P. J.; Goswami, A.; Baruah, S. D. *J. Appl. Polym. Sci.* **2002**, *85*, 1236-1245.

158. Pyun, J.; Jia, S. J.; Kowalewski, T.; Patterson, G. D.; Matyjaszewski, K. *Macromolecules* **2003**, *36*, 5094-5104.

159. Gao, J.; Li, J.; Benicewicz, B. C.; Zhao, S.; Hillborg, H.; Schadler, L. S. *Polymers* **2012**, *4*, 187-210.

160. Cash, B. M.; Wang, L.; Benicewicz, B. C. *J. Polym. Sci., Part A: Polym. Chem.* **2012**, *50*, 2533-2540.

161. Tsujii, Y.; Ejaz, M.; Sato, K.; Goto, A.; Fukuda, T. *Macromolecules* **2001**, *34*, 8872-8878.